VILNIUS UNIVERSITY
CENTER FOR PHYSICAL SCIENCES AND TECHNOLOGY

MILDA MALAKAUSKAITĖ-PETRULEVIČIENĖ

SOL-GEL SYNTHESIS AND CHARACTERIZATION OF CALCIUM HYDROXYAPATITE THIN FILMS ON DIFFERENT SUBSTRATES

Doctoral dissertation
Physical sciences, chemistry (03 P)

Vilnius, 2016

The disssertation was carried out from 2012 to 2016 at Vilnius University.

Scientific supervisor: Prof. Dr. Habil. Aivaras Kareiva (Vilnius University, Physical Sciences, Chemistry - 03 P).

Evaluation board:

Chairman:

Prof. Dr. Jurgis Barkauskas (Vilnius University, Physical Sciences, Chemistry - 03 P).

Members:

Prof. Habil. Dr. Eimutis Juzeliūnas (University of Klaipėda, Physical Sciences, Chemistry - 03 P).

Dr. Konstantinas Leinartas (Center for Physical Sciences and Technology, Physical Sciences, Chemistry - 03 P).

Dr. Vladimir Sivakov (Leibniz-Institute of Photonic Technology, Physical Sciences, Chemistry - 03 P).

Prof. Dr. Vida Vičkačkaitė (Vilnius University, Physical Sciences, Chemistry - 03 P);

The official discussion will be held on 2 p.m. 16th September 2016 at the meeting of the Evaluation Board at the Auditorium of Inorganic Chemistry of the Faculty of Chemistry of Vilnius University.

Address: Naugarduko 24, LT-03225 Vilnius, Lithuania. Tel. 2193108. Fax: 2330987.

The summary of doctoral dissertation was mailed on the …. of July 2016.

The dissertation is available at the Library of Vilnius University, at the Library of Institute of Chemistry CPST and at VU web page: *www.vu.lt/lt/naujienos/ivykiu-kalendorius*

VILNIAUS UNIVERSITETAS
FIZINIŲ IR TECHNOLOGIJOS MOKSLŲ CENTRAS

MILDA MALAKAUSKAITĖ-PETRULEVIČIENĖ

KALCIO HIDROKSIAPATITO PLONŲ SLUOKSNIŲ ANT ĮVAIRIŲ PADĖKLŲ SINTEZĖ ZOLIŲ-GELIŲ METODU IR APIBŪDINIMAS

Daktaro disertacija
Fiziniai mokslai, Chemija (03 P)

Vilnius, 2016

Disertacija parengta 2012-2016 metais Vilniaus universitete.

Mokslinis vadovas – prof. habil. dr. Aivaras Kareiva (Vilniaus universitetas, fiziniai mokslai, chemija - 03 P).

Disertacija ginama Vilniaus universiteto Chemijos mokslo krypties gynimo taryboje:

Pirmininkas – prof. dr. Jurgis Barkauskas (Vilniaus universitetas, fiziniai mokslai, chemija – 03P).

Nariai:
prof. habil. dr. Eimutis Juzeliūnas (Klaipėdos universitetas, fiziniai mokslai, chemija – 03P);

dr. Konstantinas Leinartas (Fizinių ir technologijos mokslų centras, fiziniai mokslai, chemija – 03P);

dr. Vladimir Sivakov (Leibnico fotoninių technologijų institutas, fiziniai mokslai, chemija – 03P).

prof. dr. Vida Vičkačkaitė (Vilniaus universitetas, fiziniai mokslai, chemija – 03P);

Disertacija bus ginama viešame Chemijos mokslo krypties gynimo tarybos posėdyje 2016 m. rugsėjo mėn. 16 d. 14 val. Vilniaus universiteto Chemijos fakulteto Neorganinės chemijos auditorijoje.
Adresas: Naugarduko 24, LT-03225 Vilnius, Lietuva. Tel.: 2193108. Faksas: 2330987.
Disertacijos santrauka išsiuntinėta 2016 m. liepos mėn.....d.
Disertaciją galima peržiūrėti Vilniaus universiteto, FTMC Chemijos instituto bibliotekose ir VU interneto svetainėje adresu: *www.vu.lt/lt/naujienos/ivykiu-kalendorius*

Contents

List of abbreviations

ACP - amorphous calcium phosphate

AFM - atomic force microscopy

ALP - alkaline phosphatase

APS - atmospheric plasma spraying

ASTM - the American Society of the International Association for Testing and Materials

BCPs - biphasic calcium phosphates

BMP-2 - bone morphogenetic protein-2

BMPs - bone morphogenetic proteins

BSP - bone sialoprotein

CAM - coctact angle measurements

CaP - calcium phosphate

CDHAp - calcium-deficient hydroxyapatites

CHAp - calcium hydroxyapatite

CPCs - calcium phosphate ceramics

cpTi - commercially pure titanium

CTAB - cetyltrimethylamonium bromide

CTP - cytidine 5’-triphosphate disodium salt

DCP - anhydrous dicalcium phosphate

DCPD - dicalcium phosphate dihydrate

EDTA - ethylenediaminetetraacetic acid

EDX- energy dispersive X-ray spectrometry

EPD - electrophoretic deposition

FDA - the Food and Drug Administration

FTIR - Fourier transform infrared spectroscopy

GTPS - gas tunnel type plasma spraying

HDPE - high-density polyethylene

HVOF - high velocity oxy-fuel

HVSFS - high-velocity suspension flame spraying

IBAD - ion beam assisted deposition

ISO - the International Standard Organization

KAc - potasium acetate

LPS - liquid plasma spraying

NCPs - non-collagenous proteins

OAp – oxyapatite

OCN - osteocalcin

OCP - octacalcium phosphate

OHAp - oxyhydroxyapatite

OPN - osteopontin

PAMAM - poly(amido-amine)□

PLD - pulsed laser deposition

PMMA - para-Methoxy-N-methylamphetamine

PPS - powder plasma spray

PVA - polivinylalcohol

RF - radio-frequency

SBFs - simulated body fluids

SEM - scanning electron microscopy□

SPS - suspension plasma spraying

TCP - tricalcium phosphate

TeCP - tetracalcium phosphate

VEGFs - vascular endothelial growth factors

VPS - vacuum plasma spraying

XRD - X-ray diffraction

RMS, R_q - root mean square

α-TCP - α-tricalcium phosphate

β-TCMP, Mg-TCP - Mg-substituted tricalcium phosphate

β-TCP - β-tricalcium phosphate

1. Introduction

Ageing population, changing lifestyle and better quality of life require better healthcare [1]. A few million patients need bone grafts or bone graft substitutes and teeth implants. Usually implants are needed due to bone cysts and tumours, check-up of orthopaedic implants, spine fusion, trauma and etc. [1, 2].

Bone is a dynamic natural organic-inorganic tissue consisting of 10-20% collagen fibrils, 60-70% well-arrayed, nano-crystalline, rod-like inorganic materials, which are 25-50 nm long and have a water content of 9-20% (and also contain small quantities of other organic materials, such as proteins, polysaccharides and lipids) [3–5]. The basic bone mineral is calcium hydroxyapatite $Ca_{10}(PO_4)_6(OH)_2$ (CHAp).

The broad range of materials are used for the synthetic bone graft substitutes. They should have mechanical properties as high or better than those of a cortical bone ("load-bearing" property), they should be resorbable (or degradable) to prevent fatigue fractures at long implantation times and they should promote bone formation ("osteoinductivity") [2]. Metal implants should be with surface biological properties for the adsorption of proteins, adhesion of cells and tissue integration. Chemistry, wettability and nanometer-sized roughness of surface are very important properties of metal implants, which will affect the tissue repair process and long-term behaviour of the biomaterial–tissue interface in the recipient patient [6, 7]. Challenge for researchers is to control surface properties at cell and protein levels in the nanometer size range [8].

In recent years, 70-80% of medical implants have been made of metallic biomaterials, which have been used especially for hard tissue replacement [9]. Metals and their alloys should have mechanical reliability, strength, stiffness, toughness and impact resistance [1]. Dental implants are usually made of commercially pure titanium or titanium alloys [1, 10, 11]. Also for medical application to reach better surface biocompatibility, researchers have tried to use other substrates, such as C/C substrate, magnesium alloys, silicon and

quartz substrates [12–16]. However, titanium easily oxidizes, and bioinert titanium oxide does not readily form a strong interface with round tissue; therefore the modification of titanium surface by coating it with calcium phosphate (CaP) and CHAp to improve ossteoconductivity, biocompatibility and implant-hard tissue ossteointegration properties was chosen [9, 10, 17, 18]. Calcium hydroxyapatite has been used in dentistry since 1970s and in orthopaedics - since 1980s due to its chemical similarity to the inorganic component of bone matrix [2, 4, 19]. Bone grafts substituted with CHAp showed greater advantages in clinical application compared to allografts or uncoated metallic implants [4, 5, 20]. The main advantages of CHAp are its biocompatibility, osteoconductivity, osteoinductivity and biodegradability with host tissue [4, 9, 21, 22]. However, pure sintered CHAp was determined to have low resorption rate, and in some cases it might provoke complications due to mechanical mismatch between CHAp and bone.

The aim of this doctoral work was to fabricate calcium hydroxyapatite thin films on quartz, silicon and titanium substrates using aqueous sol-gel method. The syntheses of calcium hydroxyapatite thin films on different substrates using sol-gel method for medical application are relatively new, because there are not much scientific data on the synthesis of calcium hydroxyapatite thin films from aqueous solution. The main attention and many publications are focused on syntheses of calcium hydroxyapatite powders.

The main objectives of the dissertation are the following:

1. Development of an aqueous sol-gel synthesis route for the production of calcium hydroxyapatite ($Ca_{10}(PO_4)_6(OH)_2$; CHAp) thin films on titanium substrate using dip-coating and spin-coating techniques.
2. Development of an aqueous sol-gel synthesis route for the production of calcium hydroxyapatite ($Ca_{10}(PO_4)_6(OH)_2$; CHAp) thin films on silicon substrate using dip-coating and spin-coating techniques.
3. Development of an aqueous sol-gel synthesis route for the production of calcium hydroxyapatite ($Ca_{10}(PO_4)_6(OH)_2$; CHAp) thin films on quartz substrate.

4. Investigation of calcium hydroxyapatite thin films fabricated on silicon substrate using FTIR spectroscopy.
5. Comparison of obtained results of CHAp coatings on different substrates using two preparation technique, such as dip-coating and spin-coating processing.

2. Literature Review

2.1. Calcium compounds in human bone

Bone is one of the most important biological structures which consists of organic and inorganic phase with highly hierarchical structure [23]. The structure of the Ca-P solid phase in bone was first identified using chemical and X-ray diffraction analyses data by *de Jong* in 1926 as a crystalline calcium phosphate similar to geological apatite [24]. Bones are natural composite materials, where one of the main components is an inorganic component carbonated hydroxyapatite ($Ca_{10}(PO_4)_6(OH)_2 \cdot CaCO_3$), in bone literature used under name dahllite [23, 25–28]. The inorganic part of the bone constitutes about 65% of bone mass and the remaining part is made up of 25% of organic component (collagen) and 10% of water [25, 26, 29]. Inorganic and organic parts of bone are closely related. Bone apatite crystals are irregularly shaped platelets, nanometer sized crystals with an average length of 50 nm, 30-45 nm in width and thicknesses of just 2-5 nm, oriented in their *c* axis parallel to one another and scattered in the collagen fibrils.

Moreover CHAp has some very important incorporation of impurities, such as ionic carbonate, sodium and magnesium ions (4–6% carbonate; 0.9% Na; 0.5% Mg) [25, 26, 30, 31]. Carbonate in the apatite influences dissolution of apatite mineral and plays significant role in biological process such as bone resorbtion. It has been mentioned in literature that all synthetic or natural carbonate-containing phosphates have been found to either have an apatitic structure or to be amorphous [32]. In bone apatite, carbonate can be found in two anionic sites of structure. Carbonate ions occupying monovalent anionic (OH^-) sites are generally designated as type A, and carbonate ions in trivalent anionic sites (phosphate) - as type B [32, 33]. The B-type carbonated apatite is mostly found in bone, with A/B ratio in the range of 0.7-0.9. The higher value of the A/B ratio was observed in old tissue than that in young one [34]. B-carbonated apatite showed decreased crystallinity and also increased solubility in both in vitro and in vivo tests. However, the surface of A-type carbonated

calcium hydroxyapatite has lower affinity for bone cells osteoblasts leading to lower cell attachment and collagen production, which was attributed to decrease polar component of the surface of the A-carbonated biomaterial [34]. It has been shown that pure A-type $Ca_{10}(PO_4)_6(OH)_2$ does not occur in natural apatite. There is always some ions of F^- present [35]. Moreover, in addition to the mentioned inorganic ions, bone mineral also contains various quantities of fluoride, chloride, strontium, zinc, copper and iron [33, 36]. All these elements affect bone mineral characteristics, such as crystallinity, mechanical properties and degradation behaviour. Actually, the Ca/P ratio ranges from 1.37 to 1.87 in natural bones, indicating that natural minerals can contain additional ions, such as strontium, zinc, carbonate and etc. [5, 37]. Systematic studies by X-ray diffraction analysis, infrared spectroscopy and chemical analysis led to the conclusion that biological apatite should be expressed by formula $(Ca,Na,Mg)_{10}(PO_4,HPO_4,CO_3)_6(OH,Cl,F)_2$ (compared to pure calcium hydroxyapatite, CHAp, $Ca_{10}(PO_4)_6(OH)_2$) [30]. Composition of inorganic phase of adult human bone is summarized in Table 1 [38, 39] .

Table 1. Compositional values of inorganic components of adult human bone.

Component	Bone	CHAp
Calcium [wt.%]	34.8	39.6
Phosphorus (as P) [wt.%]	15.2	18.5
Ca/P (molar ratio)	1.71	1.67
Sodium [wt.%]	0.9	
Magnesium [wt.%]	0.72	
Potassium [wt.%]	0.03	
Carbonate (as CO_3^{2-}) [wt.%]	7.4	
Fluoride [wt.%]	0.03	
Chloride [wt.%]	0.13	
Pyrophosphate,(as $P_2O_7^{4-}$) [wt.%]	0.07	
Total inorganic [wt.%]	65	100
Total organic [wt.%]	25	
Water [wt.%]	10	
a axis [Å][a]	9.41	9.430
c axis [Å][a]	6.89	6.891
Crystallinity index, (CHAp=100)	33-37	100
Typical crystal size [nm]	50x25x4	200-600

Ignition products (800 °C)	CHAp + CaO	CHAp
Elasticity modulus (GPa)	0.34-13.8	10
Compressive strength (MPa)	150	100

[a] Lattice parameters: ±0.003 Å.

Bone is a dynamic tissue, which is constantly remodeling and self-repairing, therefore small size and non-stoichiometry of crystals lead to mineral phase with solubility needed for bone cell osteoclasts. The mineral phase of bone consists of two calcium phosphate pools that coexist; an amorphous component and a poorly crystallized component resembling hydroxyapatite [40]. During the bone formation process, other calcium phosphate compounds are also observed. One group of researchers argued that CHAp crystals formed via the traditional solution crystallization process (nucleation and growth), while a handful of others pointed to the deposition of an amorphous calcium phosphate (ACP) precursor [26, 37]. If ACP is allowed to remain in contact with water (as a slurry) at pH values above 7 a transformation to hydroxyapatite occurs (process is autocatalytic) [40]. Under in vitro conditions, amorphous calcium phosphate is transformed into intermediate phases such as octacalcium phosphate (OCP) and β-tricalcium phosphate (β-TCP), which transform to most thermodynamically stable phase of hydroxyapatite; at lower pH values, the intermediate phase seems to be dicalcium phosphate dihydrate (DCPD) [25, 26, 37, 38]. The transformation of ACP to CHAp involves the following three basic steps: 1) the dissolution and hydration of ions from the solid ACP surface; 2) the movement of these hydrated ions from the surface of the ACP and 3) the nucleation and subsequent growth of CHAp crystals [19]. Solution pH, temperature and composition are the main factors influencing the formation of different types of calcium phosphates in biological and synthetic systems. Calcium phosphates can transform from one form to another depending on solution pH in biological environment. For example ACP, DCPD and OCP transform to CHAp in neutral and basic pH presenting HCO_3^- or CO_3^{2-} or to Mg-substituted tricalcium phosphate $(Ca,Mg)_3(PO_4)_2$ (β-TCMP or Mg-TCP) in acid, neutral or basic pH in presence of Mg^{2+} ions, or (F,OH)-

apatites in presence of F^- ions [30].

Some transformations in bone composition occur as a result of ageing. Young bone has lower crystallinity than a matured bone (the bands in infrared spectra generated by bone crystals are broadened and overlap [32]), moreover, an increase of calcium content, a decrease of HPO_4^{2-} and growth of the Ca/P ratio in bone mineral have been observed with age [39, 41].

2.1.1. Structure and composition of natural bone

Bone and cartilage constitute the skeletal system, which performs two main functions. The first function is a structural function, which is to support and protect vital organs, bone marrow and muscle attachment. The second function is an important metabolic function, which is serving calcium and phosphate ions needed for maintenance of serum homeostasis by contributing to buffering changes in hydrogen ion concentration [38, 42, 43]. Genes are responsible for processes of cellular differentiation, which firstly establish pattern skeletal system of cartilage and finally, in latter stages, replace them with bone through the differentiation of osteoblasts [42].

The following are possible bone structures: macrostructure (cortical and trabecular bone); microstructure (Haversian systems, osteons, single trabeculae); the sub-microstructure (lamellae); nanostructure (fibrillar collagen and embedded mineral) and sub-nanostructure (molecular structure of constituent elements, such as mineral, collagen, and non-collagenous organic proteins) (see Fig. 1).

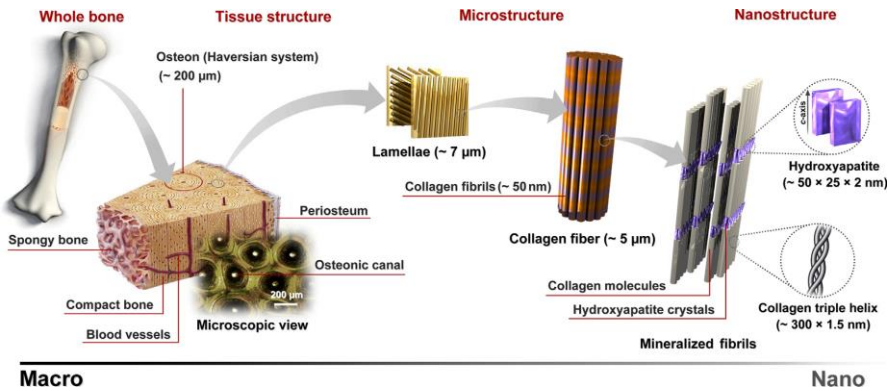

Fig. 1. Hierarchical structural organization of bone [44].

Two types of normal mature human bone macrostructure have been observed, namely, cortical and trabecular [38, 42, 44–46]. Although macroscopically and microscopically they are different, their chemical composition is identical. Cortical bone makes up 80% of skeleton and is dense and compact with high resistance to bending and torsion. Cortical bone constitutes the entire outer part of skeletal structures. The major part of cortical bone is calcified, and its main function is to provide mechanical strength and protection, but also it can participate in metabolic process during prolonged mineral deficit. Trabecular bone constitutes 20% of skeletal mass and as much as 80% of bone surface, because it is very porous. The diameter of pores may range from few micrometers to millimeters. Trabecular bone is lighter, less dense and more elastic, it is filled with a gel-like tissue known as bone marrow and performs many metabolic functions.

Bone has mineralized structure composed of biopolymer (mainly collagen), cells, vessels and crystals of calcium compounds (carbonated apatite, dahllite) [4]. Carbonated apatite is the principal mineral, which makes up 65% of natural bone. Organic matrix, which constitutes 25% of the natural bone, consist of proteins, type I collagen (90% of the organic matrix) with some non-collagenous proteins (e.g., proteoglycans), lipids and osteogenic factors (i.e., growth factors, such as bone morphogenetic proteins (BMPs), and vascular endothelial growth factors (VEGFs). Bone cells are called osteoblasts, osteoclasts, osteocytes and bone–lining cells. Bone collagen has a typical fibrous structure, the diameter whereof ranges from 100 to 2000 nm [45]. Collagen acts as a structural organic matrix where mineral crystals grow with a specific crystalline orientation. In Fig. 2 are showed how mineral crystals are assembled with collagen fibrils.

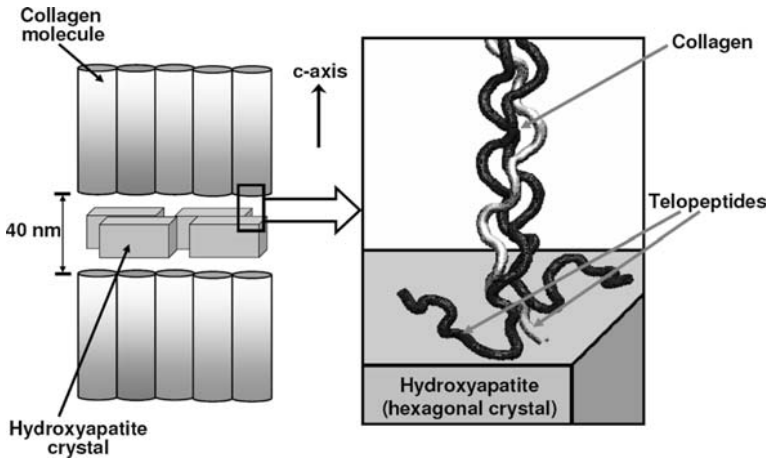

Fig. 2. CHAp connection with collagen [47].

2.1.2. Properties of natural bone

The main function of biological apatite is to provide toughness and rigidity to the bone, whereas collagen provides tensile strength and flexibility. Minerals bind to collagen through non-collagenous proteins, which make up about 3-5% of the bone, and through active sites for biomineralization and cellular attachment [48]. The remaining 9% of the mass consists of water, which is also very important for cells and for mechanical properties of the bone, such as plasticity [30, 39, 45, 46]. In addition to the above-mentioned constituent parts, other very important ions (such as carbonate, citrate, sodium, magnesium, fluoride, chloride and potassium) form the bone structure, which influence mechanical properties of the bone and affect proper functioning thereof [46, 47].

All these components form the smallest structural blocks of bone structure, which are repeated several times for functional bone. Hierarchical structures serve many biological functions, such as mechanical support for cells, and many promotional and regulatory cellular functions, such as cell adhesion, proliferation, differentiation, and vascularization in physiological environment [49]. Mechanical properties depend on hierarchical structure at all levels of the bone. The size, shape, orientations and arrangements of crystals in collagen fibrils regulate mechanical functions in the bone [49].

Bone cells, namely, osteoblasts, osteocytes, osteoclasts and bone-lining cells, are responsible for the bone formation process. This process is initiated by the action of osteoblasts, special cells that synthesize and release collagen matrix in the form of a jelly substance, and the osteoids, which are subsequently mineralized by controlled deposition of calcium phosphate [46, 49]. Osteoblasts do not function individually and are found in clusters along the bone surface; they are responsible for mineral diffusion in and from the bone [42, 46]. Osteoblasts remain trapped inside the mineral phase, evolving towards osteocytes, which are responsible for bone formation activity [42]. Osteocytes are responsible for maintaining the bone and function as transporting agents of minerals between the bone and blood [45]. Collagen and matrix proteins are responsible for apatite nucleation and inhibition or modulation of apatite crystals growing, while osteoclasts are responsible for bone destruction process [50]. This dynamic process of bone formation and destruction is very important for its growth during the development stages of the body, preserving its shape and consistency, and enabling its regeneration in case of fracture [25]. It also forms storage and hauling mechanisms for two very important elements, namely, calcium and phosphorus, which acts as storages in bones. All these processes must be well-balanced to maintain the bone healthy.

During the bone formation process, the primary and secondary stages are observed with different bone structures and different formation mechanisms. Epyphysial cartilage, which is a primary bone formation stage, is a combination of ground substance and very loose fine (10-20 nm) fibril bundles of collagen. There is also a high occurrence of matrix vesicles, which deliver either crystals or a high concentration of ions to the mineralization front. Mineralization is rapid and unorganized, forming woven bone microstructure. In this stage, crystals do not form close connection with collagen. Clusters of calcium hydroxyapatite form within the proteoglycan matrix, which then form calcification nodules or calcospherites due to the arrangement of crystal clusters. In this stage, collagen found in cartilage has been observed; it acts as

mineral deposition therein and does not play any significant role in direct mineralization process [26].

In the secondary bone formation process, the primary woven bone is remodeled into a more optimal structure, such as parallel–fibered or lamellar bone, which is organized into concentric lamellae (3-8 lamellae) that make up osteons of the Haversian canal system in humans [46]. Osteon looks like a 200-250 μm cylinder, which is almost parallel to the long axis of the bone [46]. Collagen fibrils in the secondary bone are secreted by osteoblasts; they are larger than those in the primary bone, with a mean diameter of 78 nm, and are closely packed in lamellar structure. Non-collagenous proteins (NCPs), many of which are highly charged from carboxylated groups of aspartic and glutamic acids and phosphate from phosphoserine, are near mineralization sites [26]. Also NCPs plays an important role in the mineralization process. During the bone formation process, mineral crystals are orientated by collagen fibrils within which they form. Crystals are very small, just few unit cells thick and they would be termodinamically unstable if they would not be embedded into organic matrix [26].

Bone functions depend on very important physicochemical properties, such as interconnecting porosity, biodegradability, bioactivity, osteoconductivity and osteoinductivity. Porosity is a very important bone property, because it allows body fluids and cells to access various regions of the osseous tissue [39]. Pore size ranges from 10 to 50 μm and from 100 to 300 nm in cortical bone, and from 200 to 600 μm in trabecular bone. The size and interconnection of bone porosity is essential for vascularization, diffusion of nutrients and cells, and tissue ingrowths. Bone structure and composition allows cell attachment, migration, proliferation and differentiation, promoting bone formation, repair and regeneration [30]. Osteoconductivity allows the bone to repair and regenerate itself [41].

Lipids, which account for about 2%, play an important role in the biomineralization process, which starts in only 10 days after the collagen matrix is laid-down [45].

Hierarchical structure and composition of the bone leads to strength mechanical properties [48, 50]. Mechanical properties differ depending on its location in the skeletal system [46]. This is due to different functions of bones in daily activities. Mechanical properties depend on bone components: mineral crystals, collagen and water. Bone contains about 9% of water and with the loss of water bone exhibits different mechanical properties. Tensile strength, stiffness and hardness were observed to increase with the loss of water. Dry bone exhibits lower anelastic deformation compared to wet bone, which indicates that water has a significant effect on mechanical properties of the bone [47]. Elastoplasticity, viscoelasticity and viscoelasticity – plasticity have been used to determine bone's mechanical properties [51]. Elastic properties of bone minerals depends on purity of calcium hydroxyapatite due to vacancies and substitutions in the natural crystals [46]. Table 2 lists biomechanical properties of bone.

Table 2. Biomechanical properties of bone [45].

Properties	Measurements	
	Cortical bone	Trabecular bone
Young's modulus (GPa)	14-20	0.05-0.5
Tensile strength (MPa)	50-150	10-20
Compressive strength (MPa)	170-193	7-10
Fracture toughness (MPa $m^{1/2}$)	2-12	0.1
Strain to failure	1-3	5-7
Density (g/cm^3)	18-22	0.1-1.0
Apparent density (g/cm^3)	1.8-2.0	0.1-1.0
Surface/bone volume (mm^2/mm^3)	2.5	20
Total bone volume (mm^3)	1.4×10^6	0.35×10^6
Total internal surface	3.5×10^6	7.0×10^6

2.2. Synthetic calcium phosphates

Calcium hydroxyapatite has received great attention in industry and medical application fields [25]. CHAp and TCP bioceramics are used as fillers, spacers and bone graft substitutes to repair and for reconstruction of diseased or damaged parts of human bones because of their biocompatibility, bioactivity,

non-toxicity, non-inflammatory behaviour, non-immunogenicity, stability under physiological environment and osteoconduction characteristics with respect to host tissue [52–57]. To date, calcium phosphate biomaterials have been widely used clinically in the form of powders, granules, dense and porous blocks and various composites [58]. Nanophase CHAp properties, such as surface grain size, pore size, wettability, etc., could control protein interactions (for example, adsorption, configuration and bioactivity) thus modulating subsequent enhanced osteoblast adhesion and long-term functionality [58, 59]. CHAp particles can be used as adsorbents in chromatography to separate proteins and enzymes, catalysts for dehydration and dehydrogenation of alcohols, methane oxidation, artificial teeth and bones; also, CHAp is of great interest in the industry of fertilizers and pharmaceutical products, water treatment processes [53, 60–66]. CHAp is the most stable and least soluble (K_{sp} value are around $2.9 \cdot 10^{-58}$ over the pH ranges of 3.5 to 9.7) of monophasic calcium phosphates [67]. Bioactivity of CHAp depends on the morphology, particle size and phase purity of CHAp, which are influenced by synthesis route [55, 57, 68–70]. The calcium-deficient hydroxyapatites (CDHAp) are of greater biological interest than stoichiometric calcium hydroxyapatite [71]. It has been suggested that CDHAp play an important role in several processes, such as bone remodeling and bone formation. Schematic view of hydroxyapatite application is represented in Fig. 3 [72].

Biphasic calcium phosphates (BCPs) are very important mixtures of calcium hydroxyapatite and tricalcium phosphate. BCPs ceramics combine low solubility and osteoconductivity of apatite with the osteoinductivity of a more soluble phase, such as β-TCP [67]. Monophasic stoichiometric CHAp has a limited ability and interfaces with new bone tissue and also can limitedly stimulate development of new bone tissue [71]. In contrast β-TCP-based bone substitute materials have a fast degradation rate, which may lead to clinical implant failure due to their inadequate osteoconductive properties [73].

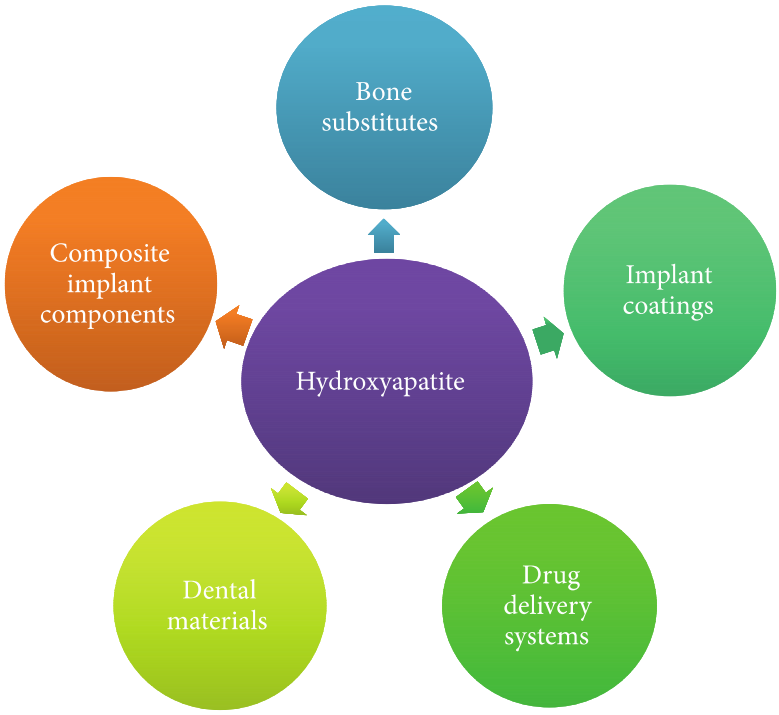

Fig. 3. Schematic view of application of calcium hydroxyapatite.

Therefore the focus was placed on more soluble calcium phosphates, from CHAp to biphasic calcium phosphates (CHAp and β-tricalcium phosphate mixtures (β-TCP; β-$Ca_3(PO_4)_2$)), β-TCP, α-tricalcium phosphate (α-TCP; α-$Ca_3(PO_4)_2$), octacalcium phosphate (OCP; $Ca_8H_2(PO_4)_6 \cdot 5H_2O$), anhydrous dicalcium phosphate (DCP; $CaHPO_4$) and dicalcium phosphate dihydrate (DCPD; $CaHPO_4 \cdot 2H_2O$) [70, 71].

Surface layers of TCP enhance bonding with adjacent host bone. This stimulates osteoclastic resorption and osteoblastic new bone formation within the resorbed implant [1, 19]. Whereas CHAp, β-TCP, α-TCP and OCP are mostly resorbed by osteoclasts, DCPD and possibly DCP may be resorbed by a simple dissolution [2]. BCPs may be produced physically mixing CHAp and β-TCP, or chemically by sintering calcium-deficient apatites at high temperatures resulting in mixture of two different phases. Specific chemical properties of BCPs depend on CHAp and β-TCP content in the mixture [21].

2.2.1. Structural features of calcium hydroxyapatite

CHAp has hexagonal $P6_3/m$ crystal structure, however stoichiometric and perfectly pure CHAp can crystallize in the monoclinic system [72, 74, 75]. The monoclinic form was discovered much later than the hexagonal form. The space group for stoichiometric monoclinic CHAp is $P2_1/b$ with unit cell parameters of a=9.421 Å, b=2a, c=6.881 Å and $\gamma=120^o$ [76]. The unit cell parameters of hexagonal crystal cell are a = b = 9.432 Å, c = 6.881 Å and $\gamma=120^o$. The overall XRD patterns of hexagonal and monoclinic CHAp are almost identical; however the pattern of monoclinic CHAp has additional weak lines the intensities whereof are less than 1 % of the strongest hexagonal CHAp line [74].

Important structural features of stoichiometric hydroxyapatite are its structural hydroxyl groups arranged at the edges of unit cells, forming the columns –OH–OH–OH— (see Fig. 4.) [25].

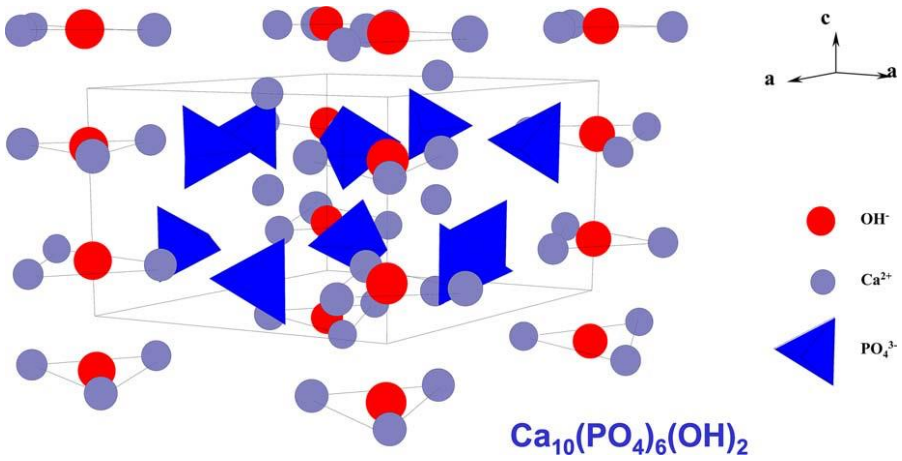

Fig. 4. Structure of calcium hydroxyapatite.

Oxygen atoms of these groups are spaced in such a way that they are unable to form hydrogen bonds. Hydroxyapatite includes two types of calcium cations referred to as Ca (I) and Ca (II). The atoms of calcium Ca (I) are located at the edges of a hexagonal unit cell, while the atoms of calcium Ca (II) form equilateral triangles with the column of structural hydroxyl groups in the middle. Phosphate ions are the largest ions that build unit cells and determine

their structure [72, 76]. Fig. 5. presents structure of calcium hydroxyapatite to crystallographic c and a axis, showing the OH^- channels and the different types of Ca ions [22].

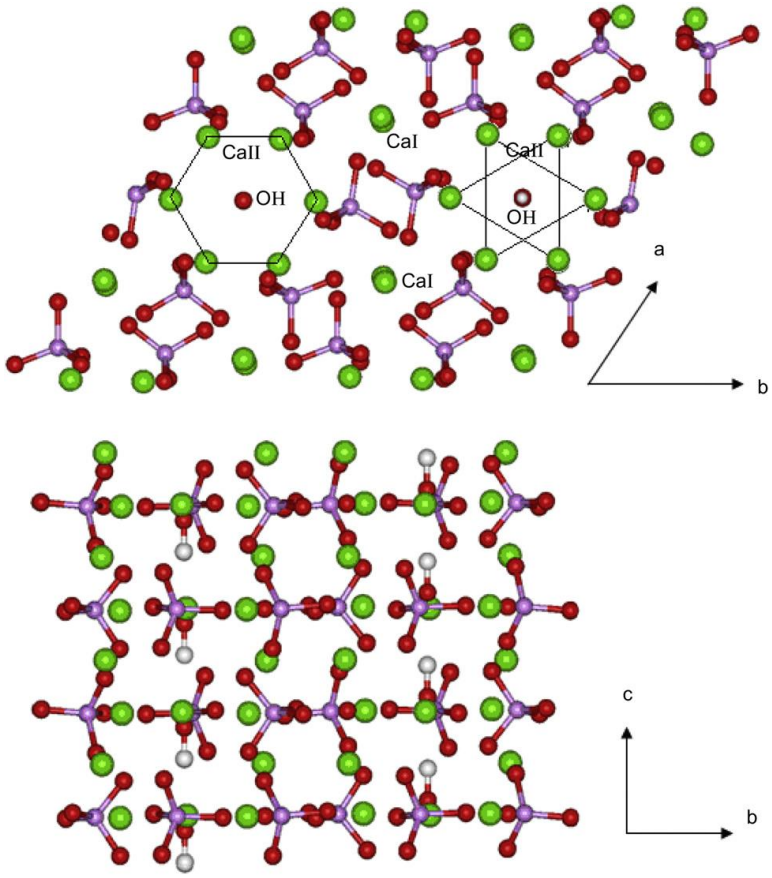

Fig. 5. Structure of calcium hydroxyapatite to crystallographic c and a axis, showing the OH^- channels and the different types of Ca ions (Ca-green; O-red; P-purple; H-white).

The arrangement of phosphate ions in the crystal structure is such as to provide the channel structure wherein calcium atoms are located within two different surroundings, Ca (I) and Ca (II). Ca (I) one is parallel to the c-axes bounding nine oxygen atoms, i.e., 3 atoms in each of the positions O (1), O (2) and O (3). Ca (II) surroundings contain one O (1), one O (2), four O (3) and one OH^- ion. Ca (II) has a larger atomic radius than Ca (I). The substitution of carbonate group occurs either in the PO_4^{3-} position (for the B type of apatite) or in the OH^- position (for the A type of apatite) [57, 61, 77–79]. In Fig. 6. different types of Ca and oxygen ions arrangements in the structure are presented [80].

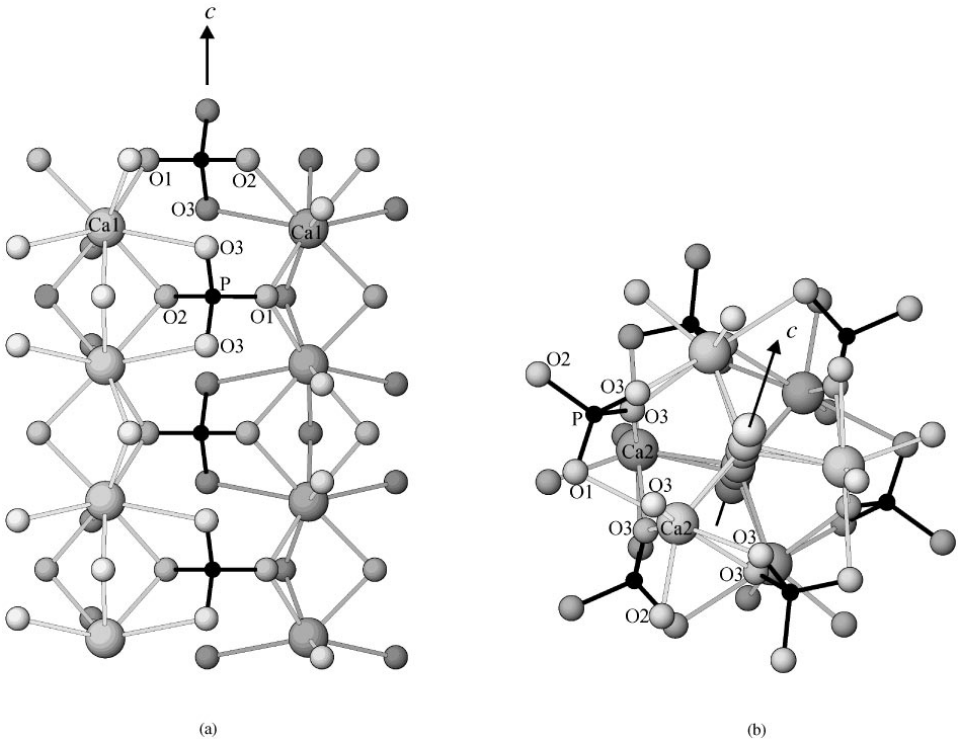

Fig. 6. Types of calcium polyhedra in the structure of apatite. (a) columns of ninefold coordinated Ca1 polyhedra and (b) triangles of sevenfold coordinated Ca2 polyhedra.

CHAp hexagonal structure possesses two different binding sites called C and P sites on the crystal surface, where proteins can be bind. After dispersing CHAp particles in aqueous media, calcium atoms (CaII) (C sites) are exposed on the CHAp surface by dissolution of OH^- ions at the particle surface. Therefore, the C sites are arranged on *ac* or *bc* crystal faces in a rectangular manner with the interdistance in the a or b directions equal to 0.943 nm and the interdistance in the c direction equal to 0.344 nm (c/2). The P sites are arranged hexagonally on the *ab* crystal face with a minimum distance of 0.943 nm. The C sites are rich in calcium ions or positive charges and thus bind to acidic groups of proteins, but the P sites are negatively charged and therefore attach to basic groups of proteins [61, 77–79].

An important aspect is that CHAp structure is so tolerant to ionic substitutions, because Ca sites can contain various divalent (Ca^{2+}, Mg^{2+}, Sr^{2+}, Cd^{2+}, Pb^{2+} and Ba^{2+}) and trivalent cations (Al^{3+}, Fe^{3+}) [53]. Small quantities

of some ions may cause changes/improvements in biological, physicochemical or mechanical properties [72, 81, 82].

2.2.2. Physical properties of calcium hydroxyapatite

Surface roughness, porosity, charge, solubility of CHAp, crystallinity and stoichiometry (e.g. calcium to phosphate (Ca/P) ratio) are very important for bioactivity, osteoconductivity and osteoinductivity [60, 67]. Bioactivity is a very important property of bioactive materials, because this property is due to ability to form a direct bond between tissues and the material resulting in a uniquely strong interface. Bioactivity is associated with the formation of bone apatite-like (carbonated calcium hydroxyapatite, CHAp) on surfaces of biomaterial [83]. Osteoconductivity is also a very important property, which allows cellular infiltration and attachment, cartilage formation and calcified tissue deposition in biomaterial [83]. Osteoinductivity is the ability of a material to recruit and induce progenitor or undifferentiated cells to differentiate towards the osteoblastic lineage [67]. Common markers of the osteoblastic phenotype include type I collagen, alkaline phosphatase (ALP), bone morphogenetic protein-2 (BMP-2), osteopontin (OPN), osteocalcin (OCN) and bone sialoprotein (BSP) [67].

Properties of calcium phosphates, which influence biological processes including protein adsorption, cell adhesion and cell differentiation are presented in Fig. 7 [17].

In recent years, great attention was placed on the fabrication of bioceramics with high level of porosity. The size and density of interpore connections are very important factors for osteoconduction into the porous of CHAp. Pore size, pore shape, pore interconnectivity and total porosity of the scaffold play a crucial role in successful tissue regeneration [4, 5, 10, 19]. Bone substitute materials have clinical success when they interact with tissue structures and cells, which interconnect into a macroporous (of diameter >100 μm) structure of bone substitute materials. Microporosity (of diameter < 10 μm) has been demonstrated to allow body fluid circulation, whereas macroporosity (of

diameter > 100 μm) - to provide a scaffold for bone cell colonization [83]. The optimal pore size must be larger than 50-100 μm or even 250-500 μm for penetration of bones and implant absorption [19, 52]. Moreover, pore size affects the biocompatibility of synthetic ceramics [19].

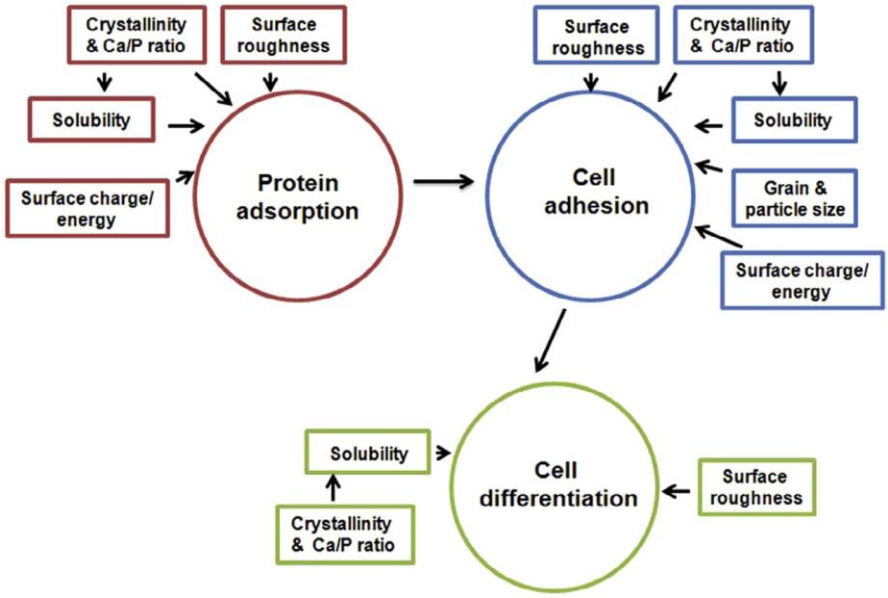

Fig. 7. Properties of calcium phosphates, which influence biological processes.

Lager pores size and lower macroporosity show greater ingrowth of biomaterial compared to bioceramics with smaller pore size and higher macroporosity [83]. Porosity of pores ranging from 20 nm to 500 μm was shown enhance protein adsorption significantly. CHAp particles with higher porosity and diameter of pores can adsorb more proteins than particles with lower porosity. In addition, a larger number of micropores was also shown to enhance the adsorption of proteins, such as fibrinogen and insulin, but not type I collagen [67]. In the review, Samavedi et al. mentioned some comparative studies on surface roughness, establishing that higher roughness of surface leads to better adsorption of proteins. Protein adsorption also depends on surface charge and solubility. Hydrophilicity or hydrophobicity is a very important property due to denaturation of proteins. A surface of higher hydrophilicity level is more desirable, because a better interaction with

biological fluids, cells, proteins and tissues has been observed compared to that of hydrophobic surface [7, 67]. Protein absorption on CPC can also be affected by electrostatic interactions with both cationic calcium sites and anionic phosphate sites; however, adsorption also depends on the structure of proteins.

Ionic strength and pH of the aqueous environment also affect protein adsorption. The solubility of CPCs (ACP > TCP > BCP > CHAp) may also influence protein adsorption by affecting the equilibrium ion concentration near the material surface [67]. Solubility constants are presented in Table 3 [17].

Table 3. Solubility of CPC and osteoconductivity.

CPC	Solubility (~K_{sp})	Ca/P ratio	Osteoconductivity
CHAp	Poor (10^{-58})	1.67	+
TCP	Fair (10^{-25}-10^{-29})	1.5	++
ACP	High (10^{-23}-10^{-25})	1.15-1.67	+++
BCP	Variable (dependent on TCP/CHAp ratio)	1.5-1.67	++++

Dissolution of BCP depends on CHAp/β-TCP ratio: a higher ratio leads to lower dissolution of bioceramics (see Fig. 8) [37].

Dissolution process also is affected by microporosity and macroporosity of bioceramics: decreasing crystal size and increasing microporosity and macroporosity lead to higher dissolution [83].

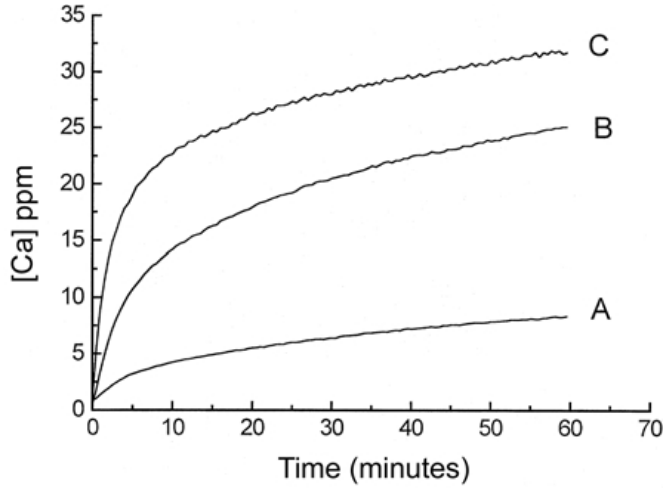

Fig. 8. Effect of CHAp/β-TCP ratios on the dissolution properties of BCP: the higher the ratio, the lower the extent of dissolution. Dissolution experiments conducted in 0.1 M KAc, pH 6, and 37 °C. The release of calcium ions to the acidic buffer was monitored using calcium-selective ion electrode. The CHAp/b-TCP ratios of the BCP samples: (a) 80/20; (b) 40/60 and (c) 20/80.

2.2.3. Synthesis methods

Composition, physicochemical properties, morphology and crystal sizes of synthetic calcium hydroxyapatite are very sensitive to the preparation conditions [84, 85]. Depending on synthesis methods and conditions impurities and additional products can be observed. For example, common impurity phases in synthetic apatites prepared by precipitation from supersaturated aqueous solutions are calcium phosphate compounds, such as amorphous calcium phosphates (ACP) with variable compositions of $Ca_3(PO_4)_{2-2x}(HPO_4)_{3x}\cdot nH_2O$, octacalcium phosphate (OCP), $Ca_8(HPO_4)_2(PO_4)_4\cdot 5H_2O$, and calcium hydrogenphosphate dihydrate (DCPD), $CaHPO_4\cdot 2H_2O$.

CHAp powders can be synthesized by solid state reaction, wet synthesis, precipitation, sol-gel and hydrothermal methods [44, 84–90]. A solid state reaction process is a relatively simple and chemically hazard free process, which can yield large amounts of material having desirable structure and properties [91]. This procedure relies on diffusion of ions among powder raw materials and thus requires high temperature processing (< 1250°C) to initiate

the reaction [92]. Solid state reaction requires high temperatures and a long heat treatment, but the products are well crystallized and stoichiometric. The solid state process has high reproducibility and low processing costs in spite of the risk of contamination during milling [93, 94]. Calcium and phosphorous compounds used as starting materials in the solid state reaction process are dicalcium phosphate anhydrous ($CaHPO_4$), dicalcium phosphate dihydrate ($CaHPO_4 \cdot 2H_2O$), monocalcium phosphate monohydrate ($Ca(H_2PO_4)_2 \cdot 2H_2O$), calcium pyrophosphate ($Ca_2P_2O_7$), calcium carbonate ($CaCO_3$), calcium oxide (CaO) and calcium hydroxide ($Ca(OH)_2$). Scheme of solid state process is presented in Fig. 9 [49].

The wet-chemical precipitation method was originally suggested in 1976 [85]. These precipitation methods are among most widespread techniques due to their simplicity, availability and the use of relatively inexpensive raw materials [92]. In application of this method, chemical reactions occur between calcium and phosphorus ions under controlled pH and temperature of the solution [95, 96].

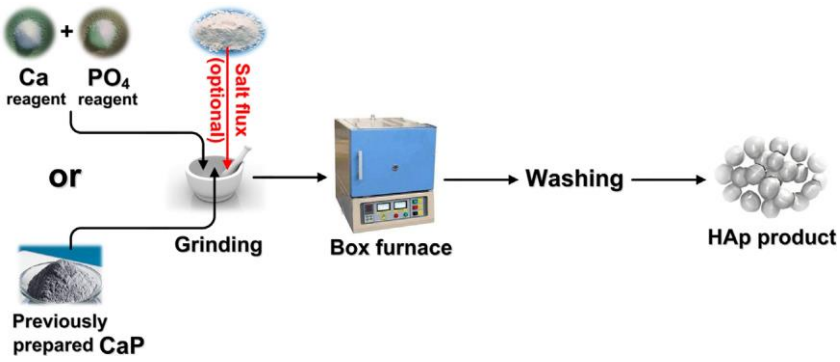

Fig. 9. Preparation of CHAp powder via solid-state method.

The precipitation method does not require high temperatures (temperatures stay below 100 °C), while high percentages of pure products and nanometric-size crystals can be obtained [85]. However, reactions require fine-tuning to optimize morphology and minimize crystal growth. Furthermore, a number of surfactants (e.g. PVA) or dispersants (e.g. ammonium polyacrylate,

ethanolamine) have been investigated with the aim of reducing particle agglomeration. After precipitation process powder is typically calcined at 400-600 °C (or even at higher temperatures) in order to obtain a stoichiometric apatite structure [96]. In some cases, a well-crystallized CHAp phase was only developed while approaching a sintering temperature of 1200 °C [92, 95, 96]. In application of this method, many factors influence the properties of hydroxyapatite, such as starting materials, pH, stirring speed, temperature, ageing time, etc. [85, 92, 95]. For example, fast precipitation process leads to chemical inhomogeneity in the final product, however slow titration and dilution processes must be used to improve chemical homogeneity and stoichiometry of the resulting CHAp [95, 96]. Scheme of wet precipitation method is presented in Fig. 10 [49].

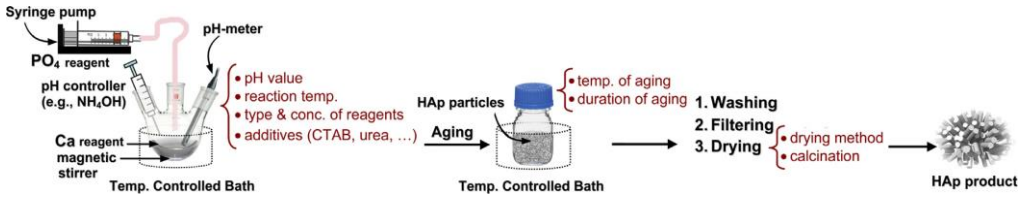

Fig. 10. Preparation of CHAp nanoparticles via chemical precipitation.

Hydrothermal synthesis offers a relatively simple and effective way to prepare a high degree of crystallinity, with a Ca/P close to the stoichiometric value and well-dispersed CHAp nanoparticles [84, 97]. Hydrothermal processing can be defined as any heterogeneous reaction in the presence of aqueous solvents or mineralizers under high pressure and temperature conditions to dissolve and recrystallize (recover) materials that are relatively insoluble under ordinary conditions [98]. Hydrothermal process occurs often using water as a solvent (with precursor soluble ions) and heating it in a sealed vessel [92]. Additives, such as ethylenediaminetetraacetic acid (EDTA), cetyltrimethylamonium bromide (CTAB) and poly(amido-amine) (PAMAM) are utilized to modify morphology of CHAp nanoparticles during hydrothermal synthesis [97]. Temperature of the solvent can increase up to a boiling point, and then autogenous pressure occurring within the vessel exceeds the ambient

pressure. It is very important to choose the optimal pH value of reaction and hydrothermal temperature and also duration of hydrothermal treatment, because these factors affect CHAp morphology and particle size (Fig. 11.) [44, 99].

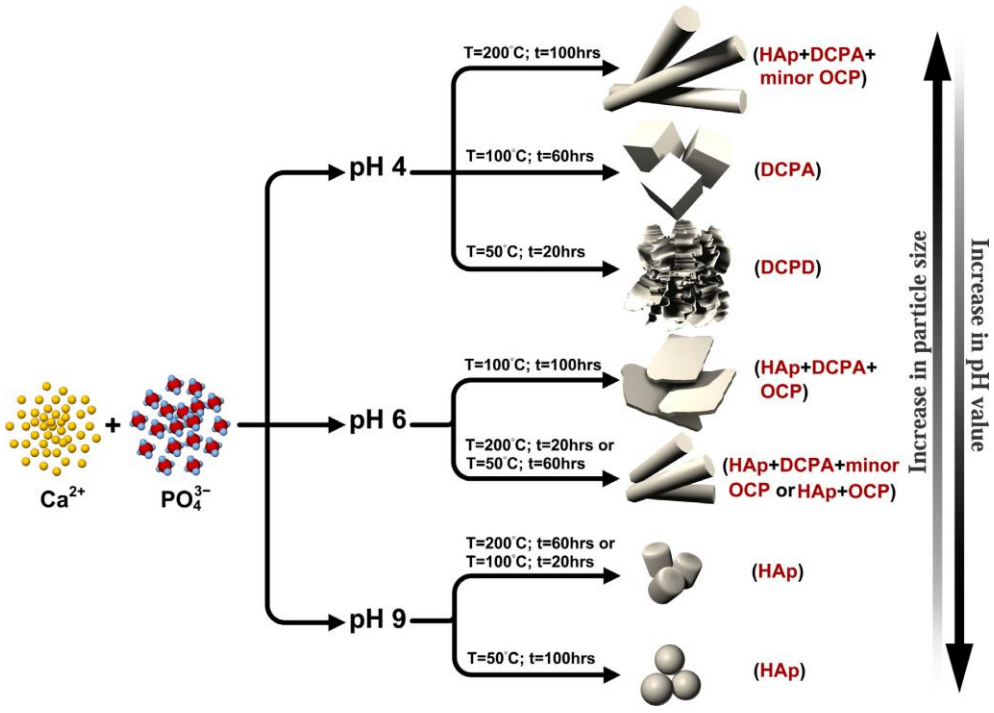

Fig. 11. Effect of pH, temperature, and duration of hydrothermal treatment on phase, morphology and particle size of the CaP powder.

These methods can be performed at substantially lower temperatures. The main difference compared to other low temperature methods such as wet chemical precipitation and sol-gel synthesis is the required post heat treatment to crystallize the CHAp, whereas crystalline CHAp can be produced in one step via hydro- and solvothermal synthesis. The main disadvantages of this method include the use of a limited size reaction vessel and complex equipment. Microwave-hydrothermal method enables the synthesis of the ultra-fine and high purity powders for shortening working time. This method has some advantages, such as heating throughout the media, rapid heating, fast reaction, high yield, excellent reproducibility, narrow particle distribution, high purity and high efficient energy transformation [100, 101].

The sol-gel method is a very attractive technique to produce ultra-fine and pure ceramic powders, fibers, coatings, thin films and porous membranes under mild conditions [96, 102]. This method is treated as a promising way for convenient synthesis because of few facilities used, high output and easily controllable operation processes [103, 104]. The sol-gel reaction occurs under low temperature in molecular mixing level of calcium and phosphorous precursors resulting in high purity, crystallinity, homogeneity and thermal stability of CHAp [58, 87, 95, 105]. This process allows forming fine-grain microstructure containing a mixture of nano-to-submicron particles with crystalline structure [106]. Advantages of the sol-gel process are the following: (a) the ability to produce high purity material; (b) the ability to change physical characteristics, such as pore size distribution and pore volume; (c) the ability to vary compositional homogeneity at a molecular level; (d) the ability to introduce several components in one step and (e) the ability to produce samples in different physical forms [102, 103, 107]. The synthesis of CHAp in application of the sol–gel method requires a correct molar ratio of 1.67:1 between Ca and P in the final product [106]. Fig. 12 presents a common structure of sol-gel process [103].

Different starting materials can be used to synthesize CHAp using different fabrication methods (Table 4).

CHAp crystals synthesized using sol-gel method are very efficient to improve the contact and stability at the artificial/natural bone interface observed in in-vitro and in-vivo environments [106].

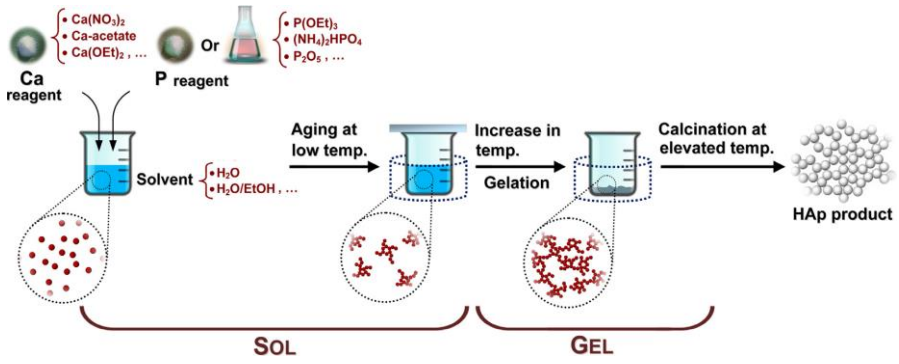

Fig. 12. CHAp synthesis process via sol-gel method.

Table 4. Precursors used to synthesize CHAp powders.

Ca precursor	P precursor	Method	References
$Ca(NO_3)_2$	$(Na)_2HPO_4$	Hydrothermal	[97]
$Ca(OH)_2$	$CaHPO_4{\cdot}2H_2O$ H_3PO_4		[99, 101]
$Ca(NO_3)_2{\cdot}4H_2O$	$NaH_2PO_4{\cdot}2H_2O$ $(NH_4)_3PO_4$ $(NH_4)_2HPO_4$		[82, 108, 109]
$CaCl_2$	cytidine 5'-triphosphate disodium salt (CTP)	Microwave-assisted hydrothermal	[100]
$Ca(NO_3)_2{\cdot}4H_2O$	$(CH_3O)_3P$ $NH_4H_2PO_4$ $P(C_2H_5O)_3$ P_2O_5	Sol-gel	[96, 102, 104, 106, 107, 110]
$Ca(OH)_2$	2-ethylhexyl-phosphate		[102]
$CaCO_3$	$Ca_2P_2O_7$	Solid-State	[111]
$Ca(NO_3)_2{\cdot}4H_2O$	$(NH_4)_2HPO_4$	Wet precipitation	[58, 84, 85, 88, 112]
$Ca(OH)_2$	H_3PO_4 $(NH_4)_2HPO_4$		[58, 102]

2.3. Thin films of calcium hydroxyapatite as bone graft materials

Metallic biomaterials, such as stainless steel, cobalt-based alloy, titanium and its alloys are widely used as artificial hip joints, bone plates and dental implants due to their excellent mechanical properties, high tensile strength, high yield strength, resistance to cyclic loading (fatigue), resistance to time dependent deformation (creep) as well as corrosion resistance and endurance [113–115]. However, there are some problems with metallic implants due to corrosion and release of ions in biological fluids after implantation, which leads poor implant fixation or even rejection of implant due to a lack of properties, such as osteoconductivity and osteoinductivity, and infections due to bacterial adhesion and colonization at the implantation site [113, 116, 117]. For example, unmodified titanium is prone to bacterial infections that may eventually lead to inflammation and destructive failure of the implant [118].

To overcome these surface problems, surface modification was established, including chemical treatment, physical and biological methods [113].

In the 1980s, de Groot et al. published their work on the development of plasma-sprayed hydroxyapatite implants. At the same time, Furlong and Osborn, two leading surgeons in the orthopaedics field, began implanting plasma-sprayed stems in patients [20, 119, 120]. In fabricating bioceramics for medical implants restoring hard tissue, the main attention has been placed on mechanical properties, design and biocompatibility [114]. Calcium hydroxyapatite thin films are currently used as biomaterials for many applications in both dentistry and orthopaedics, because they form a real bond with the surrounding bone tissue after implantation, therefore prolongs the lifetime of prostheses [117, 121–125]. Due to poor mechanical properties (brittle and break easily) of CHAp, it cannot be used for load-bearing implants, therefore CHAp was coated on titanium substrate and its alloys to combine mechanical performance of the metallic and the bioactivity of CHAp [117, 119, 121, 126–132]. Clinical results showed that implants coated with calcium hydroxyapatite have much longer life times after implantation than uncoated devices, and they have been found to be particularly beneficial for younger patients [20, 119]. Moreover, Eulenberger et al. determined that a period of time of about 100 days was needed for recovery after the implantation of a metallic implant, however this time can be reduced to only 20 days through the use of hydroxyapatite (CHAp), leading to rapid bond development between CHAp and the surrounding bone tissue [133]. The main reason of using CHAp coating on metallic substrates is to keep mechanical properties of metal, such as load-bearing ability, and at the same time to take advantage of the coating's chemical similarity, osteoconductivity and biocompatibility with the bone, allowing direct bone formation across its surface by attachment, proliferation and differentiation of bone- forming cells [117, 123, 132, 134–139]. Implants can be made in different shapes, such as plates, rods, screws and pins, depending on site of their implantation [117].

The main disadvantage of CHAp implants is the rate of bone bonding after implantation, which is relatively low compared to bioactive glasses and glass ceramics. Therefore the suggestion was made to incorporate in the structure additional elements, which are found in physiological bone, for a faster integration after implantation. Incorporated ions (such as magnesium, silicon, fluorine and carbonate) affect the dissolution rate of apatites, and this has been shown to enhance the proliferation of human osteoblast-like cells in vitro and to encourage osseointegration [119, 140–142].

2.3.1. Substrates

Medical implants are usually made of commercially pure titanium or titanium alloys (a+b alloys, Ti–6Al–4V, Ti–Al– Nb and b-Ti alloys), cobalt-based alloys (Co–Cr–Mo, Co–Ni–Cr–Mo, Co–Cr–W–Ni), stainless steel (primarily type 316L), Ni–Ti alloys, Au-based materials, and Ag–Sn alloys [1, 10, 11, 114, 136, 143–145]. Other substrates to improve properties of implants, adhesion between coatings and substrates, quality of CHAp coatings, also to simplify equipment and find the fastest and cheapest method to develop bone and dental implants were also developed and investigated: quartz and glass [146–148], silicon [148, 149], MgO [148], NiTi [150], Mg and its alloys [151–156], alumina and zirconia [157], and polymers [158].

Historically, the most popular metal has been titanium and its alloys due to their superior mechanical properties, such as tensile strength and fatigue strength, chemical stability, corrosion resistance and biocompatibility under in vivo conditions [1, 9, 17, 18, 114, 117, 128, 159–165]. Titanium as a pure metal was implanted into laboratory animals for the first time in 1940 [114]. Commercially pure titanium (cpTi) has various degrees of purity (graded from 1 to 4). This purity is characterized by oxygen, carbon and iron content. Most dental implants are made of grade 4 cpTi as it is stronger than other grades. Titanium alloys are mainly composed of Ti6Al4V (grade 5 titanium alloy) with greater yield strength and fatigue properties compared to pure titanium [7]. The two most commercially used specifications for implants are pure Ti (ASTM

F67) and Ti–6Al–4V (ASTM F136) [166]. Pure titanium can be used when primary importance of implant is corrosion resistance, however Ti–6Al–4V (ASTM F136) is an alpha–beta alloy, the microstructure, mechanical behaviour and chemical stability whereof depend on the type of heat treatment and mechanical working [114]. Mechanical properties of Ti-based metallic materials are presented in Table 5 [114].

Table 5. Mechanical properties of Ti-based metallic materials.

Alloy designation	Elastic modulus (GPa)	0.2% offset yeld strength (MPa)	Ultimate tensile strength (MPa)	Elongation (%)
Pure Ti	102-110	170-480	240-550	15-24
Ti–6Al–4V	110	860	930	10-15
Ti–6Al–7Nb	105	795	860	10
Ti–13Nb–13Zr	79-84	836-908	973-1037	10-16

Stainless steels are iron based alloys with a minimum of 10.5% Cr as an alloying element needed to prevent the formation of rust. Stainless steel (18Cr–8Ni) was first used in orthopaedic surgery in 1926. For implant applications they must have the resistance to pitting and crevice corrosion from body plasma [114]. 316L stainless steel is biocompatible and has been used for many decades as a permanent surgical implant material due to its lower cost, excellent fabrication properties, good corrosion resistance and availability [145].

Cobalt-based alloys are most commonly used representative Co alloys for biomedical applications. The presence of Cr imparts corrosion resistance and small amounts of other elements, such as iron, molybdenum or tungsten, can render very good high temperature properties and abrasion resistance. Various types of Co–Cr alloys used in implant applications include Co–Cr–Mo (ASTM F75), Co–Cr–Mo (ASTM F799), Co–Cr–W–Ni (ASTM F90) and Co–Ni–Cr–Mo–Ti (ASTM F562) [114].

Due to excellent mechanical properties and biocompatibility, magnesium

and its alloys have attracted increasing attention for load-bearing biocompatible implant applications [151]. Moreover, Mg is also an essential element for bone metabolism promoting the formation of new bone tissue; being a cofactor for many enzymes, it stabilizes the structures of DNA and RNA. The major disadvantage of using magnesium in many engineering applications is its low corrosion resistance, which may manifest in pitting corrosion, especially in electrolytic, aqueous environments [151].

Comparison of mechanical properties between Implant Materials and bone is presented in Table 6 [167].

Table 6. Comparison of mechanical properties between implant materials and bone.

Material	Young's Modulus (GPa)	Tensile Strength (MPa)
Alumina	365	6-55
Sintered CHAp	70-90	50-110
CHAp coating	0.5-5.3	>51
316L stainless steel	193	540
Co-Cr alloys	230	900-1540
Ti-6Al-4V, wt %	106	900
PMMA bone cement	3.5	70
HDPE	1	30
Cortical bone	7-30	50-150
Cancellous bone	0.1-1	1.5-3

2.3.2. Preparation techniques

Several coating methods have been used to deposit CHAp coatings on metal substrates: plasma spray [113, 114, 117, 121, 123], magnetron sputtering [113, 114, 123, 168–170], laser ablation [123], sol-gel technique [114, 117, 123, 133, 136, 168, 171, 172], dip-coating [117, 121, 170, 173], pulsed laser deposition [113, 114, 117, 121, 133, 168, 171], electrophoretic deposition [114, 117, 121, 133, 168, 171], ion beam assisted deposition [113, 114, 117, 133, 168], micro-arc oxidation [114, 168] and electrochemical deposition [20, 133, 168]. All these techniques are employed to enhance short- and long-term performance of implants by encouraging bone ingrowth and providing enhanced fixation.

Depending on the selected technique, different morphology of coating, various phases of calcium phosphate compounds and different thickness of coatings can be prepared. The selected method for the preparation of CHAp coatings onto the substrate could affect coating characteristics, such as adhesion strength and reliability [117]. Among the listed techniques, plasma spraying is the only process which is approved by the Food and Drug Administration (FDA), USA, for biomedical coatings. However, plasma-sprayed hydroxyapatite coatings have poor mechanical properties on tensile strength, wear resistance, hardness, toughness and fatigue [117, 174]. Also dentists hesitate to use implants with plasma-sprayed CHAp because of poor coating-substrate bonding and fragility of coating, which often causes serious clinical problems [174]. For this reason, other techniques were employed to improve properties and quality of coatings. In subsequent literature review, some CHAp thin films deposition techniques are discussed.

2.3.2.1. Dip-coating technique

Dip-coating process starts with immersing substrate in the solution; second step is withdrawal of substrate while liquid film is entrained on surface of substrate; a thin film on substrate is formed upon evaporations of solvents and any accompanying chemical reactions in the liquid film [117]. Dip-coating process is very fast and allows achieving a complete transition within a few seconds. Dip coating is fairly popular in the industry and laboratory applications due to its low cost, simple processing steps and high coating quality [117].

In application of the dip-coating technique, calcium hydroxyapatite coatings can be homogenous with thickness in the range of 0.05-0.5 μm. The surface of CHAp can be well controlled using this method. Moreover, processing time for dip coating can be very short, even for substrate with complex shapes. The coating layer is deposited on the surface of the substrate without decomposition or reaction with metal substrate. Dip-coating process schematically is presented in Fig. 13 [117].

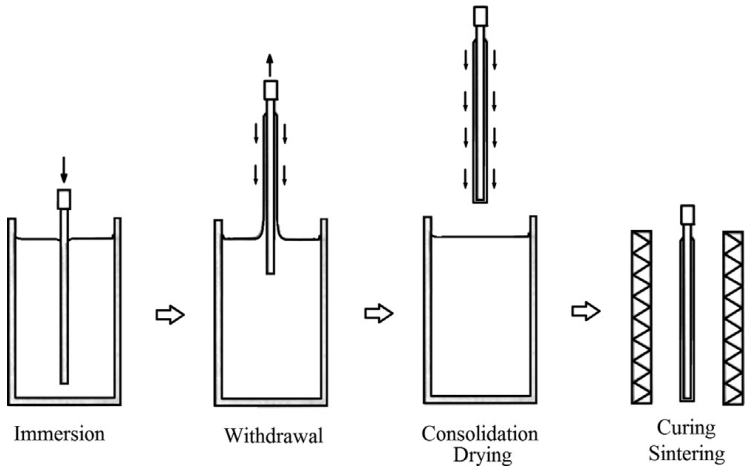

Fig. 13. Fundamental stages of dip coating (the finer arrows indicate the flow of air).

2.3.2.2. Spin-coating technique

Spin coating has been used for several decades for the fabrication of thin films [9, 110, 175–178]. A typical process involves depositing a small amount of fluid resin onto the centre of a substrate, and then substrate is accelerated rapidly to the desired rotation rate (typically around 3000 rpm) [179, 180]. Liquid flows radially due to centrifugal force, and the excess is ejected off the edge of the substrate. The film continues to thin slowly until disjoining pressure effects cause the film to reach an equilibrium thickness or until it turns solid-like due to a dramatic rise in viscosity from solvent evaporation. Final film thickness and other properties depend on the nature of resin (viscosity, drying rate, percent solids, surface tension, etc.) and the parameters chosen for the spin process [179, 180]. Schematic diagram of the spin-coating process is shown in Fig. 14 [181].

There are two methods of spin-coating process: static and dynamic. Static dispense means simply depositing a small puddle of fluid on or near the center of the substrate. The amount of fluid depends on the viscosity of fluid and the size of the substrate to be coated. Higher viscosity and higher substrate require greater solution amounts before a high speed spin step. Dynamic dispense means depositing a small amount of fluid on substrate rotating them at low speed. Typically a speed of about 500 rpm is used in this step of the process. It

serves to spread fluid over the substrate. Later on, substrate is accelerated at high speed to thin the fluid to near its final desired thickness. Spin speed of 1500-6000 rpm is usually used, depending on properties of fluids and on the substrate. This step can take from 10 seconds to a few minutes. The thickness of thin films depends on a selected spinning rate. Generally, a higher speed and longer spinning time create thinner films [180].

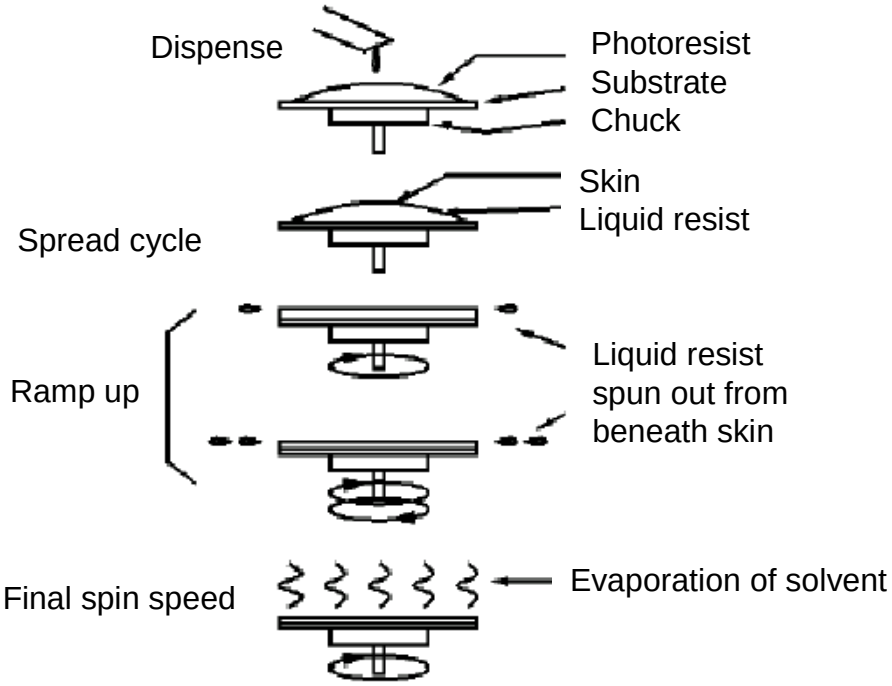

Fig. 14. Schemati c diagram of the spin-coating process.

2.3.2.3. Other techniques

Plasma spray deposition technique. Powder plasma spray (PPS) is the first and most popular commercial method to make thin coatings of CHAp [113, 114, 121, 122, 161]. There are different types of a thermal spray process: atmospheric plasma spraying (APS), vacuum plasma spraying (VPS), suspension plasma spraying (SPS), liquid plasma spraying (LPS), etc.), high-velocity suspension flame spraying (HVSFS), high velocity oxy-fuel (HVOF), gas tunnel type plasma spraying (GTPS), detonation gun spraying etc., which are elaborated to fabricate a bioactive CaP-based coatings [113, 168]. Because

of being operated under extremely high temperatures, namely, 6000-10000 °C, main disadvantages of these coatings include mixture of calcium phosphate phases, such as crystalline hydroxyapatite, amorphous hydroxyapatite, oxyhydroxyapatite, tetracalcium oxide, calcium oxide and tricalcium phosphate phases, non-uniform thickness, poor crystallinity, poor integrity, uneven resorption, poor porosity and low adhesion between coating and substrate [117, 121–123, 133, 170, 182–186]. When an additional amorphous phase is placed on the outer surface of coating, it promotes the growth of osseous tissue compared to crystalline sintered hydroxyapatite. However, high dissolution of the amorphous phase could affect implant stability. The location of the amorphous phase can especially be detrimental in the long term, if the amorphous phase is in regions adjacent to the substrate, where preferential dissolution of amorphous phase can lead to delamination and, hence, an implant failure [187]. One of the main problem of coatings deposited applying a plasma spray method is a greater coating thickness (50–200 μm), which affects fatigue under tensile loading conditions [114, 142]. Also, increasing thickness can lead to cracks forming at the substrate/coating interface. For example, the amorphous hydroxyapatite phase, which generally makes up 5% to 20% of plasma-sprayed coatings, degrades much more rapidly than the crystalline hydroxyapatite phase [122]. In addition, plasma-sprayed coatings contain more molten particles, defects and cracks, the function whereof is to degrade coating integrity [122]. For these reasons, plasma-sprayed coatings have exhibited mechanical failure at the coating–substrate interface [122].

Plasma-spray process occurs by spraying molten or heat-softened material onto the surface to provide coating [114]. Material in the form of powder is injected into a high-temperature plasma flame, where it is rapidly heated and accelerated at a high velocity towards a substrate for coating [114, 117, 142, 187, 188]. In the plasma-spray process He, Ar, N_2, H_2 and a mixture of these gases are used. Plasma spray process is presented in Fig. 15 [117].

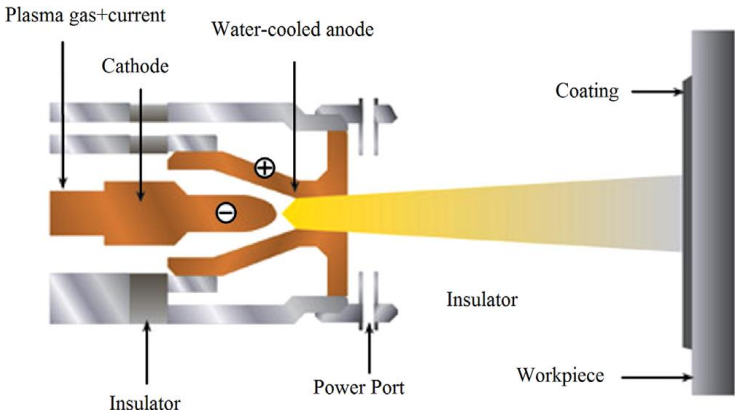

Fig. 15. A schematic diagram of thermal spray coating.

Pulsed laser deposition technique. Pulsed laser deposition (PLD) is a universal technique used to ablate a target material and condense it on the surface of a substrate material to form a wide range of thin films and multi-layered structures in any kind of materials by using appropriate lasers [114, 121]. For the first time, high-quality calcium hydroxyapatite thin films were deposited on Ti–6Al–4V substrates using a pulsed laser deposition technique in 1992 by Cotell et al., and since then the process has been improved significantly to obtain a well-adhered and highly crystalline CHAp thin films under certain conditions [117, 121, 189]. Typical equipment of a pulsed laser deposition consists of a laser source, an ultrahigh vacuum deposition chamber equipped with a rotating target and a fixed substrate holder with pumping systems (see Fig. 16) [113, 114, 121].

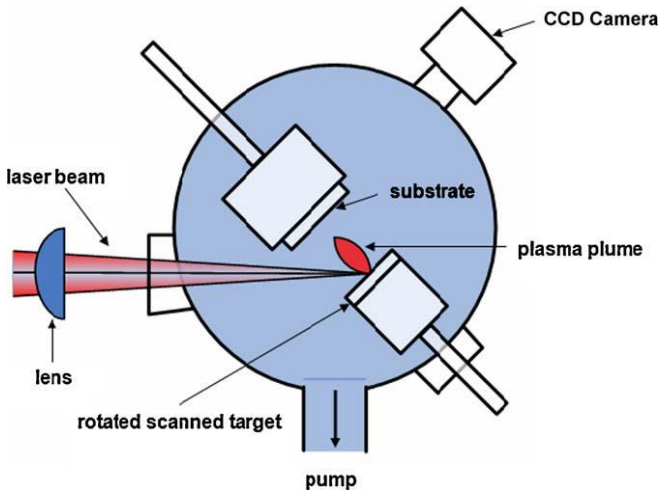

Fig. 16. Schematic of a PLD setup.

Pulsed laser deposition mechanisms consist of a sample irradiation of an intense laser beam. A small amount of material is vaporized on the surface and ejected away from the sample. Due to CHAp decomposition, the laser-target interaction produces molecules, such as $Ca_4P_2O_9$, $Ca_3(PO_4)_2$, CaO, P_2O_5 and H_2O [113]. In application of the PLD method, different substrate temperature can be chosen to provide thin films with different fine texture and roughness depending on coating application. The main disadvantage and limitation of this process is the splashing of particulate deposition on the film [117].

Magnetron sputtering technique. The magnetron sputtering technique is an ionic sputtering method, where a highly energetic ion beam strikes a solid target and knocks of the atoms from the surface onto the substrate [114, 117]. The magnetron sputtering process was used for depositing metals, alloys and compounds onto a wide range of materials with thickness ranging from <1 μm to about 5 μm [114, 141, 190]. Using this method, different type of coatings can be synthesized (hard, wear-resistant, low-friction, corrosion-resistant coatings, decorative coatings and coatings with specific optical or electrical properties) [191]. This method has some advantages, such as a high deposition rate, high-purity films, extremely high adhesion of films, ability to coat heat-sensitive substrates, excellent uniformity on large area substrates [114, 192]. Using this technique, coatings can be <1 μm thick with controlled microstructure, dense, uniform and well-adhered to metallic, ceramic or polymeric substrates [117, 119]. Due to the above-mentioned advantages of the magnetron sputter deposition technique, many researchers have explored the deposition of CaP films on metallic materials for implant applications by this technique. Scheme of magnetron sputtering deposition technique is presented in Fig. 17 [114].

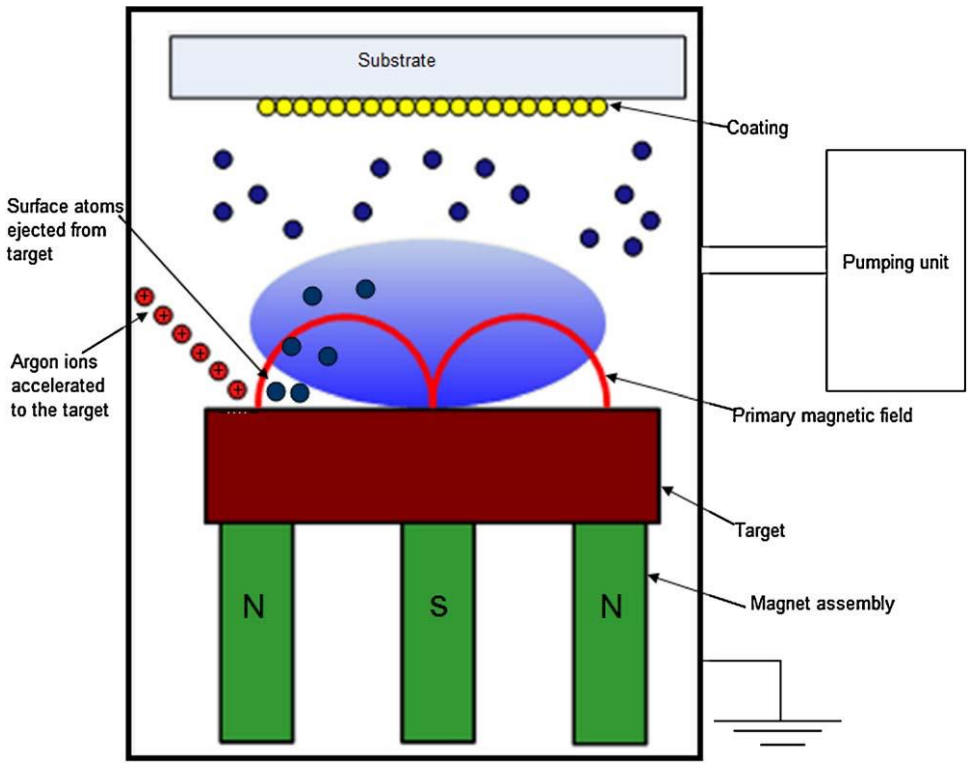

Fig. 17. Schematic of a magnetron sputter deposition system.

Radio-frequency (RF) magnetron sputtering. Research group consisting of Yamashita, Jansen, Wolke et al. used radio-frequency magnetron sputtering technique for the first time to prepare CHAp coatings [113]. The equipment of this technique for CaP coatings includes vacuum chamber, RF generator, matching network, magnetron and cooling system (see Fig. 18) [113, 193]. Parameters, such as discharge power, gas flow rate, working pressure, substrate temperature, deposition time, post-heat treatment or negative substrate bias, can be controlled and also they influence quality of CaP coatings. Substrate can be kept at constant temperatures during the deposition process or can be subjected to plasma irradiation without additional heating. Different types of coatings (pure CHAp, Si-CHAp, carbonated CHAp, and Zn, Mg, and Al-doped CaPs) can be prepared [113, 142, 166, 192].

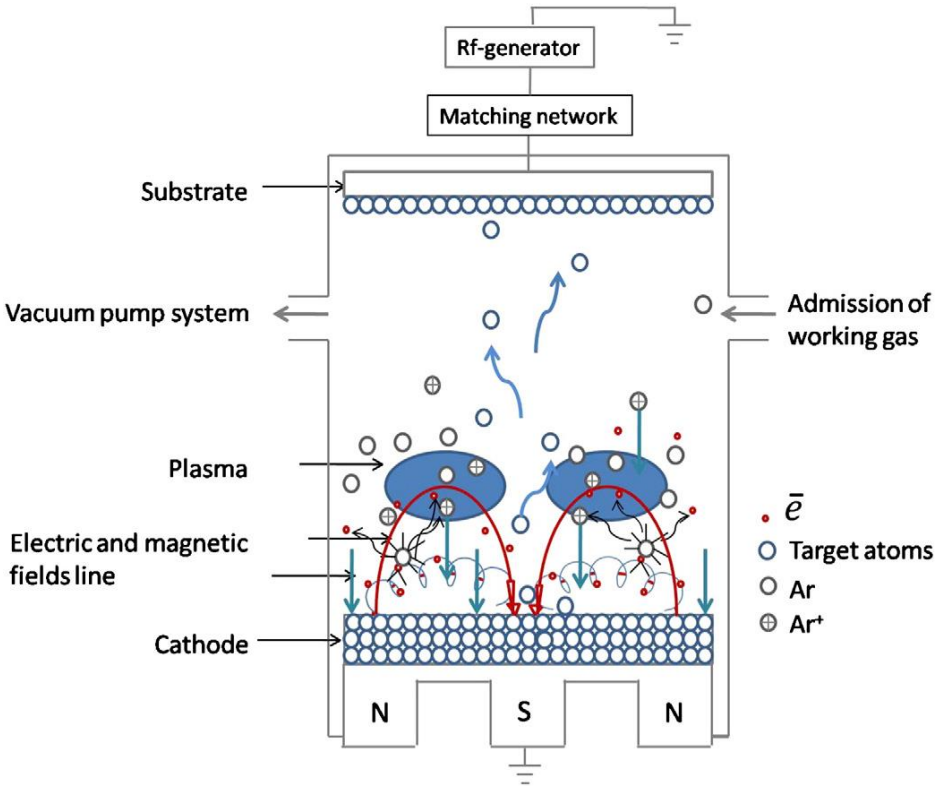

Fig. 18. Schematic diagram of the typical RF magnetron sputtering facility.

Ion beam assisted deposition technique. A typical IBAD system (Fig. 19) consists of two main parts: electron or ion beam bombarding and vaporizing a CHAp bulk target to produce an elemental cloud towards the surface of a substrate and a source for simultaneous irradiation of a substrate with highly energetic inert (e.g. Ar^{+}) or reactive (e.g. O_2^{+}) gas ions to assist in the deposition of CHAp [113, 114, 117]. A few angstroms to several (2-4 μm) micrometres-thick CaP coatings can be prepared. High bond strength associated with the IBAD prepared films is considered a consequence of an atomic intermixing interfacial layer which can be a few μm thick [113].

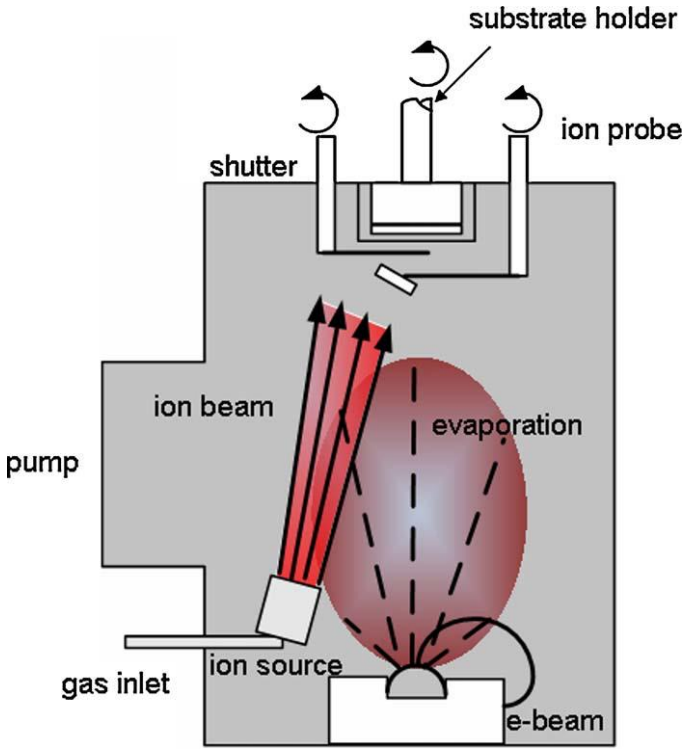

Fig. 19. Scheme of ion beam assisted deposition technique using a single ion source.

Electrophoretic deposition technique. Electrophoretic deposition (EPD) techniques involve the deposition of coatings from charged powder particles suspended in liquid medium onto substrate electrode under the influence of an electric field [114, 117]. EPD process can be divided into two types depending on which electrode deposition occurs. When the particles in suspension are positively charged, the deposition takes place on the cathode and the process is called cathodic electrophoretic deposition. If the particles in suspension are negatively charged, the deposition takes place on the anode and the process is called anodic electrophoretic deposition [114]. The main advantages of electrophoretic deposition technique include the following: coatings can be deposited on any kind of surfaces, such as flat, cylindrical or any other shaped substrate with minor changes in electrode design and positioning; process is quick and does not require any complicated apparatus; different compounds can be deposited; coatings are strongly adhered and homogeneous like in any other dip and spray coating technologies; produced coatings are of a wide

range of thickness - from less than 1 μm to more than 100 μm thick. Scheme of electrophoretic deposition technique is presented in Fig. 20 [114, 117].

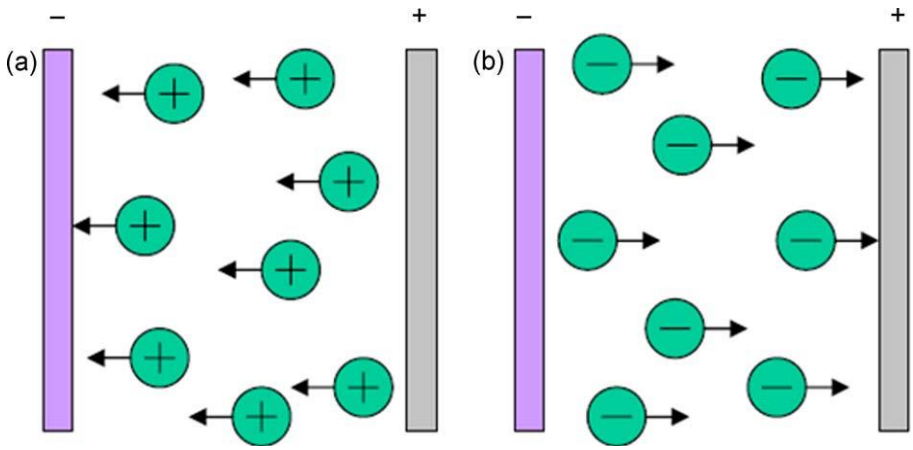

Fig. 20. Schematic illustration of electrophoretic deposition process: (a) cathodic EPD and (b) anodic EPD.

One disadvantage of this process is that water cannot be used as solvent, because the application of voltage to water causes the evolution of hydrogen and oxygen gases at the electrodes which could adversely affect the quality of deposits formed [114]. Another limitations of the technique include low adhesion strength, decrease in porosity and cracking on the coated surface due to post-process heat treatment shrinkage [117].

Sol-gel technique. The sol-gel process is a low-cost, easy, well-controlled wet method to develop CaP coatings from calcium and phosphate containing precursor solutions on different substrates for medical implants due to its ability to produce crystalline films at relatively low temperatures, possibility to tailor the microstructures, and its convenience for complex shape coatings [11, 110, 114, 194–196]. The sol-gel thin films coating process can be divided into the following steps: (a) preparation of sol by hydrolysis and condensation reactions using organic or inorganic routes [114, 117, 197, 198]; (b) ageing of sol at a suitable temperature for arriving at desired properties (e.g., optimum viscosity) [114, 117]; (c) sol coating on substrate in application of the casting, spinning, drawing, coating, emulsification, dipping, spraying or other process [114, 117]; (d) coated sol drying, usually followed by heating, to obtain the

desired product [114, 117]. Sol-gel techniques have some advantages, such as: (1) produced coatings show excellent adhesion; (2) high homogeneity and purity coatings; (3) process is under control; (4) low temperature of synthesis allows adding thermolabile organic or inorganic compounds and biologically important molecules, such as polymers and/or medicaments, in the structure; (5) corrosion resistance performance due to the ability to form thick coating [114, 117, 196, 199]. The sol-gel coating technique is a simple, economic and effective method to produce high-quality coatings [114, 117]. Thickness of coatings can be less than 0.1μm [178].

Electrochemical deposition technique. Various calcium phosphate coatings, including carbonated apatite, brushite, octacalcium phosphate and CHAp, can be deposited using electrochemical deposition technique [20]. Electrochemical deposition technique has some advantages, such as good and controllable composition and structure of coatings and the use of low temperatures, which allow for the formation of highly crystalline deposits with low residual stresses, and the ability to deposit on non-line-of-site, porous or complex surfaces [20]. The structure of the coating can be controlled by changing the composition, pH and temperature of the electrolyte, as well as the applied potential or current density.

Deposition of apatite coatings from simulated body fluids (SBFs). Deposition of apatite coatings from simulated body fluids is a biomimetic deposition method. The biomimetic approach has some advantages, such as (1) being a low-temperature process applicable to any heat-sensitive substrate, including polymers; (2) forming bonelike apatite crystals having high bioactivity and good resorption characteristics; (3) being evenly deposited on, or even into, porous or complex implant geometries; (4) being able to incorporate bone-growth-stimulating factors [200]. The biomimetic process consists of soaking metal implants in simulated body fluids at physiological temperature and pH [200]. Coatings are deposited by immersing metal, glasses and polymers in SBFs. SBFs have the same temperature, pH and inorganic composition as human blood plasma, and it is unknown whether these

conditions are optimal for a coating process. Coatings are obtained by immersing substrates for a long time (7-14 days). During this time, the composition of SBFs is replenished for apatite crystal growth, also pH and temperature are kept constant [200]. Due to low solubility product of CHAp and limited concentration range for metastable phase, this operation is extremely difficult and might lead to local precipitation or uneven coatings. Such an intricate and long process can hardly be applicable in the coating prostheses industry [200].

It must be mentioned, that during long heat treatment in the range of temperatures 900-1300°C hydroxyapatite starts to decompose by dehyroxylation process forming oxyhydroxyapatite (OHAp) [201–204]. OHAp has a large number of vacancies in its structure, a bivalent oxygen ion and a vacancy substitute for two monovalent OH^- ions of CHAp, which can be presented by a formula: $Ca_{10}(PO_4)_6(OH)_{2-2x}O_xV_x$, where V stands for vacancy. When x=1, oxyapatite ($Ca_{10}(PO_4)_6O$; OAp) is formed [185, 187, 205]. The XRD patterns of calcium hydroxyapatite and calcium oxyhydroxyapatite are almost identical [205]. The following decomposition of OHAp yielding calcium phosphates, mainly tricalcium phosphate (TCP) and tetra-calcium phosphate (TeCP) [201, 204]. Steps of decomposition process: CHAp→OHAp→OAp→TCP+TeCP [204]. Hydroxyapatite starts to decompose by evaporating water and forming partially or completely dehydrated oxyhydroxyapatite:

Step 1: $Ca_{10}(PO_4)_6(OH)_2 \rightarrow Ca_{10}(PO_4)_6(OH)_{2-2x}O_x + xH_2O$, with $0 \leq x \leq 1$.

Step 2: $Ca_{10}(PO_4)_6(OH)_{2-2x}O_x \rightarrow Ca_{10}(PO_4)_6O + (1-x)H_2O$

If *x* reaches a critical value the destruction of the apatite channel structure occurs, and an equilibrium with tricalcium phosphate (TCP, $Ca_3(PO_4)_2$) and tetracalcium phosphate (TeCP, $Ca_4(PO_4)_2O$) exists [202, 203]:

Step 3: $Ca_{10}(PO_4)_6O \rightarrow Ca_4(PO_4)_2O + Ca_3(PO_4)_2$

or $2Ca_{10}(PO_4)_6O \rightarrow 2Ca_3(PO_4)_2 + Ca_2P_2O_7 + 3\ Ca_4P_2O_9$

Oxyapatite remains stable under dry conditions and will readily transform

to hydroxyapatite in the presence of moisture, according to reaction (1), where V represents a vacancy [187]:

$2OH^-(s) \rightarrow O^{2-}(s) + V(s) + H_2O(g)$ (1)

Overview of calcium hydroxyapatite thin films deposition techniques is presented in Table 7.

Table 7. Different techniques to deposit CHAp coatings [117, 120].

Technique	Thickness	Advantages	Disadvantages
Thermal spraying	30-200 μm	High deposition rates; low cost	Line of sight technique; high temperatures induce decomposition; rapid cooling produces amorphous coatings
Pulsed laser deposition	0.05-5 μm	Coating with crystalline and amorphous; coating with dense and porous	Line of sight technique
Sputter coating	0.5-5 μm	Uniform coating thickness on flat substrates; dense coating	Line of sight technique; expensive time consuming;
Ion beam assisted deposition	< 0.03-4μm	Low temperature process; high reproducibility and reliability; high adhesion; wide atomic intermix zone are coating-to-substrate interface	Crack appearance on the coated surface
Electrophoretic deposition	<1-200μm	Uniform coating thickness; rapid deposition rates; can coat complex substrates	Difficult to produce crack-free coatings; requires high sintering temperatures

Sol-gel	< 1-2.0 μm	Can coat complex shapes; Low processing temperatures; relatively cheap as coatings are very thin	Some processes require controlled atmosphere processing; expensive raw materials
Dip coating	0.05-0.5 μm	Inexpensive; coatings applied quickly; can coat complex substrates	Requires high sintering temperatures; thermal expansion mismatch
Biomimetic coating	< 30 μm	Low processing temperatures; can form bonelike apatite; can coat complex shapes; can incorporate bone growth stimulating factors	Time consuming; Requires replenishment and a constant of pH of simulated body fluid

2.3.3. Properties of calcium hydroxyapatite thin films

Calcium hydroxyapatite thin films derived for medical application must meet the minimum requirements described by the Food and Drug Administration, USA (FDA), and the International Standard Organization (ISO) (Table 8) [113, 114, 120, 168]. The CHAp coating permits a faster osteointegration due to its bone tissue bonding properties [206, 207]. CHAp coatings must be non-toxic, non-carcinogenic, with little or no foreign body reaction, chemically stable or corrosion-resistant and have certain chemical, physical and mechanical properties, which satisfy critical quality specifications [114, 119, 168, 208].

Biological response of CHAp coatings depends on thickness (this will affect coating adhesion and fixation), phase composition, phase purity, chemical purity, crystallinity (this affects the dissolution and biological behaviour), Ca/P ratio, microstructure, surface roughness, porosity, implant type and surface

texture, which affect the resulting mechanical properties of the implant, such as cohesive and bond strength, elasticity, yield stress, ductility, toughness, wear resistance, tensile strength, shear strength, Young's modulus, residual stress and fatigue life [114, 119, 168]. Changes in these properties can produce coatings with varied bioactivity and durability. Osteoconductivity accelerate bone growth and attachment to implant interface, thus providing improved implant fixation and lifetime [123]. Physical properties of calcium hydroxyapatite is presented in Table 9 [122].

Table 8. FDA requirements for CHAp coatings [113, 114, 120, 168].

Properties	Specification
Thickness	Not specific
Crystallinity	62% minimum
Phase purity	95% minimum
Ca/P atomic ratio	1.67-1.76
Density	2.98 g/cm^3
Heavy metals	<50 ppm
Tensile strength	>50.8 MPa
Shear strength	>22 MPa
Abrasion	Not specific

Table 9. Physical properties of calcium hydroxyapatite [122].

Property	Typical values
Density (g cm^{-3})	3.15
Young's modulus (GPa)	85-90
Knoop hardness (MPa)	3450
Tensile strength (MPa m^{-2})	120
Poisson coefficient	0.3
Thermal expansion (x10^{-6} K^{-1})	11
Melting point (°C)	1660
Specific heat (cal g^{-1} K^{-1})	0.15
Thermal conductivity (W cm^{-1} K^{-1})	0.01

In an implanted prosthesis, the stability and the adherence of implant/coating and coating/bone interfaces strongly affect its performance [209]. A number of in vivo studies showed that failures mainly occur at the

metal/coating interface. The longer the period of implantation, the higher is the probability of a failure at this interface (since the strength of the bone/CHAp interface tends to increase with time during the early stages of post-operative recovery) [209]. It is very important for substrate and coating to be in adherence and for coating not to pull away after implantation. Tsui et al. claimed that the cohesive and adhesive integrity of coatings considerably affect the long term performance of CHAp-coated implants [117, 209]. Adhesive strength is usually evaluated based on surface roughness, coating properties, residual stress and mechanical interlocking between the coating and the substrates, whereas the cohesive strength is determined by coating properties, such as microstructure and crystallinity [117].

Also, to achieve long term stability of coatings, the dissolution behaviour of coating is a critical factor, because it induces the precipitation of bone-like apatite on the implant surface [113, 210]. The two primary factors that control the dissolution characteristics of a coating are (1) inherent material properties, such as chemical composition, presence of secondary phases, crystallinity, particle size, surface morphology and roughness, and (2) environmental factors, such as media composition and pH [210].

It has been suggested that coating for orthopaedic implants should have low porosity, strong cohesive strength, good adhesion to the substrate, a high degree of crystallinity and high chemical and phase stability [168, 209]. There is a general agreement that chemical purity of CHAp should be as high as possible (95%), with a Ca/P ratio of 1.67 [168].

Another source has mentioned that the main requirement for bone materials is very high porosity (above 70-80%) with full interconnectivity [119]. A well-connected 3D porous structure with optimum pore size is critical for the osteoconduction and osteoinduction of the implant [211]. Optimal pore size is ranging from 50– 150 μm to 300 μm [211]. Furthermore, CHAp coatings with a porous structure might provide an advantage for loading and delivering the antibiotic, drug and growth factor, which is an important direction for future development of high-performance calcium phosphate coatings for orthopaedic

implants [211].

Requirements for ideal bone substitute materials include biocompatibility, biodegradability, osteoinduction and osteopromotion/osteoconduction porosity, stability under stress, resorbability/degradability, plasticity, sterility, stable and long-term integration of implants [19, 21]. Requirements for CaP coatings are listed in Table 10 [113, 168].

Table 10. Key requirements of CaP coatings of implants and specific functions [113, 168].

Requirement	Definition/function
Biocompatibility	Ability of a material to perform with an appropriate host response in a specific application
Bioactivity	Ability to interact with the surrounding bone and soft tissues
Osteoconductivity	Ability to provide scaffold for the formation of new bone
Dominant crystalline phase	Prevent resorption (dissolution) of the coating in body fluids
Amorphous phase	Promote early osseointegration
Dissolution of CHAp	Programmed dissolution rate in body fluids to match the in vivo healing process
Defined elemental composition	Match elemental composition of bone mineral phase
Specific surface morphology of interfacial matrix (interface 2)	Enable osteoblasts attachment and differentiation, and bone material ingrowth (fixation to the bone)
Interfacial stability and strong adhesion to an implant (interface 1)	Prevent mechanical failures under load bearing conditions
Therapeutic capabilities	Templates for the in situ delivery of drugs and growth factors at the required times

2.3.4. Importance and role of calcium hydroxyapatite thin films in bone and teeth implants

Calcium hydroxyapatite thin films on substrates can be used in bone and teeth implants, because they restore the function of load-bearing joints which

are subjected to high level of mechanical stresses, wear and fatigue in the course of normal activity. These devices include prostheses for hip (Fig. 21(a), knee (Fig. 21(b), ankle, shoulder (Fig. 21(c), and elbow joints (Fig. 21(d)). They also include fracture fixation devices, such as wires, pins, plates, screws, etc. [114]. Dental implants are used to restore lost tooth by replacing both the tooth and its root (Fig. 22). Here a metallic implant (titanium) is first inserted into the gum (gingival) so that bone cells grow tightly around it and anchor it firmly. Then an abutment is placed over the anchor followed by an artificial tooth (crown) attached to the abutment. Titanium is most commonly used as an implant material as it osseointegrates rapidly to the surrounding tissues and thereby forms a tight seal against any kind of bacterial invasion [114]. However, a CHAp coated titanium implant is more biocompatible and osteoconductive, therefore shows faster integration.

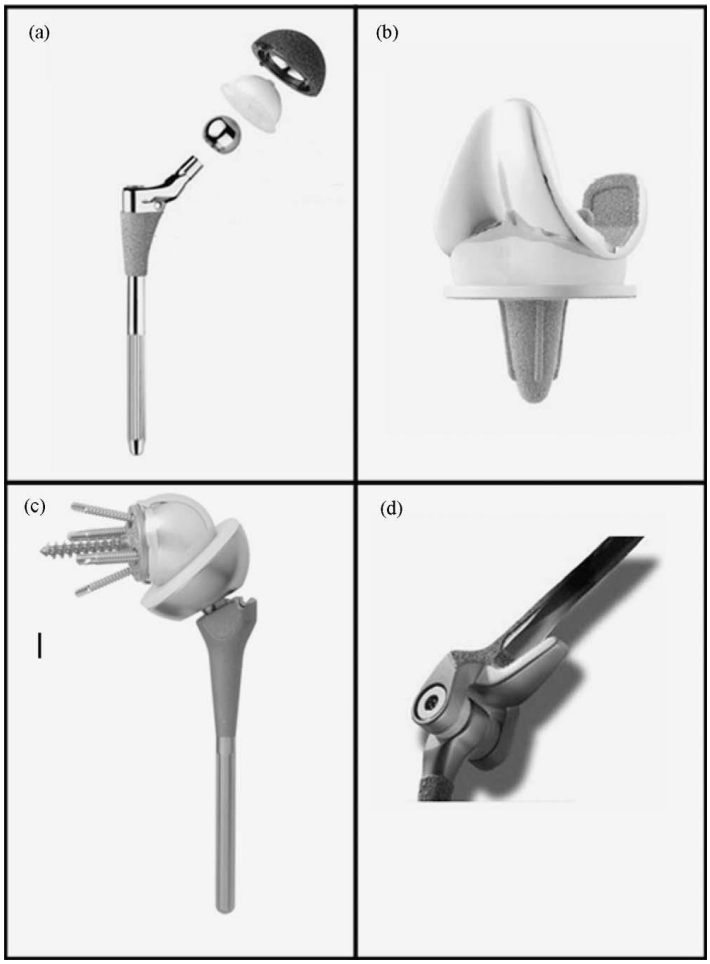

Fig. 21. Orthopedic implant devices used for load bearing applications: (a) hip implant, (b) knee implant, (c) shoulder implant and (d) elbow implant.

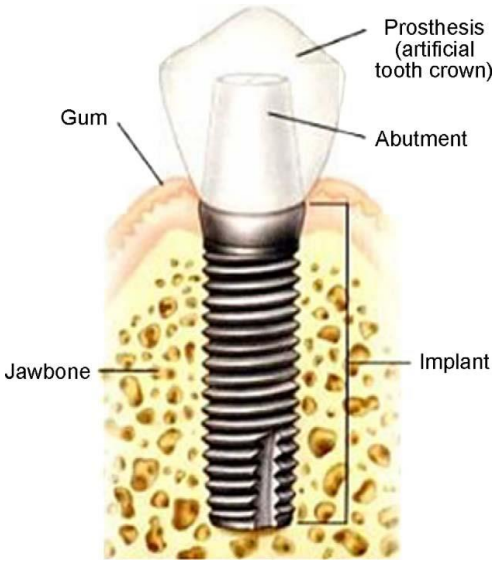

Fig. 22. A dental implant.

It is very important to avoid inflammation after implantation, because it can lead to rejection of the implant. Implant infection has been associated with biofilm formation, and bacterial cells growing within the biofilm exhibit increased resistance to antibacterial agents [14, 212]. Orthopaedic implant failure may come as a result of bacterial infections from both Gram-positive and Gram-negative pathogens, such as Staphylococcus epidermidis and Pseudomonas aeruginosa. S. epidermidis is known to be involved in approximately 30% of all bacterial colonies that form in orthopaedic implants. P. aeruginosa prosthetic and bone infections are difficult to treat and often require two-stage revision surgeries as the primary treatment [118]. The antibiotic prophylaxis therapy has been used to avoid these infections, therefore infection rates of all joint hip arthroplasties range between 0.5% and 3.0% in primary total hip arthroplasty [212]. Also silver has been used in many medical devices to avoid infections, because silver is known as the primary antimicrobial agent [118, 212, 213]. Silver-doped hydroxyapatite coatings that exhibit antimicrobial properties have been created using methods, such as sol–gel, physical vapour deposition, ion beam assisted deposition, magnetron sputtering, micro-arc oxidation and plasma spraying [14, 118, 198, 213, 214].

In dentistry, synthesis of nanosized Zn- substituted CHAp crystals has been very important, because zinc-containing compounds have the ability to release zinc ions, which in turn inhibit growth of caries-related bacteria [213].

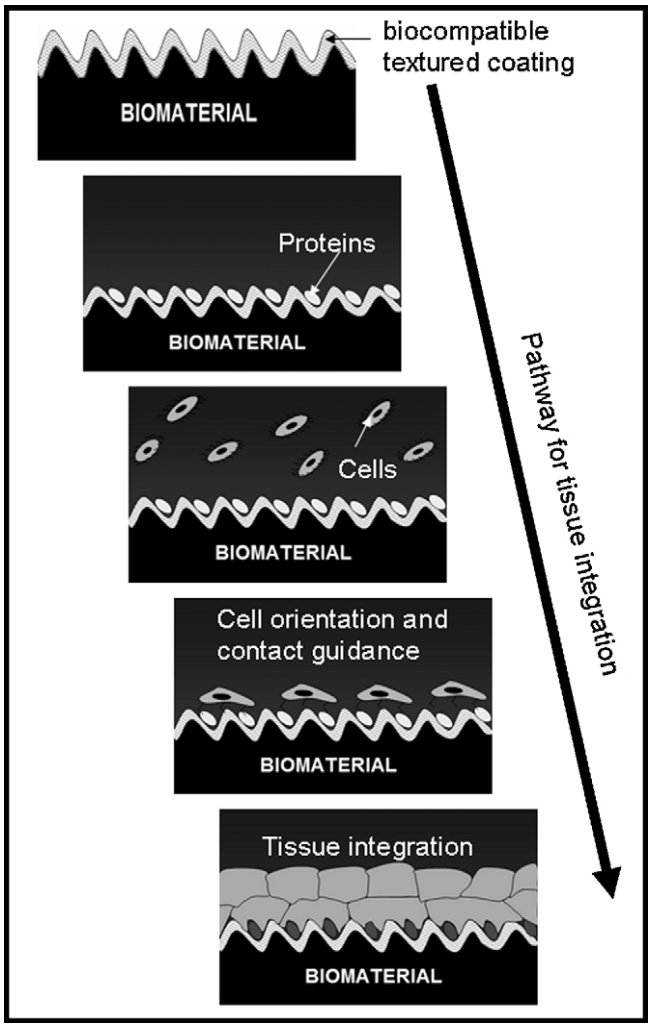

Fig. 23. Schematic illustration of the sequential reactions that take place after the implantation of an biomaterial into a living system.

The adhesion of implants occurs through two continuous processes; one is the bone ingrowth into the CHAp coating resulting in mechanical fixation. The other one is a reciprocal dissolution/precipitation reaction between coating and the bone, which is determined by the concentration of Ca^{2+}, OH^- and PO_4^{3-} ions in body fluids [215]. The final adhesion will be reached when the last deposited ions completely bond between the coating with the bone (bioactive fixation) (Fig. 23.) [7, 114, 215]. These processes are mainly affected by

CHAp and phosphate-based coatings, therefore high mechanical quality of CHAp coatings is required for dental and bone implants.

The ideal bone substitute should be biocompatible, and it should gradually be replaced by newly formed bone and preferably possess osteoinductive or osteoconductive properties [216]. Osteoinduction is a healing process in which local stimulating factors cause mesenchymal cells to disaggregate, migrate, reaggregate, proliferate and differentiate into chondroblasts or osteoblasts. In osteoconduction, the implanted material serves as a scaffold for ingrowth of capillaries, perivascular tissue and osteoprogenitor cells from the recipient bed [216].

3. Experimental

3.1. Materials and Reagents

Materials and reagents used to prepare calcium hydroxyapatite coatings are listed in Table 11.

Table 11. List of reagents.

Reagent	Chemical formula	Purity	Producer
Calcium acetate monohydrate	$Ca(CH_3COO)_2 \cdot H_2O$	99.9 %	Fluka
1,2- ethandiol	$C_2H_6O_2$	99.0 %	Alfa Aesar
Ethylenediamine tetraacetic acid (EDTA)	$(HO_2CCH_2)_2NCH_2CH_2N(CH_2CO_2H)_2$	99.0 %	Alfa Aesar
Triethanolamine (TEA)	$(HOCH_2CH_2)_3N$	99.0 %	Merck
Phosphoric acid	H_3PO_4	85.0 % (concentration)	Reachem
Poly(vinyl alcohol) (PVA7200)	$[-CH_2CHOH-]_n$	99.5 %	Aldrich

3.2. Synthesis of calcium hydroxyapatite thin films

Calcium hydroxyapatite coatings on titanium, silicon and quartz substrates were prepared by sol-gel method in aqueous solution by dip-coating and spin-coating techniques. The molar ratio of Ca/P was kept 1.67 like in calcium hydroxyapatite. Synthesis scheme of Ca-P-O sol-gel is presented in Fig. 24. In the sol-gel process, 2.6425 g of $Ca(CH_3COO)_2 \cdot H_2O$ was dissolved in 50 mL of distilled water under continuous stirring for 30 min at 65 °C. Next, 1,2-ethandiol was added and stirred for 15 min. Afterwards to this solution 4.82185 g of EDTA was added as complexing agent and triethanolamine was slowly dripped into the solution. After 10 h of stirring, 0.61mL 85.0 % phosphoric acid was added to the solution. To prepare PVA solution 3 g of

PVA powder was added to 97mL of distilled water under continuous stirring for 2 h at 90 °C. Finally, PVA solution was added to the above solution.

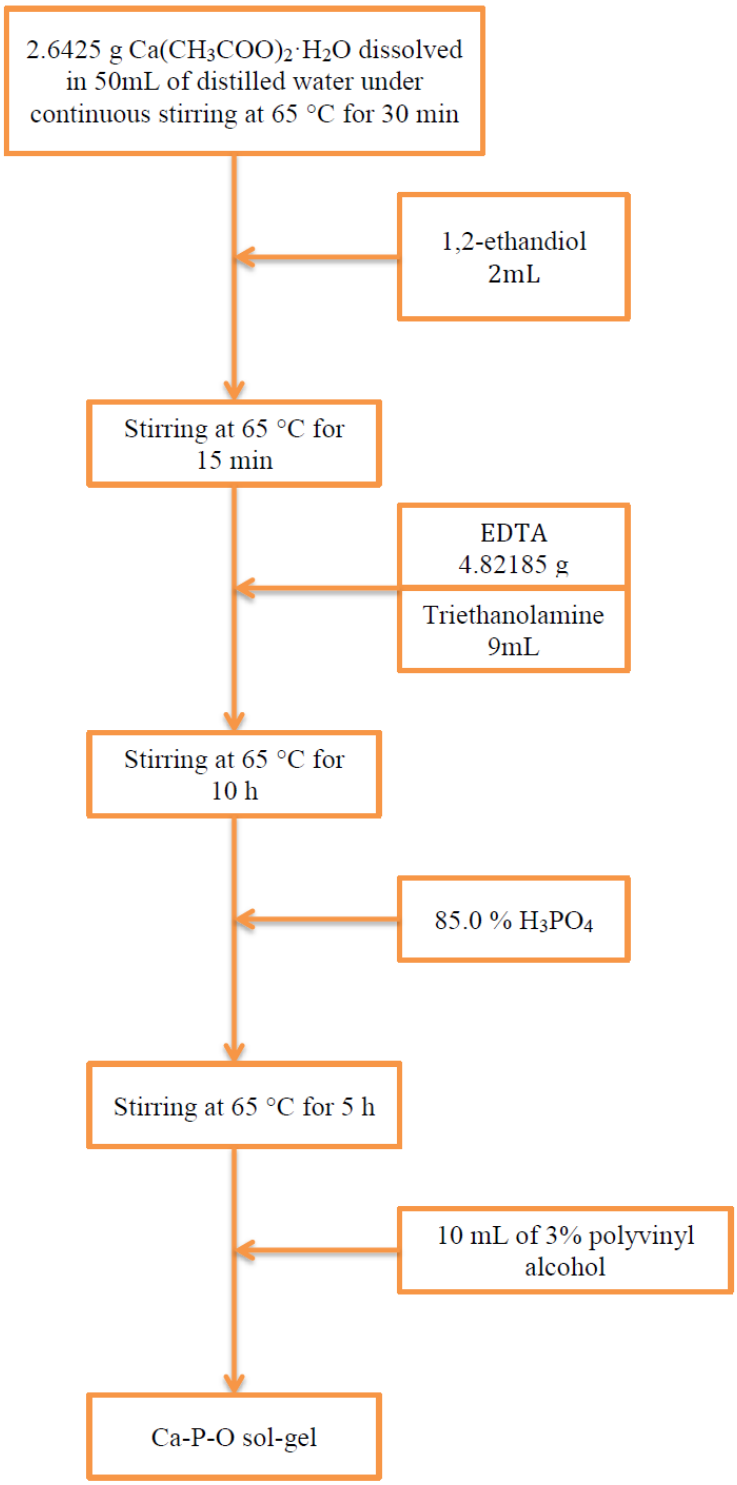

Fig. 24. Synthesis scheme of Ca-P-O sol-gel.

The stock solution was used for the preparation of CHAp coatings on titanium, silicon and quartz substrates using dip-coating and spin-coating techniques.

3.2.1. Preparation of substrates

The substrates were carefully prepared by different cleaning procedures depending on type of substrate before dip-coating and spin-coating procedures.

Preparation of titanium substrate. Titanium surface was polished with fine sandpaper till the surface became bright. After washing with acetone, ethanol and distilled water the Ti substrates were storied in 5 M solution of NaOH at 60 ^{o}C for 24 h. Again, before dipping the substrates were washed abundantly with distilled water and finally dried in air.

Preparation of silicon and quartz substrates. The substrates were cleaned with piranha solution, acetone, ethanol and distilled water.

3.2.2. Dip-coating technique

The substrates used in the dip-coating procedure had slightly different measurements (Ti - 1×2 cm; Si - 1.5×1.5 cm and SiO_2 - 1×1 cm).

The standard immersing (85 mm/min) and withdrawal rates (40 mm/min) for dip-coating process were applied for all the samples. The dipping procedure was repeatedly performed 1, 5, 15 and 30 times on all substrates. After evaporation of solvent the substrates were dried in an oven for 10 min at 110 ^{o}C and heated at 1000 ºC for 5 h with heating rate of 1 ^{o}C/min after each dip-coating procedure.

3.2.3. Spin-coating technique

The diameters of substrates used in spin-coating process were 2.2 cm – Ti and Si and 2.5 cm - SiO_2.

For the spin-coating process a speed of 2000 rpm and duration of 60 s were used. After each spin-coating the samples were annealed at 1000 °C for 5 h with heating rate of 1 °C/min. Spin-coating and annealing procedures were repeated 1, 5, 15 and 30 times. Another samples with 5, 8 and 10 layers of

coatings on silicon substrate were prepared for FTIR analyses in the same conditions.

Samples on titanium substrate were prepared with 5 layers of calcium hydroxyapatite where samples after each spin-coating procedure were dried in an oven for 10 min at 110 ^{o}C and finally after last spin-coating procedure samples were annealed at 850 ^{o}C for 5 h with heating rate of 1 °C/min.

Another group of samples were prepared with $CaTiO_3$ sublayer. For this reason 5 layers of calcium titanate was coated on titanium substrate with the same drying and annealing conditions described before and finally 5 layers of calcium hydroxyapatite were coated on calcium titanate after each spin-coating procedure drying in an oven for 10 min at 110 ^{o}C and finally after last spin-coating procedure annealing samples in 850 ^{o}C for 5 h with heating rate of 1 °C/min.

Also third group of samples on titanium substrate were prepared using different annealing temperatures. Titanium substrate was coated with 5 and 15 layers of calcium hydroxyapatite after each spinning procedure drying samples in an oven for 20 min at 200 °C or 400°C. Finally, after last spin-coating procedure all samples were annealed at 1000 °C for 5 h with heating rate of 1 °C/min.

3.3. Instrumentation and characterization techniques

Dip-coating and spin-coating procedures were carried out with Dip coater D KSV and Spin coater P6700. Overview of used instruments and analysis methods are presented in Table 12.

Table 12. Overview of used instruments.

XRD	Rigaku miniFlex II diffractometer	Bruker AXE D8 Focus diffractometer	
SEM	Hitachi SU-70	JEOL JSM 8404	
AFM	Veeco Bioscope 2		

FTIR spectroscopy	Perkin-Elmer FTIR Spectrum BX II spectrometer	ALPHA FTIR spectrometer (Bruker)	
Raman spectroscopy	Confocal Raman spectrometer/microscope LabRam HR 800	inVia (Renishaw) spectrometer	
CAM	KVS Instrument CAM 100		
Thickness of coatings	VEECO Dektak 6M Stylus Profiler	Helios NanoLab 650	J.A. Woollam M2000X
UV-vis reflectance spectrometry	Perkin-Elmer Lambda 35		

The X-ray diffractometers operated with Cu $K_{\alpha 1}$ radiation. The measurements were recorded at the standard rate of 1.5 2θ/min. The spectral resolution of FTIR spectroscopes was set at 4 cm^{-1}. Spectra were acquired from 100 scans. Calcium phosphates were deposited on round silicon plates with diameter of 21.5 mm and width of 0.6 mm. The bare Si plate annealed at 1000 ^{o}C for 5 h was used for collection of background spectrum. Parameters of the bands were determined by fitting the experimental spectra with Gaussian-Lorentzian shape components using GRAMS/A1 8.0 (Thermo Scientific) software. The Raman spectra were registered using 632.8 nm laser for excitation; inVia (Renishaw) spectrometer equipped with thermoelectrically cooled (–70 ^{o}C) CCD camera and microscope. To determine hydrophobic and hydrophilic properties of coatings the contact angle measurements were recorded. A micro-droplet of water (volume 6 μl) was allowed to fall onto the sample from a syringe tip to produce a sessile drop. Besides, for the measurement of thickness of layers the profilometer (VEECO Dektak 6M Stylus Profiler), the ellipsometer (J.A. Woollam M2000X) and scanning electron microscope (Helios NanoLab 650) were additionally used.

4. Results and discussion

4.1. Sol-gel synthesis and characterization of calcium hydroxyapatite thin films synthesized on titanium substrate.

Thin films of calcium hydroxyapatite on titanium substrate were developed using sol-gel approach from Ca-P-O sol-gel by dip-coating and spin-coating techniques.

4.1.1. Dip-coating approach

Fig. 25 represents the XRD patterns of films obtained from Ca-P-O sol-gel using dip-coating technique.

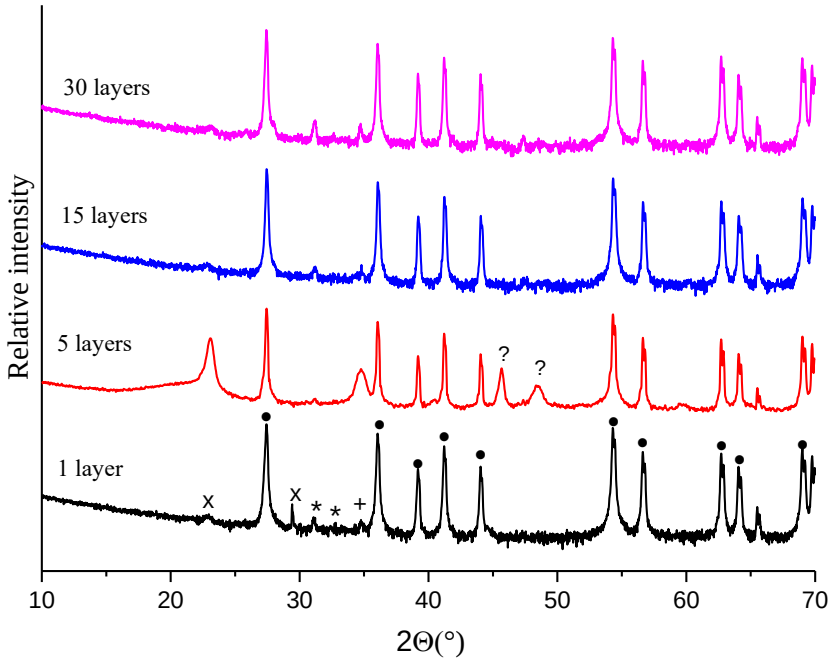

Fig. 25. XRD patterns of the Ca-P-O sol-gel samples annealed at 1000 °C after each dipping procedure for 5 h in air. Diffraction lines are marked: * - $Ca_{10}(PO_4)_6(OH)_2$ [PDF: 74-0566], + - $Ca_3(PO_4)_2$ [PDF: 70-2065], • - TiO_2 [PDF: 21-1276], x – Ti_xO_y and ? – unidentified.

As seen from Fig. 25, after first immersing, withdrawal and annealing procedure the peaks attributable to the $Ca_{10}(PO_4)_6(OH)_2$ ($2\theta \approx 31.8°$ and 32.2°) and $Ca_3(PO_4)_2$ ($2\theta \approx 35.0°$) crystalline phases are observed. The XRD diffraction pattern also contains not intensive peaks of Ti_xO_y and very sharp

diffraction lines attributable to TiO_2 (rutile) crystalline phase, and no formation even traces of anatase could be observed. The formation of TiO_2 during heat treatment of Ti substrate at elevated temperatures is very likely. The additional experiments evidently confirmed this assumption. Fig. 26 shows XRD patterns of Ti substrates repeatedly heated at 1000 ºC for 5 h with heating rate of 1 ^{o}C/min. As seen, the surface of Ti is fully converted to rutile oxide phase after heating at 1000 ºC. According to the literature data, the formation of TiO_2 during the synthesis of CHAp thin films on Ti substrate usually also proceeds [217, 218].

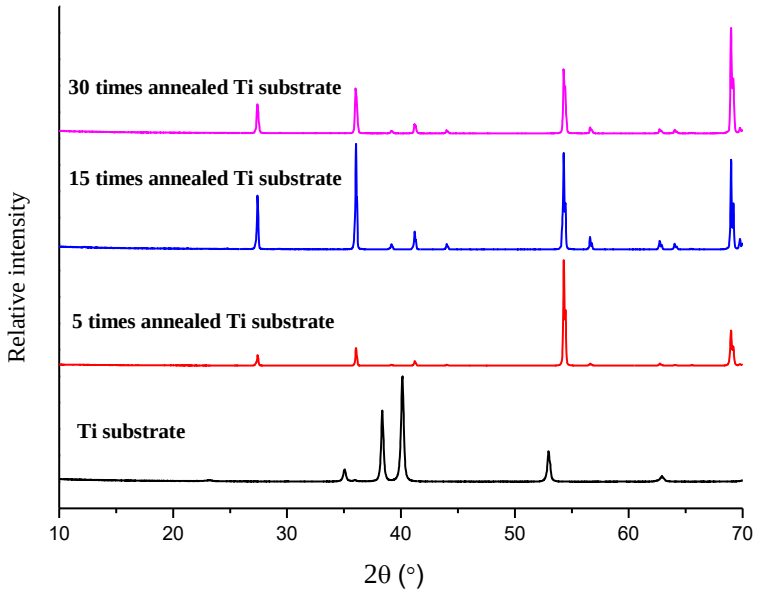

Fig. 26. XRD patterns of Ti substrates repeatedly heated at 1000 ºC for 5 h with heating rate of 1 ^{o}C/min.

Interestingly, the repetition of immersing, withdrawal and annealing procedures for 5, 15 and 30 times did not change phase composition of coating dramatically. No characteristic peaks to other phosphate or titanate crystalline phases appear in the XRD patterns. However, such repeating slightly increased the intensity of peaks attributable to the phosphates. Surprisingly, these results demonstrate that the number of coating procedures does not influence on the crystallization of calcium phosphate coatings. Thus, suggested sol-gel

chemistry route could be used for the preparation of CHAp-TCP coatings containing titanium dioxide onto Ti substrate.

Apparently, characterization of Ti substrates repeatedly heated at 1000 ºC using FTIR spectroscopy confirms the XRD analysis results. FTIR spectra of the Ti samples calcined at 1000 °C contain low intensity broad bands at 3450 cm^{-1} and 1610 cm^{-1}. The intensities of these bands, which could be assigned to the adsorbed water during the exposure of dried samples to air [219], remained unchanged with calcination temperature. In addition, there is a broad band at 1000–550 cm^{-1} which is assigned to the characteristic metal-oxygen (Ti–O) vibrations.

The FTIR spectra of the corresponding films obtained from Ca-P-O sol-gel using dip-coating technique are presented in Fig. 27.

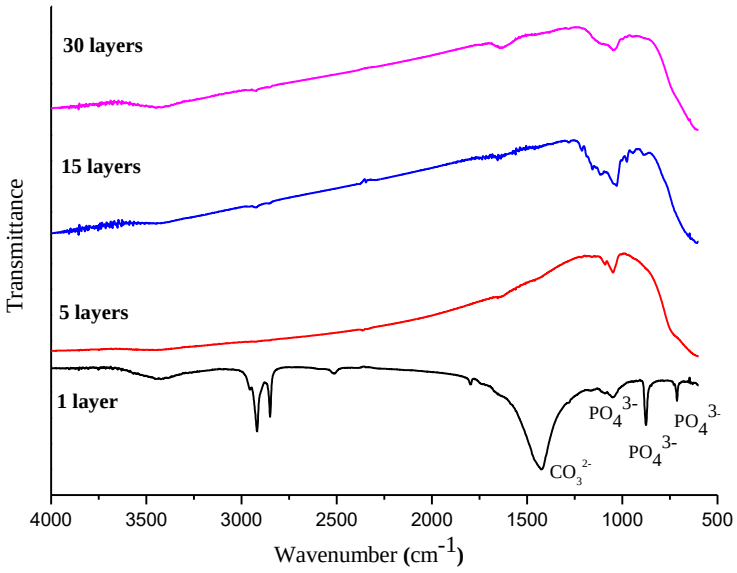

Fig. 27. FTIR spectra of the Ca-P-O sol-gel samples annealed at 1000 °C after each dipping procedure for 5 h in air.

In the spectrum of the sample obtained after one immersing, withdrawal and annealing procedure the peaks in the range of 1100-575 cm^{-1} attributable to the P-O vibrations in PO_4^{3-} ($Ca_{10}(PO_4)_6(OH)_2$ and $Ca_3(PO_4)_2$) are visible [220]. The corresponding characteristic bands of stretching vibrations of CO_3^{2-} are at

~1450 cm^{-1} [221]. Also, very intensive peaks in the range of 3000-2250 cm^{-1} could be observed in the FTIR spectrum of this sample. However, the origin of these vibrations is not clear. As a result of long-range heating the peaks at 3000-2250 cm^{-1} and 1450 cm^{-1} disappeared. Besides, in all spectra the bands at 3450 cm^{-1} and 1610 cm^{-1} are visible as well. Therefore the FTIR spectra indicate the presence of phosphates in the samples.

The textural properties of different specimens were investigated by scanning electron microscopy (SEM). Fig. 28 shows SEM micrographs of pure titanium substrates heated at 1000 °C and obtained at different magnifications. As seen from Fig. 28, the surface of titanium substrate consists of the regular shaped crystallites with a size of 3-10 μm. It is obvious that these grains are rhombohedral titanium dioxide crystallites formed during annealing of Ti substrate in air. The size of TiO_2 crystallites increases with increasing duration of annealing. Quite different surface morphology was determined for the sol-gel synthesized phosphate films on the titanium substrate.

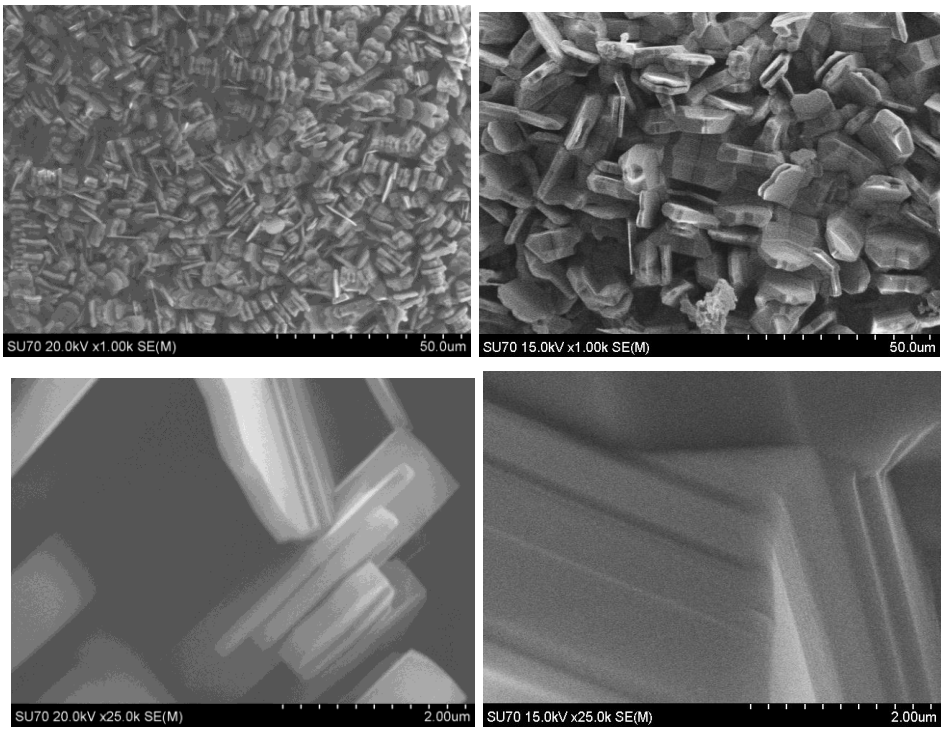

Fig. 28. SEM micrographs of Ti substrates repeatedly heated at 1000 ºC for 5 h with heating rate of 1 ºC/min: 5 times (at left) and 15 times (at right).

The SEM micrographs of the corresponding CHAp-TCP samples are displayed in Figs. 29 and 30.

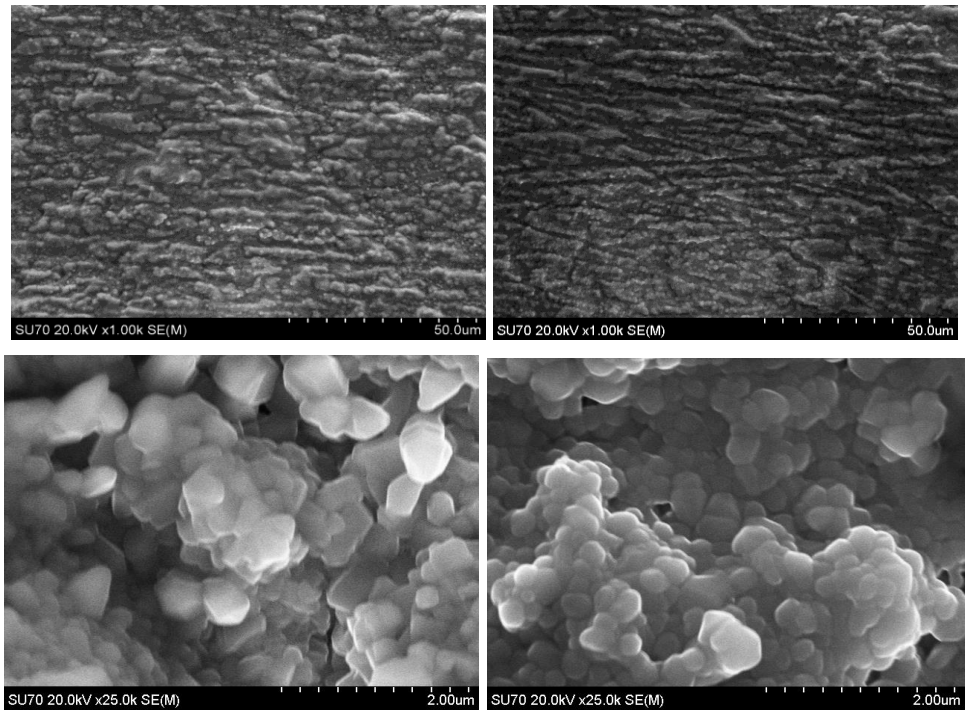

Fig. 29. SEM micrographs of samples containing 1 layer (at left) and 5 layers (at right).

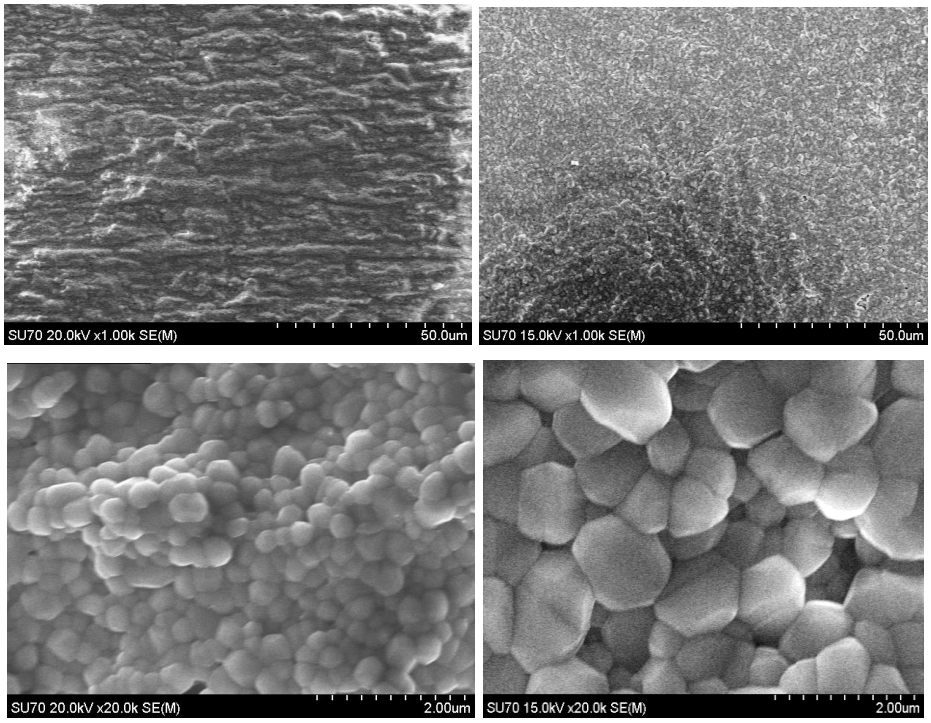

Fig. 30. SEM micrographs of samples containing 15 layers (at left) and 30 layers (at right).

The SEM micrographs clearly show that already first layer contains CHAp-TCP products which consist of aggregated spherical particles less than 300 nm in size. According to the SEM micrographs presented in Fig. 29 the coatings of 1 and 5 layers have similar structural characteristics. A progressive change in morphology of specimens is evident with increased immersing time. The formation of smaller and very homogeneously distributed spherical particles with an average grain size of 200 nm is evident for the coatings with 15 layers (see Fig. 30). The coatings of 30 layers have similar structural characteristics. However, the size of spherical particles increased significantly up to 0.6-0.8 μm with increasing amount of the layers on the substrate. Finally, the micrographs of Ca-P-O sol-gel calcined at 1000 °C show highly uniform and crystalline particles with smooth surfaces. There are no macro cracks or pores. Therefore, the proposed sol-gel technique appears to be very attractive way to make a high density, homogeneous CHAp-TCP coatings on Ti substrate.

In order to estimate hydrophobic properties of the produced thin films the contact angle measurements (CAM) were performed [222]. Surprisingly, the hydrophobicity of CHAp-TCP films was found to be slightly dependent on the number of coating procedures. The representative results are presented in Table 13. As seen, the contact angle of the Ti substrate coated with 5 layers from Ca-P-O sol-gel showed a highest contact angle (~35°). The contact angle of specimens produced with 15 and 30 dipping times has very similar values (~26-29°). The hydrophobicity of such films clearly should be dependent on the chemical composition of the coating. The composite materials containing the highest amount of crystalline $Ca_{10}(PO_4)_6(OH)_2$ phase should be more hydrophilic, since only calcium hydroxyapatite contains hydroxy groupings. Since the hydrophobic properties of the samples are relatively the same, the amount of $Ca_{10}(PO_4)_6(OH)_2$ and $Ca_3(PO_4)_2$ should be comparable. These results of contact angle measurements are in a good agreement with the results of XRD analysis.

Table 13. CAM results on CHAp-TCP coatings on Ti substrate.

Number of layers	Mean contact angle (degrees)
0	67.2 ± 0.2
1	13.7 ± 0.2
5	35.3 ±0.2
15	30.0 ± 0.2
30	26.4 ± 0.2

4.1.2. Spin-coating approach

Fig. 31 represents the XRD patterns of CHAp thin films obtained from Ca-P-O sol-gel on titanium or Ti/$CaTiO_3$ substrates using spin-coating technique. Small peaks of $Ca_{10}(PO_4)_6(OH)_2$ and $Ca_3(PO_4)_2$ are observed in the sample after 5 spin-coating and annealing procedures. Also sharp peaks of TiO_2 (rutile) are observed. However, the calcium titanate sub-layer did not promote the formation of CHAp.

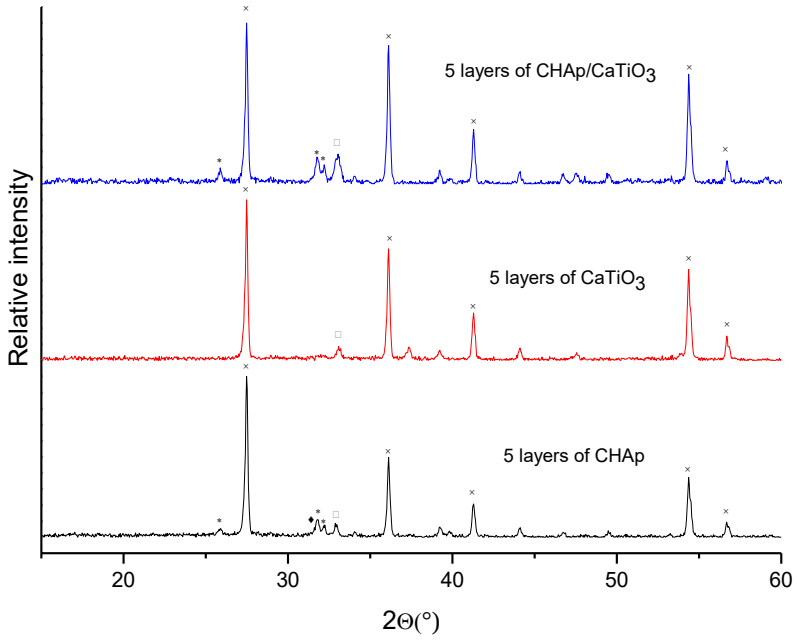

Fig. 31. XRD patterns of CHAp thin films obtained from Ca-P-O sol-gel on titanium substrate (at bottom) and calcium titanate sublayer (at top) using spin-coating technique. The XRD pattern in the middle represents sublayer of $CaTiO_3$. Diffraction lines are marked: * - $Ca_{10}(PO_4)_6(OH)_2$ [PDF: 74-0566], ♦ - $Ca_3(PO_4)_2$ [PDF: 70-2065], □ - $CaTiO_3$ [PDF: 78-1013] and x – TiO_2 [PDF: 21-1276].

4.1.3. Conclusions

It was demonstrated that an aqueous sol-gel technique is suitable for the formation of calcium hydroxyapatite/phosphate composite ($Ca_{10}(PO_4)_6(OH)_2$ and $Ca_3(PO_4)_2$) coatings on titanium substrate using dip-coating and spin-coating techniques. The XRD and FTIR measurements confirmed that the samples also contain TiO_2 (rutile). Interestingly, using dip-coating technique, the repetition of immersing, withdrawal and annealing procedures for 5, 15 and 30 times did not change phase composition of coating dramatically. The SEM micrographs clearly showed that first layer already contained CHAp-TCP products, which consist of aggregated spherical particles less than 300 nm in size. The micrographs of Ca-P-O sol-gel calcined at 1000 °C showed highly uniform and crystalline particles with smooth surfaces. There are no macro cracks or pores. The hydrophobic properties of thin films measured by CAM were associated with phase composition of CHAp-TCP coatings.

4.2. Sol-gel synthesis and characterization of calcium hydroxyapatite thin films synthesized on silicon substrate

Recently, it was demonstrated that silicon significantly improve osteoblastic response on calcium phosphate bioceramics, probably, since it presents in trace concentrations in natural bone. Therefore, this part of dissertation focuses on the synthesis of CHAp coatings on silicon substrate by the same sol-gel approach using dip-coating and spin-coating techniques. 1, 5, 15 and 30 layers of thin films were analysed and characterized using different analysis methods.

4.2.1. Dip-coating approach

Fig. 32 represents the XRD patterns of films on Si obtained from Ca-P-O sol-gel using dip-coating technique.

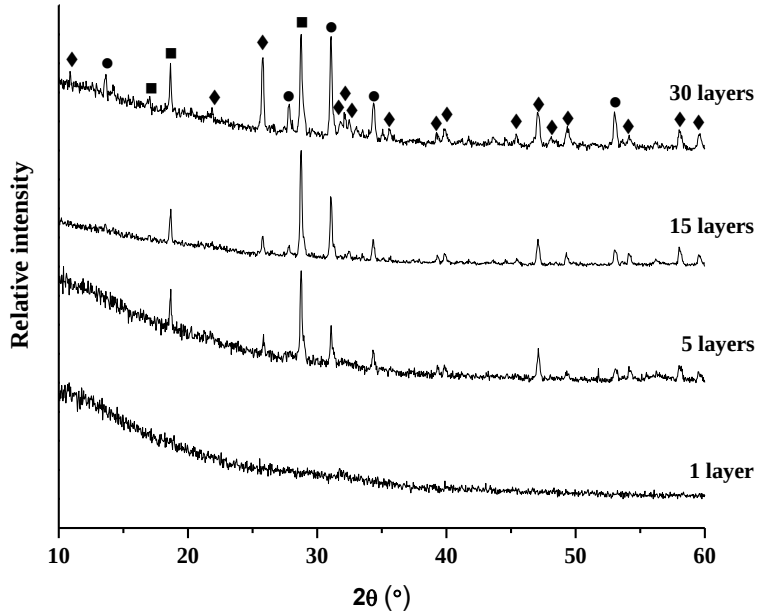

Fig. 32. XRD patterns of the Ca-P-O sol-gel samples annealed at 1000 °C after each dipping procedure for 5 h in air. Diffraction lines are marked: ♦ - $Ca_{10}(PO_4)_6(OH)_2$ [PDF: 73-1731], ■ - $Ca_3(PO_4)_2$ [PDF: 86-1585] and ● - $Ca_2P_2O_7$ [PDF: 71-2123].

These results present the influence of the number of coating procedures on the crystallization of calcium phosphate coatings. As seen from Fig. 32, after first immersing, withdrawal and annealing procedure no peaks attributable to the $Ca_{10}(PO_4)_6(OH)_2$ or $Ca_3(PO_4)_2$ crystal phases are observed. The layer formed contains only amorphous materials. However, already after five dipping and annealing times the main characteristic peaks attributable to tricalcium phosphate $Ca_3(PO_4)_2$ and dicalcium diphosphate $Ca_2P_2O_7$ (DCDP) crystal phases appear in the XRD pattern. The repetition of immersing, withdrawal and annealing procedures for 15 times did not change phase composition of coating. However, such repeating increased the crystallinity of phosphates significantly since the diffraction lines became sharper and intense. Finally, with further increasing of calcium phosphate layers up to 30, the formation of calcium hydroxyapatite is evident (diffraction lines of CHAp are marked as solid rhombus) [223]. The $Ca_3(PO_4)_2$ and $Ca_2P_2O_7$ phases also remain in the sample obtained after 30 immersing and annealing procedures.

Thus, suggested sol-gel chemistry route could be successfully used for the preparation of CHAp-TCP coatings containing dicalcium diphosphate onto silicon substrate.

The textural properties of the synthesized samples were also investigated. Fig. 33 shows SEM micrographs (secondary electron (SE) and back scattered electron (BSE) images) of pure silicon substrate and sample obtained after first immersing, withdrawal and annealing procedure calcined at 1000 °C.

The brightness of the silicon substrate on BSE image is highly homogeneous over the entire measuring area. Moreover, the SEM micrographs clearly show that already first layer contains Ca-P-O intermediate amorphous products which consist of differently shaped particles. The additional homogenization of the intermediates and further sol-gel processing are necessary to get CHAp-TCP. The SEM micrographs of other three samples are presented in Fig. 34. A progressive change in morphology of specimens is evident with increased immersing time. The formation of differently shaped particles (spherical particles and plate-like grains) with an average grain size ranging between 1 and 2 μm is evident from these investigations. According to the SEM micrographs presented in Fig. 34 the coatings of 15 and 30 layers have similar structural characteristics. There are no macro cracks or pores. However, the amount of spherical particles slightly decreases with increasing amount of the layers on the substrate. Finally, the micrographs of Ca-P-O sol-gel calcined at 1000 °C show highly uniform and crystalline particles with smooth surfaces. Therefore, the proposed sol-gel technique appears to be very attractive way to make a high density, homogeneous CHAp-TCP ceramic composites. The BSE images clearly demonstrate that most of the material is finely divided, however, the distribution of its chemical elements is not uniform.

The formation of multiphasic system composed of 3 different phases is evident. Such observations partially support previous results obtained by XRD analysis. Fig. 32 clearly shows the formation of $Ca_{10}(PO_4)_6(OH)_2$, $Ca_3(PO_4)_2$

and $Ca_2P_2O_7$ crystalline phases only in the sample obtained after 30 immersing and annealing procedures.

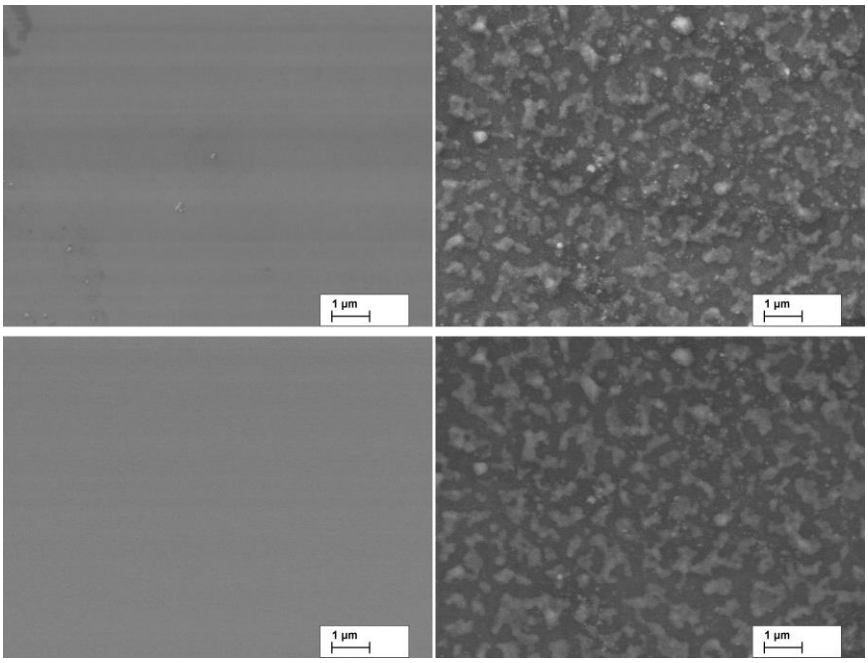

Fig. 33. SEM micrographs of silicon substrate (at left) and sample containing 1 layer of Ca-P-O sol-gel calcined at 1000 °C (at right) in SE (at top) and BSE (at bottom) modes.

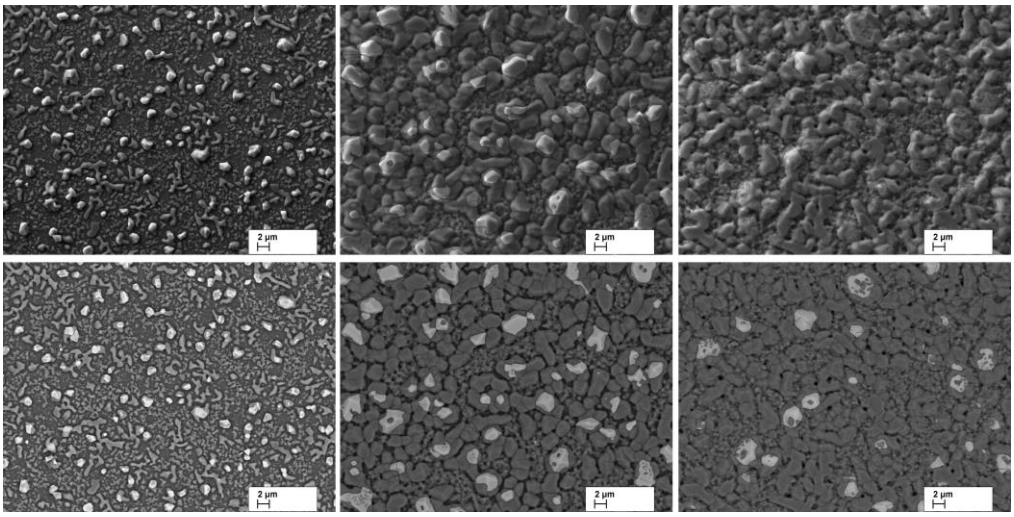

Fig. 34. SEM micrographs of sample containing 5 layers (at left), 15 layers (at middle) and 30 layers (at right) of Ca-P-O sol-gel calcined at 1000 °C in SE (at top) and BSE (at bottom) modes.

On the other hand, the negligible $\upsilon_1(PO_4)$ band attributable to CHAp [224] could be determined in the Raman spectra of the samples prepared using 5, 15 and 30 immersing and annealing procedures. The Raman spectra of the CHAp-TCP specimens are shown in Fig. 35. So, the formation of amorphous $Ca_{10}(PO_4)_6(OH)_2$ phase along with crystalline calcium phosphates is also possible [225].

Typical AFM (Atomic force microscopy) 3D images of the calcium phosphate/hydroxyapatite thin films prepared with different number of coating procedures are presented in Figs. 36-39. AFM images reveal a substantial difference of their surface morphology. The surface of 1 layer film (see Fig. 36) exhibits smooth and homogeneous surface morphology with no special surface features. Only few submicroscopic bumps of about 250 nm diameter are visible. The intensity and size of bumps on the surface increases monotonically with increasing amount of layers up to 15.

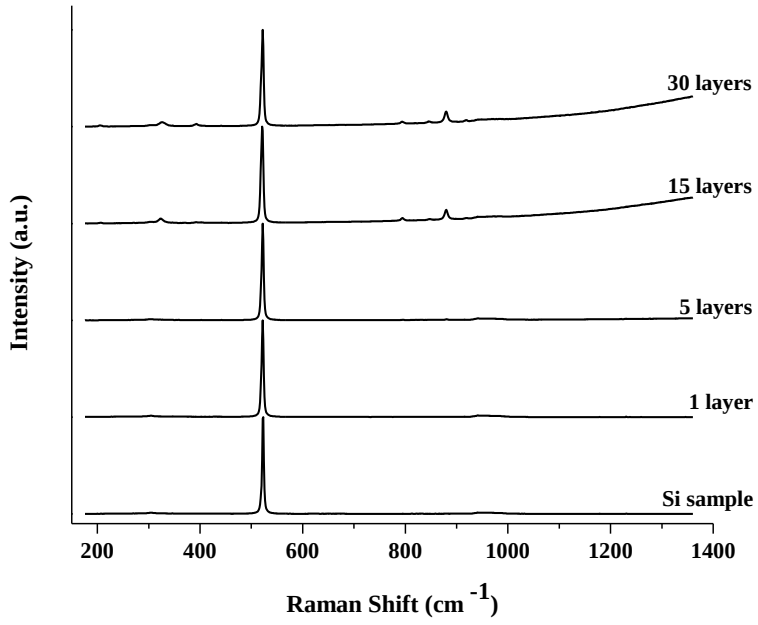

Fig. 35. Raman spectra of the Ca-P-O sol-gel samples annealed at 1000 °C after each dipping procedure for 5 h in air.

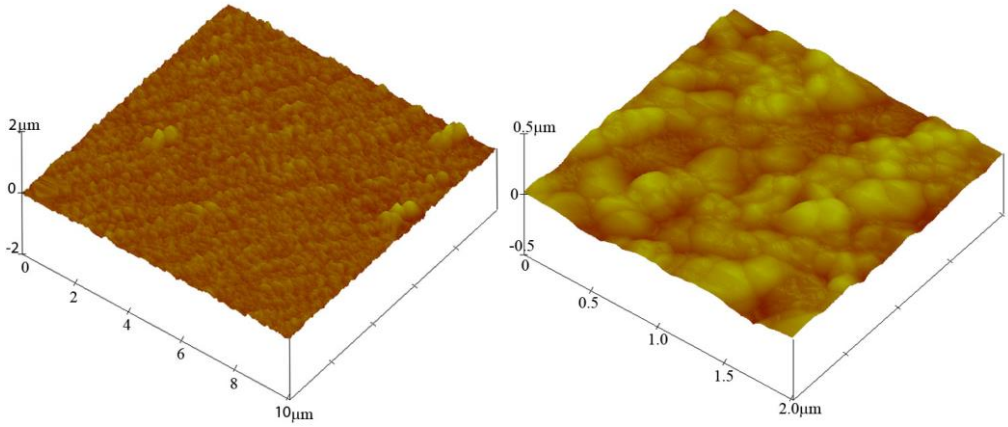

Fig. 36. Surface morphology of film (1 layer) obtained by calcination of Ca-P-O sol-gel.

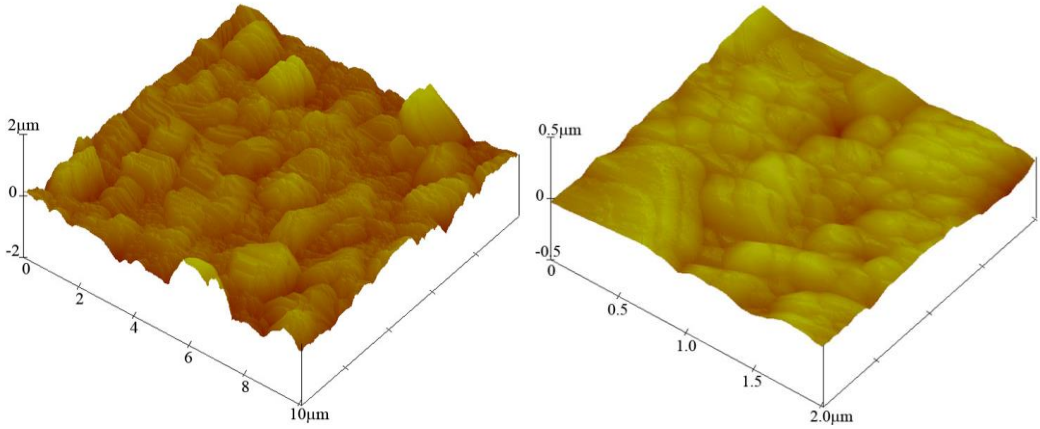

Fig. 37. Surface morphology of film (5 layers) obtained by calcination of Ca-P-O sol-gel.

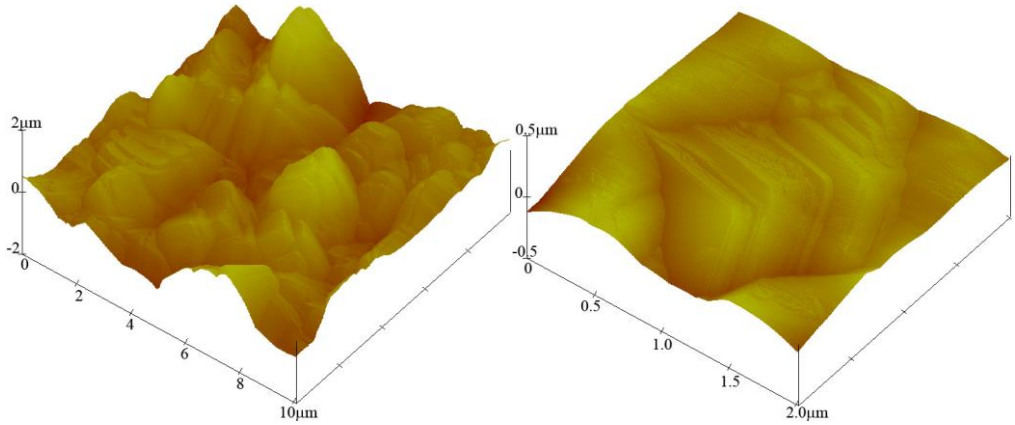

Fig. 38. Surface morphology of film (15 layers) obtained by calcination of Ca-P-O sol-gel.

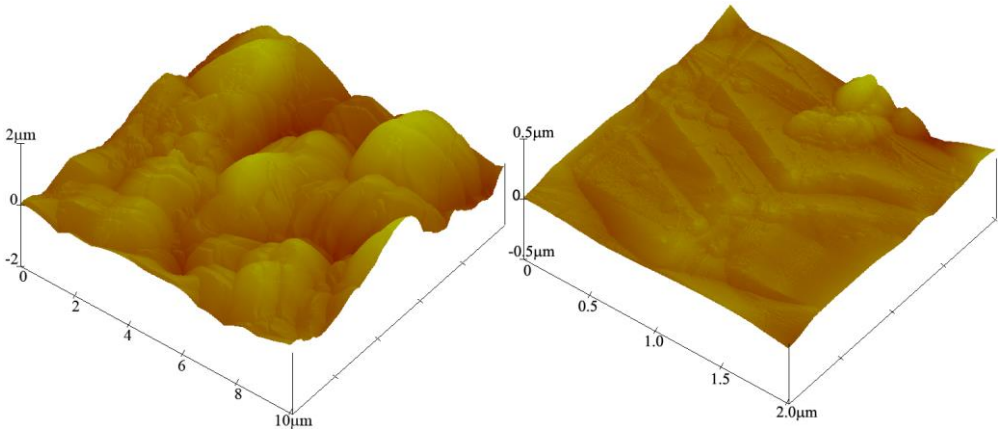

Fig. 39. Surface morphology of film (30 layers) obtained by calcination of Ca-P-O sol-gel.

The bumps on the surface of calcium phosphate films originate from the explosive elimination of the residual solvent and complexing reagents [226]. Interestingly, with further sol-gel processing (30 layers) the surface of film appeared more smooth and less defected (see Fig. 39). This may be associated with changes in phase composition of CHAp-TCP coatings. The roughnesses measured by AFM are shown in Table 14.

The RMS roughness values measured by AFM were compared for different surface areas. As seen, the tendency of variation of surface roughness remains the same. Moreover, the RMS roughness results show very good correlation with SEM results.

Table 14. Surface roughness measured by AFM on phosphate/hydroxyapatite samples.

Number of layers	RMS (Rq, nm)	
	Surface area 2/2µm	Surface area 10/10µm
0	0.2	0.2
1	17.1	20.0
5	22.2	90.7
15	45.3	174.8
30	19.1	166.1

In order to estimate hydrophobic properties of the produced thin films the contact angle measurements were performed. Surprisingly, the hydrophobicity of CHAp-TCP films was found to be slightly dependent on the number of

coating procedures. The representative results are presented in Fig. 40 and Table 15.

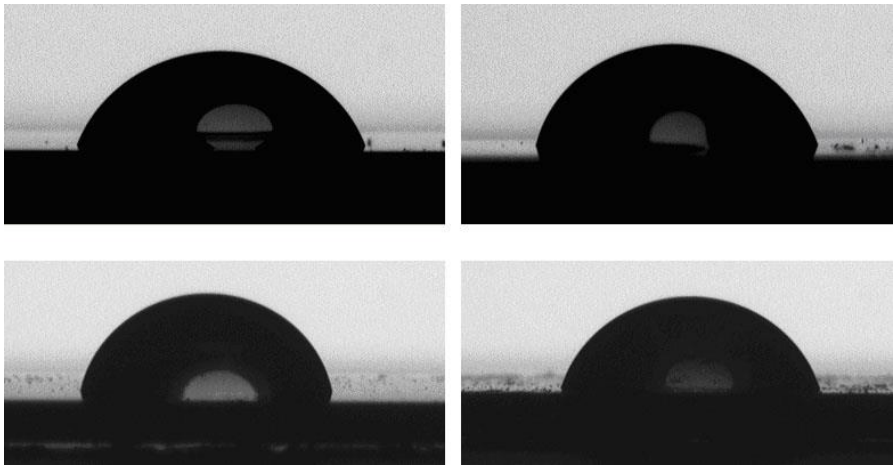

Fig. 40. Images of water droplets on the surfaces of substrate (at left, top) and CHAp-TCP coatings obtained by forming 1 layer (at right, top), 15 layers (at left, bottom) and 30 layers (at right, bottom).

Table 15. Surface properties measured by CAM on phosphate/hydroxyapatite samples deposited using different dipping times.

Number of layers	Mean contact angle (degrees)
0	67.2 ± 0.4
1	79.0 ± 0.5
5	77.3 ± 0.5
15	86.7 ± 0.5
30	75.0 ± 0.5

As seen, the contact angle of the silicon substrate is about 67^{o}. The substrate coated with 1 and 5 layers from Ca-P-O sol-gel showed a higher contact angle (~77-79°). The contact angle of specimen produced with 15 dipping times has the highest value (~87°). Finally, the contact angle of the surface coated with 30 dipping times decreased till 75°. Thus, hydrophobicity of obtained thin films clearly depends on the phase composition of the coating. The last composite material contains the highest amount of crystalline $Ca_{10}(PO_4)_6(OH)_2$ phase. Since only calcium hydroxyapatite contains hydroxy groupings, it is not

surprising that the samples with higher concentration of $Ca_3(PO_4)_2$ and $Ca_2P_2O_7$ crystalline phases possess relatively higher hydrophobic properties. Moreover, the results of contact angle measurements are in a good agreement with the results of surface roughness measured by AFM.

The optical properties of CHAp-TCP thin films synthesized using sol-gel process were also investigated. It is interesting to note, that UV-vis reflectance spectra of all samples are very similar. In Fig. 41 the UV-vis reflectance spectra of substrate and thin films obtained using different number of coating procedures are compared.

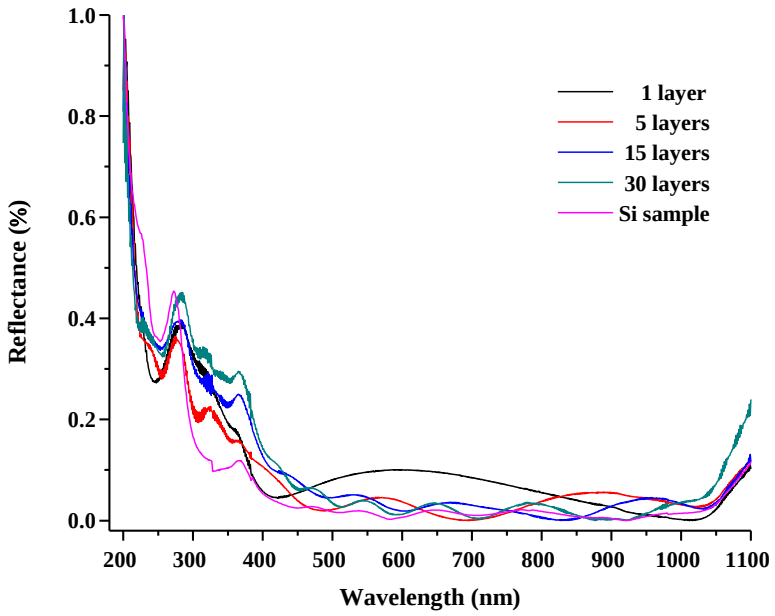

Fig. 41. The reflectance spectra of substrate and of CHA-TCP coatings obtained using different number of coating procedures.

Evidently, the reflectance spectra of substrate and thin films obtained by the sol-gel processing are very similar independent on dipping time. This observation let us to conclude that sol-gel derived CHAp-TCP films are very thin. As seen, several periodically repeating absorptions could be observed in the wavelength region of 200-450 nm. However in the higher wavelength region (≥ 450 nm), in whole wavelength region the reflectance is almost

constant, i.e. not wavelength dependent. Such composites additionally doped by rare-earth elements would have an excellent optical quality [227, 228].

4.2.2. Spin-coating approach

Fig. 42 presents XRD patterns of Si substrate and coatings obtained by spin-coating silicon with Ca–P–O sol–gel solution.

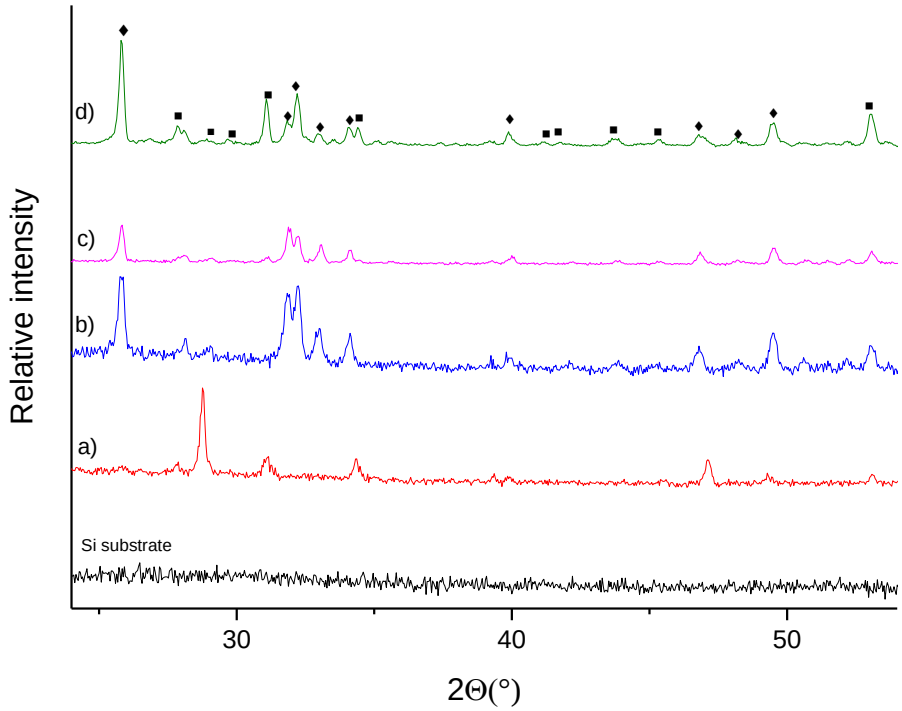

Fig. 42. XRD patterns of the Si substrate and sol-gel derived calcium hydroxyapatite films on Si substrate annealed at 1000 °C after each spinning procedure for 5 h in air. (a) 1, (b) 5, (c) 15 and (d) 30 layers. The diffraction lines are marked: ♦ - $Ca_{10}(PO_4)_6(OH)_2$ [PDF: 74-0566], ■ - $Ca_3(PO_4)_2$ [PDF: 70-2065].

The XRD analysis results also show the influence of number of spinning on the crystallization of calcium hydroxyapatite on Si substrate. The XRD pattern of sample obtained after 1 spinning contains only diffraction peaks attributable to tricalcium phosphate. The calcium hydroxyapatite is evidently forming in the end product obtained after 5 spinning and annealing procedures. In the coatings with 15 and 30 layers of Ca–P–O precursor sol-gel the calcium hydroxyapatite phase is forming as dominating crystalline phase along with

minor amount of tricalcium phosphate. Thus, the XRD analysis data proved that calcium hydroxyapatite could be easily obtained from sol–gel precursor solution on Si substrate using a spin-coating technique.

In Fig. 43 the SEM micrographs of CHAp samples containing 1, 5, 15 and 30 layers of synthesis product are presented. Obviously, the progressive changes in the surface morphology of CHAp films with increasing the spinning time are seen. The formation of small particles less than 100 nm in size proceeds on the Si surface already after first spin-coating procedure.

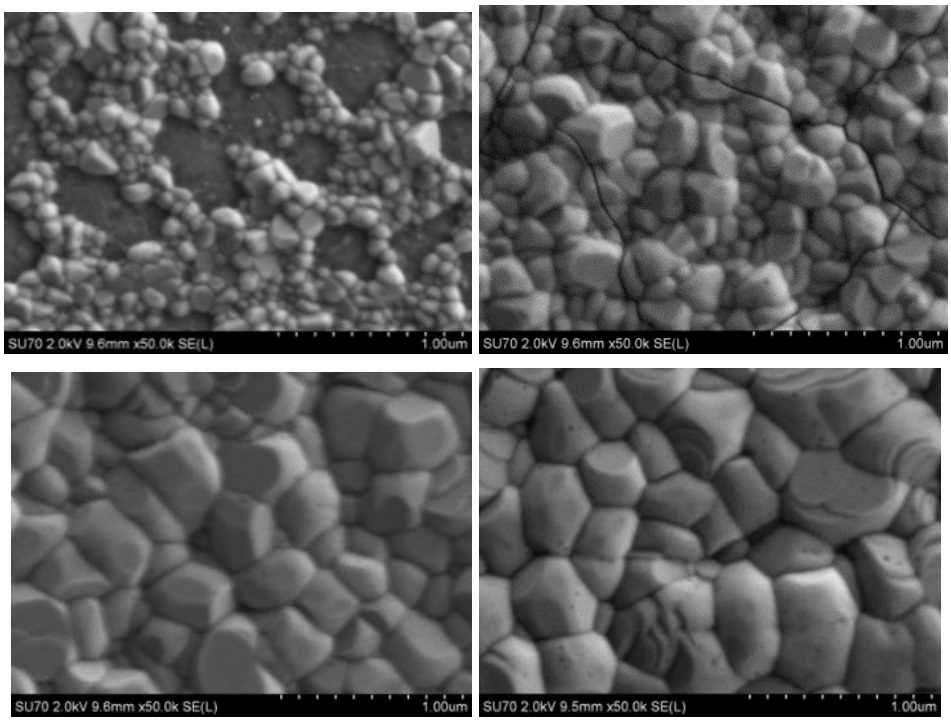

Fig. 43. SEM micrographs of samples containing 1 layer (at left, top), 5 layers (at right, top), 15 layers (at left, bottom) and 30 layers (at right, bottom) of Ca-P-O sol-gel calcined at 1000 °C after each spin-coating procedure (magnification 50000x).

However, the surface is uneven and coated incompletely with calcium phosphate. Different view is seen on the surface of CHAp sample containing 5 layers. The surface of substrate is not expressed anymore. Moreover, the silicon substrate is completely coated by calcium hydroxyapatite plate-like crystals about 100–200 nm in size with formation of small cracks [229]. The more homogeneous CHAp coatings have formed after 15 and 30 spinning and annealing procedures. Formation of regular polygons (similar to the

icosahedron) with narrow particle size distribution (300-400 nm) is evidently seen in the SEM micrographs. In Fig. 44 AFM 3D images of films containing 1, 5, 15 and 30 layers of calcium hydroxyapatite are presented. AFM images also show significant difference in the morphology between CHAp samples synthesized using different spin-coating time. The AFM images of the samples obtained after first and fifth spin-coating and annealing procedures are rather similar. The surfaces are rough and contain similar bumps. However, the CHAp sample containing 5 layers has more homogeneous surface and larger crystals which is in a good agreement with SEM results. The AFM images of the specimens containing 15 and 30 layers are quite distinctive. The surface of these CHAp films is smoother with larger crystals and more homogeneous crystal size distribution. Interestingly, at the surface area 10/10 μm large smooth areas were observed. However, the origin of such topography is not clear.

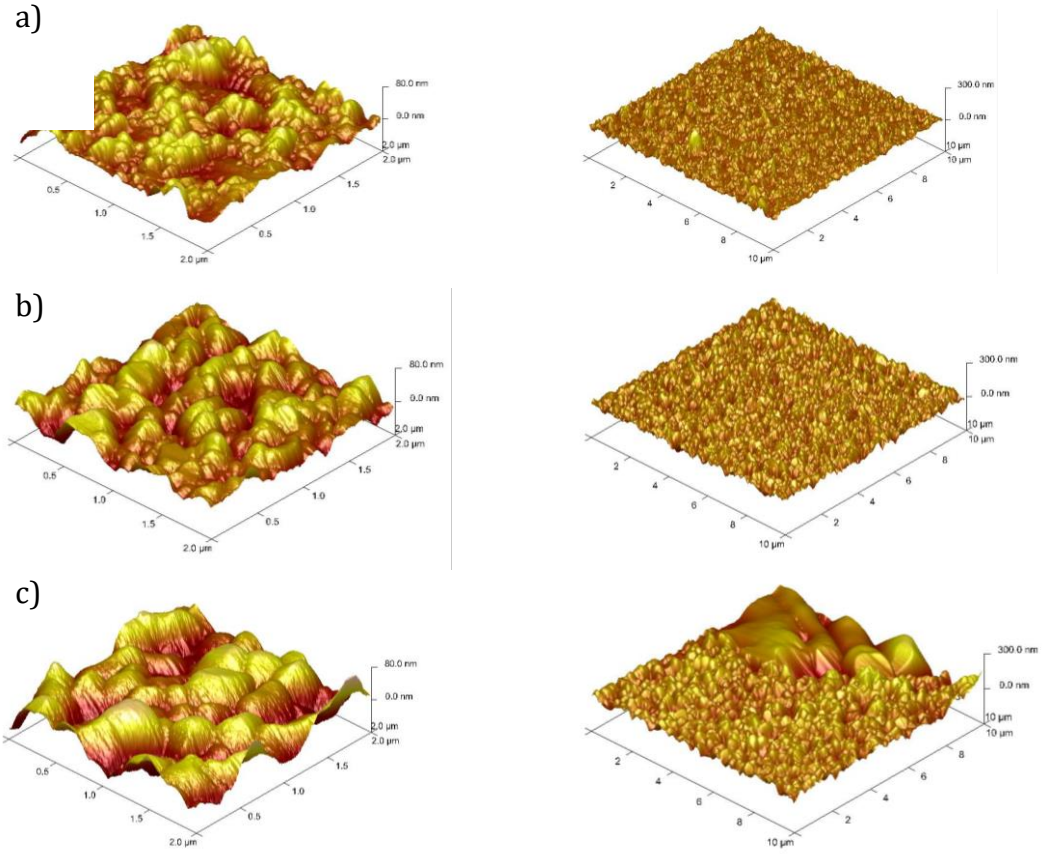

d)

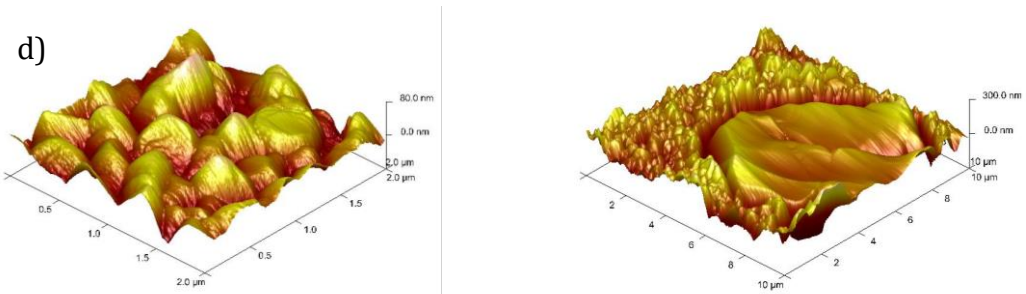

Fig. 44. AFM images of samples containing 1 layer (a), 5 layers (b), 15 layers (c) and 30 layers (d) of Ca-P-O sol-gel calcined at 1000 °C after each spin-coating procedure.

AFM results of surface roughness measurements for CHAp films are presented in Table 16. As seen from Table 16, almost linear correlation between values of roughness and number of layers could be observed. With increasing number of layers the roughness of CHAp films increased from 12.3 till 18.6 at surface area of 10/10 μm and from 16.9 till 44.2 at surface area of 2/2 μm.

Table 16. The AFM results of surface roughness measurements for CHAp films.

Number of layers	RMS (Rq, nm)	
	Surface area 2/2μm	Surface area 10/10μm
1	12.3	16.9
5	13.8	24.8
15	17.1	32.8
30	18.6	44.2

Thickness of CHAp layers was measured using profilometer and SEM analysis of cross-sections of the films (Table 17).

The results evaluated with assumption that CHAp density is 3.2 g/cm^3. Obviously, the thickness of CHAp films increases monotonically with increasing number of spin-coating and annealing procedures. Also, the results presented in Table 17 shows that the absolute values of films thickness measured by different techniques are slightly different, however the tendency of monotonic increase of thickness from ~30 nm to ~1 μm remains almost the

same.

Table 17. Thickness of CHAp films measured with profilometer and SEM.

Number of layers	Thickness (nm)	
	Profilometer	SEM
1	26	28
5	35	57
15	994	581
30	1396	943

The synthesized CHAp coatings were also investigated using FTIR spectroscopy. However, all FTIR spectra are very similar. The absorption bands in the spectra of samples containing 1 and 5 layers are less intensive. In the spectra of all samples the absorption bands located at 2300–1950 cm^{-1} which could be attributed to Si-H vibrations of silicon substrate are seen [230]. The absorption bands of ~1100 cm^{-1} and ~650 cm^{-1} belong to the P-O vibrations in the phosphate groups [231]. Absorption bands visible at ~780 cm^{-1} could be attributed to Si-O vibrations of Si substrate [230].

Fig. 45 shows Raman spectra in wavenumber region from 600 to 1250 cm^{-1} of Si substrate and CHAp sample containing 30 layers. Excitation wavelength was 632.8 nm. The spectra were recorded at the centre of the specimens. The broad band with sharp peak near 941 cm^{-1} belongs to overtone spectrum of Si substrate. Difference spectrum clearly shows the peak at 961 cm^{-1}. This band corresponds to symmetric stretching vibration of phosphate groups in $Ca_{10}(PO_4)_6(OH)_2$ [65, 232].

To determine hydrophobic and hydrophilic properties of the CHAp samples the contact angle measurements were recorded. The obtained results are presented in Fig. 46 and Table 18. The contact angle measured on the sample containing 1 layer of synthesis product is less (61.0°) than determined for the substrate (65.7°). This could be associated with fact, that the surface of sample

containing 1 layer of Ca–P–O precursor sol-gel is uneven and coated incompletely with calcium phosphate. Hydrophobic properties of films increased with crystallization of CHAp on the Si substrate. For example, in the sample containing 5 layers of CHAp the contact angle increased to 90.8°. However, with further increasing number of layers of CHAp, the hydrophobic properties of films decrease or remain very similar. For example, recently biomimetic niobium oxide coatings on stainless steel for orthopaedic applications with enhanced wettability have been fabricated [233]. The contact angle determined for these coatings varied in the range of 75.8°–83.2°. Accordingly, the sol–gel derived CHAp coatings synthesized in this work with contact angle of 79.3°–85.5° could also accelerate structural and functional connection between living bone and the surface of a load-bearing artificial implant.

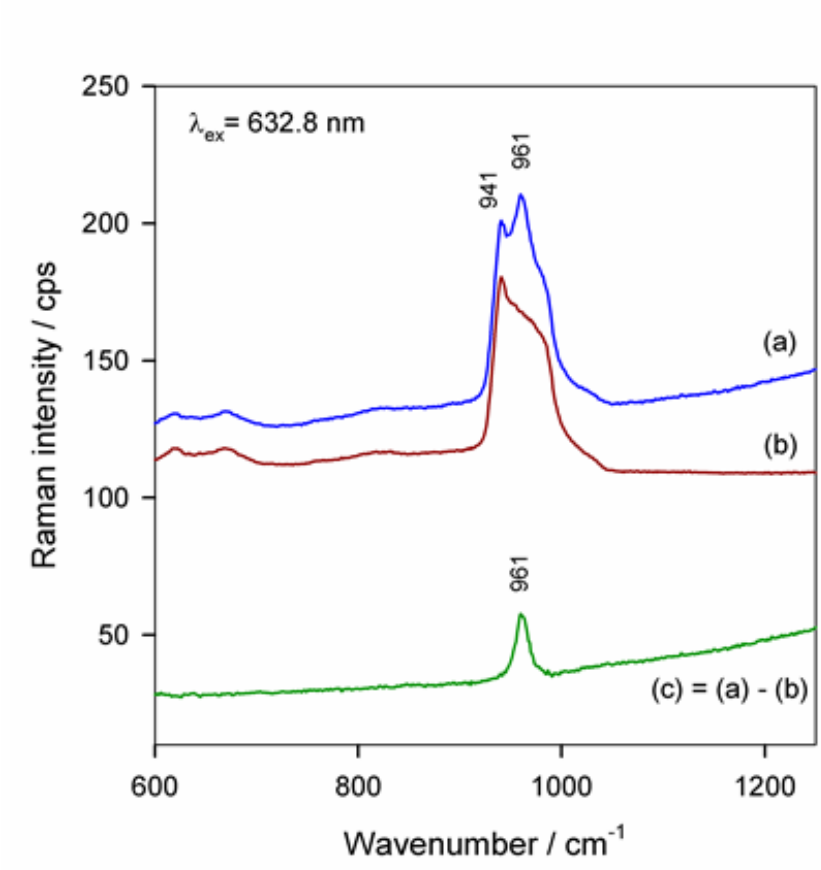

Fig. 45. Raman spectra of sample containing 30 layers (a) and Si substrate (b). Difference spectrum (c) is also shown.

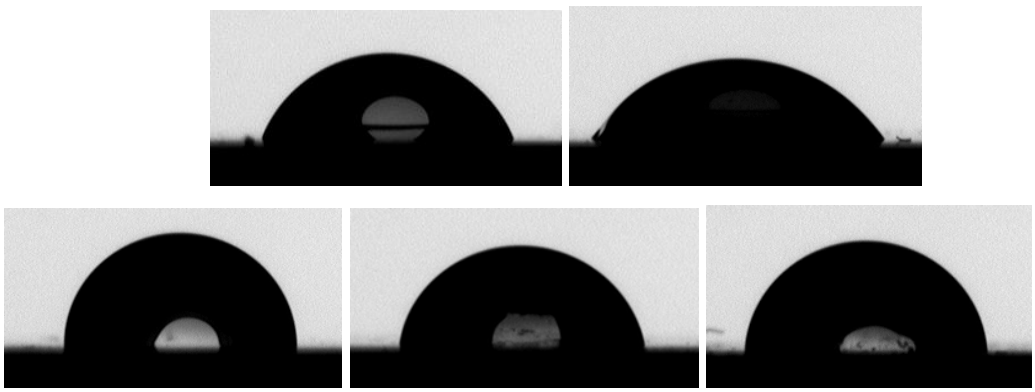

Fig. 46. Images of water droplets on the surfaces of Si substrate (at top and left) and Ca-O-P coatings continuously from 1 to 30 layers.

Table 18. Mean contact angle values measured on CHAp films.

Number of layers	Mean contact angle (degrees)
0	65.7 ± 0.4
1	61.0 ± 0.4
5	90.8 ± 0.6
15	79.3 ± 0.5
30	85.5 ± 0.5

Well-known tape adhesion test [234, 235] was carried out to evaluate the adherence of the CHAp coatings. The quality of coating adhesion measurements showed that the detachment of coating is less than 5% and could be classified between 5B and 4B according to ASTM standard. The results indicate that obtained CHAp coatings have good adhesion strength [236].

4.2.3. FTIR spectroscopy – a powerful tool for the characterization of calcium hydroxyapatite thin films on silicon substrate

The synthesized CHAp coatings on Si substrate were deeply investigated using FTIR spectroscopy. Free phosphate group PO_4^{3-} has tetrahedral symmetry (T_d) and vibrational spectrum consists of four modes. Totally symmetric stretching ν_1 (A_1) and double-degenerate symmetric deformation ν_2 (E) modes are only Raman active, while triple-degenerate asymmetric stretching ν_3 (F_2) and asymmetric deformation ν_4 (F_2) modes are active both in

infrared and Raman spectra [237–239]. In crystalline state all vibrational modes became active in infrared spectra because the crystal field induced the lowering of the symmetry. Fig. 47 shows FTIR spectra in the wavenumber region of phosphate group symmetric stretching ν_1 (975–940 cm^{-1}) and asymmetric bending ν_4 (660–520 cm^{-1}) modes [240–242].

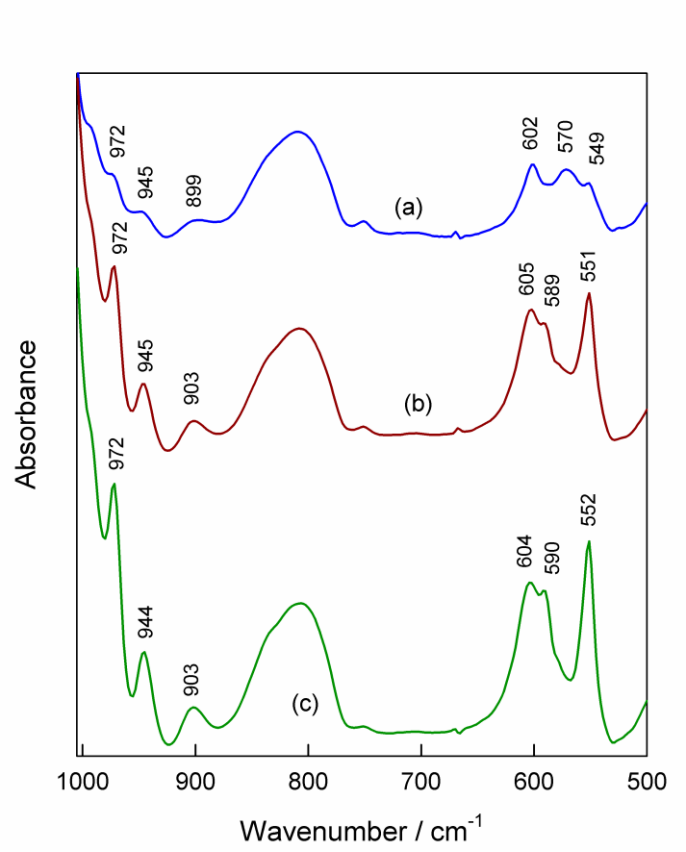

Fig. 47. FTIR absorbance spectra in region of phosphate group ν_1 and ν_4 bands of samples containing (a) 5 layers, (b) 8 layers, and (c) 10 layers of Ca–P–O sol-gel deposited by spin-coating technique and annealed at 1000 ^{o}C.

The characteristic bands in the asymmetric stretching ν_3 spectral region (1190–1030 cm^{-1}) were not analyzed because of their overlapping with intense silicon oxide band. More detailed analysis of spectral region for ν_4 band revealed the presence of 570 cm^{-1} components in the case of samples prepared from 8- (Fig. 48) and 10-layers.

Several spectroscopic arguments suggest the absence of hydroxyapatite (CHAp) structure ($Ca_{10}(PO_4)_6(OH)_2$) for all the studied samples. First of all, the specific OH^- vibration mode near 635–630 cm^{-1} [243–245] is not visible in

our FTIR spectra. Secondly, the narrow high frequency O–H stretching band near 3571 cm^{-1} [245–247] is also absent (data not shown). Finally, the stoichiometric CHAp exhibits characteristic single ν_1 mode at 961–963 cm^{-1} [240, 245, 248]. In contrast, we observed two bands located at 945 and 972 cm^{-1} in ν_1 mode spectral region. Thus, infrared spectroscopy indicates dehydration of studied samples. Mode detailed analysis of ν_1 and ν_4 spectral regions provides possibility to identify the nature of synthesized phosphates (Table 19). The well-defined ν_1 band at 945 cm^{-1} corresponds to peak position of totally symmetric vibrational mode from oxyhydroxyapatite $Ca_{10}(PO_4)_6(OH)_{2-2x}O_x$ [249]. In the limiting case (x = 1) this compound transforms to oxyapatite $Ca_{10}(PO_4)_6O$. Oxyapatite is reactive and will transform to hydroxyapatite in contact with water vapour, to lower its free energy [250]. Moreover, the XRD patterns of oxyhydroxyapatites or oxyapatites are almost identical to the XRD pattern of CHAp [205]. According to the literature data, the decomposition of CHAp can occur in very broad range of temperatures (600-1400 °C) [185, 202, 205, 251, 252]:

Step 1: $Ca_{10}(PO_4)_6(OH)_2 \rightarrow Ca_{10}(PO_4)_6(OH)_{2-2x}O_x + xH_2O$,

with $0 \leq x \leq 1$.

Step 2: $Ca_{10}(PO_4)_6(OH)_{2-2x}O_x \rightarrow Ca_{10}(PO_4)_6O + (1-x)H_2O$

If *x* reaches a critical value the destruction of the apatite channel structure occurs, and an equilibrium with tricalcium phosphate ($Ca_3(PO_4)_2$) and tetracalcium phosphate ($Ca_4(PO_4)_2O$) exists:

Step 3: $Ca_{10}(PO_4)_6O \rightarrow Ca_4(PO_4)_2O + Ca_3(PO_4)_2$

or $2Ca_{10}(PO_4)_6O \rightarrow 2Ca_3(PO_4)_2 + Ca_2P_2O_7 + 3\ Ca_4P_2O_9$

Detailed Raman and infrared spectroscopic analysis of two forms of tricalcium phosphate ($Ca_3(PO_4)_2$) revealed characteristic vibrational bands of β-$Ca_3(PO_4)_2$ structure at 972 and 945 cm^{-1} in the spectral range of ν_1 mode

[253]. Importantly, the α-$Ca_3(PO_4)_2$ form can be easily distinguished spectroscopically because of the single ν_1 band at 954 cm^{-1}. In the range of ν_4 vibrational mode the characteristic infrared bands were observed at 555 and 609 cm^{-1} for β-$Ca_3(PO_4)_2$ form and at 551, 563, 585, 597, and 613 cm^{-1} in the case of α-$Ca_3(PO_4)_2$ [253]. Position of infrared bands observed in this work both in the ν_1 and ν_4 spectral regions (Fig. 47) coincides well with the β-$Ca_3(PO_4)_2$ structure. This phase is stable in the room temperature to 1120 ^oC range [253]. Importantly, the β-$Ca_3(PO_4)_2$ structure is bioactive and surface layer might transform to hydroxyapatite at room temperature [253]. The structures of compounds obtained as a result of infrared spectroscopic studies are listed in Table 19. Comparison of the samples containing different layers shows slight difference between the 5-layer and 8/10-layer structures. Intensity of the 509 and 602 cm^{-1} bands increases almost linearly with increasing number of deposited layers (Fig. 49).

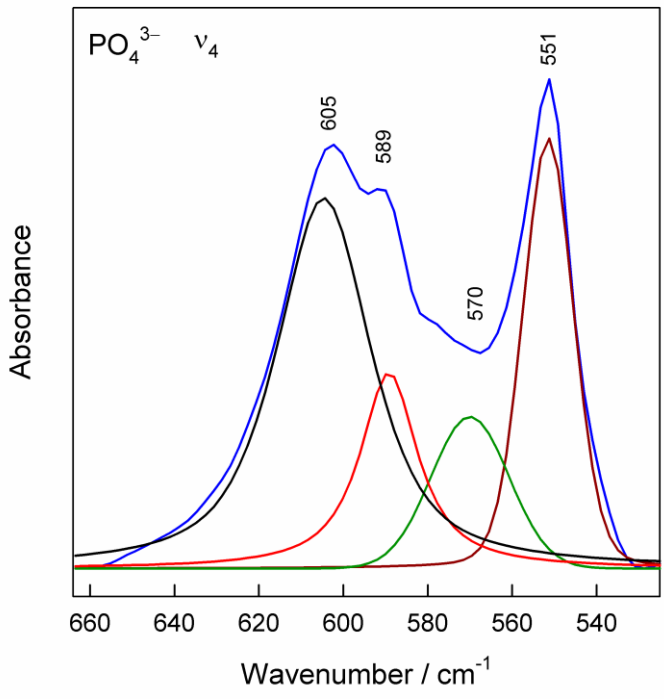

Fig. 48. FTIR absorbance spectra with fitted Gaussian-Lorentzian form components in region of phosphate group ν_4 band of a sample containing 8 layers of Ca–P–O sol-gel deposited by spin-coating technique and annealed at 1000 ^oC.

Table 19. Peak wavenumbers (cm^{-1}) and assignments of the infrared spectra for the Ca–P–O gel deposited by spin-coating technique and annealed at 1000 ^{o}C.

5 layers	8 layers	10 layers	Assignments[1]	Compound
549	551	552	ν_4 asymmetric deformation of PO_4^{3-}	β-$Ca_3(PO_4)_2$ [253]
570	570	573	ν_4 asymmetric deformation of PO_4^{3-}	$Ca_4(PO_4)_2O$ [239]/ β-$Ca_3(PO_4)_2$ [246]
–	589	590	ν_4 asymmetric deformation of PO_4^{3-};	β-$Ca_3(PO_4)_2$ [253]
602	605	604	ν_4 asymmetric deformation of PO_4^{3-}	β-$Ca_3(PO_4)_2$ [246, 253]
945	945	944	ν_1 symmetric stretching of PO_4^{3-}	$Ca_{10}(PO_4)_6(OH)_{2-2x}O_x$/$Ca_4(PO_4)_2O$/ β-$Ca_3(PO_4)_2$ [239, 249, 253]
972	972	972	ν_1 symmetric stretching of PO_4^{3-}	β-$Ca_3(PO_4)_2$ [246, 253]

[1]Based on references [237–239].

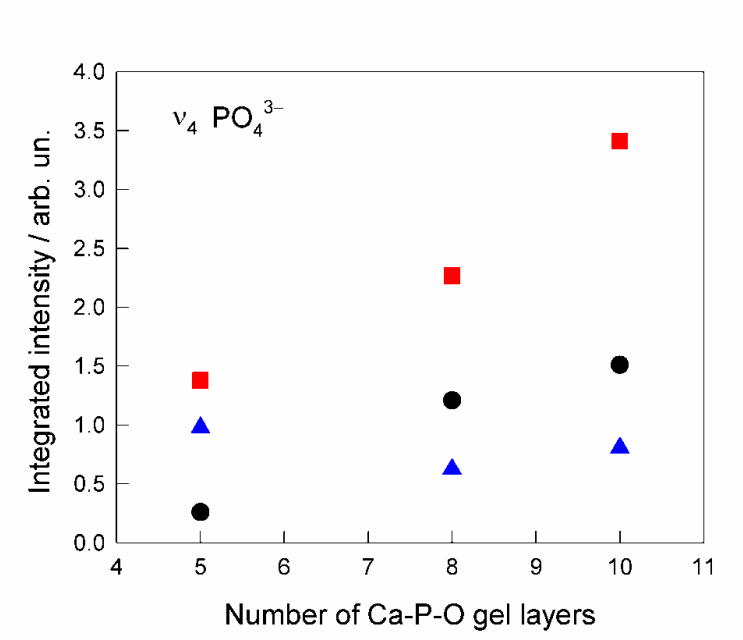

Fig. 49. Evolution of integrated intensity of ν_4 infrared absorption bands at 549 cm^{-1} (circles), 570 cm^{-1} (triangles), and 602 cm^{-1} (squares) on the number of Ca-P-O sol-gel layers.

However, in case of ν_4 mode at 570 cm^{-1}, the integrated absorption intensity remains similar for all the studied samples. This observation indicates presence of a slightly different calcium phosphate structure due to deposited initial 5 layers. Such structure might be stabilized because of the interaction of phosphate group with the substrate. Integrated absorption intensity of both ν_1 bands increases linearly with increasing number of deposited layers (Fig. 50).

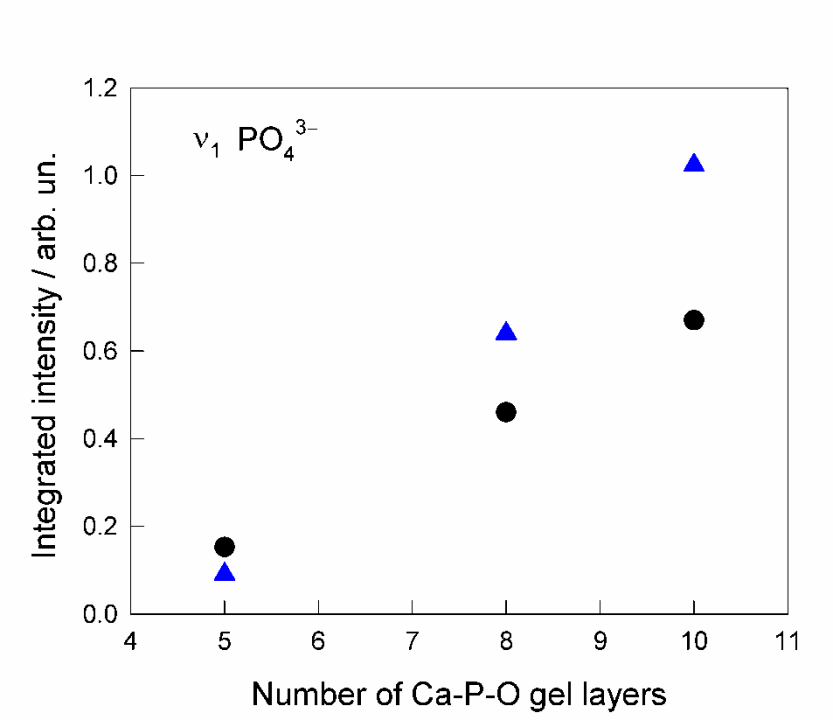

Fig. 50. Evolution of integrated intensity of ν_1 infrared absorption bands at 945 cm^{-1} (circles) and 972 cm^{-1} (triangles) on the number of Ca-P-O sol-gel layers.

4.2.4. Conclusions

The sol-gel method for the preparation of calcium phosphate/hydroxyapatite thin films on silicon substrate using dip-coating and spin-coating techniques has been developed. It was shown that adjustment of dip-coating conditions can be used to control the process of synthesis, phase purity and morphology of the bioceramic thin films. The formation of calcium phosphate/hydroxyapatite mixture is promoted by dipping time. According to XRD analysis data, the concentration of hydroxyapatite in the mixture

increases with increasing the repetition of dip-coating procedures. The formation of differently shaped particles (spherical particles and plate-like grains) with an average grain size ranging between 1 and 2 μm was determined from SEM measurements. The roughness of thin films measured by AFM and hydrophobic properties measured by CAM are associated with changes in phase composition of CHAp-TCP coatings. The results of Raman spectrometry showed the peak at 961 cm^{-1}, which corresponds to symmetric stretching vibration of phosphate groups in calcium hydroxyapatite proving the formation of high quality $Ca_{10}(PO_4)_6(OH)_2$ thin films on Si substrate using an aqueous sol–gel chemistry approach. FTIR spectroscopy revealed that intensity of ν_4 infrared absorption bands at 549 cm^{-1}, 570 cm^{-1}, 602 cm^{-1} and ν_1 infrared absorption bands at 945 cm^{-1}, 972 cm^{-1} increases with increasing the number of deposited layers. The specific OH^- vibration mode near 635–630 cm^{-1} and band near 3571 cm^{-1} was not visible in FTIR spectra. The well-defined ν_1 band at 945 cm^{-1} corresponds to peak position of totally symmetric vibrational mode from oxyhydroxyapatite $Ca_{10}(PO_4)_6(OH)_{2-2x}O_x$. Position of infrared bands observed in this work both in the ν_1 and ν_4 spectral regions coincides well with the β-$Ca_3(PO_4)_2$ structure. The results obtained demonstrated that calcium oxyhydroxyapatite, probably, have formed on Si substrate and crystallization of sol-gel derived calcium oxyhydroxyapatite depends on the number of layers.

4.3. Sol-gel synthesis and characterization of calcium hydroxyapatite thin films synthesized on quartz substrate

The results presented in this part of PhD thesis demonstrate that suggested sol-gel process is perfectly suitable for the synthesis of calcium hydroxyapatite on the quartz substrate allowing to control phase purity and morphological properties of CHAp. Again, 1, 5, 15 and 30 layers of calcium hydroxyapatite thin films were fabricated and characterized using different analysis methods.

4.3.1. Dip-coating approach

Fig. 51 presents XRD patterns of films on silica substrate obtained from Ca-

P-O aqueous precursor solution using dip-coating technique. As seen, after the first immersing, withdrawal and annealing procedures the formation of two crystalline phases $CaH_2P_2O_7$ and $Ca_{10}(PO_4)_6(OH)_2$ took place. More intensive diffraction peaks attributable to CHAp phase were observed in the XRD pattern of specimen obtained after five dip-coating procedures. Moreover, tricalcium phosphate $Ca_3(PO_4)_2$ phase has formed as well. With further increasing immersing, withdrawal and annealing to 15 times, the only peaks of calcium hydroxyapatite and calcium phosphate phases could be detected. However, the calcium hydrogen phosphate phase appeared in the sample prepared after 30 dipping procedures.

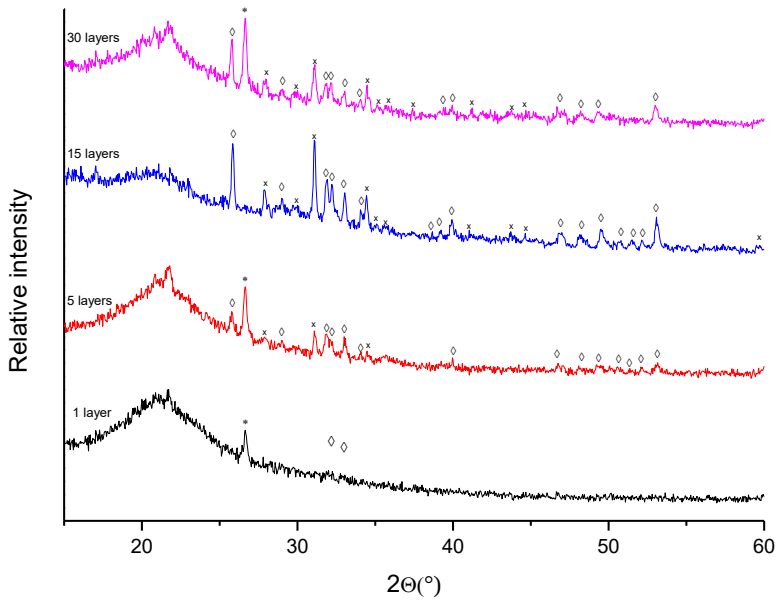

Fig. 51. XRD patterns of the Ca-P-O sol-gel annealed at 1000 °C after each dipping procedure for 5 h in air. Diffraction lines are marked: ◊ – $Ca_5(PO_4)_3(OH)$ [PDF:73-1731], × - $Ca_3(PO_4)_2$ [PDF: 70-2065] and ∗ - $CaH_2P_2O_7$ [PDF: 51-0200].

In Fig. 52 SEM micrographs of quartz substrate and the CHAp sample obtained after first immersing, withdrawal and annealing procedure is presented.

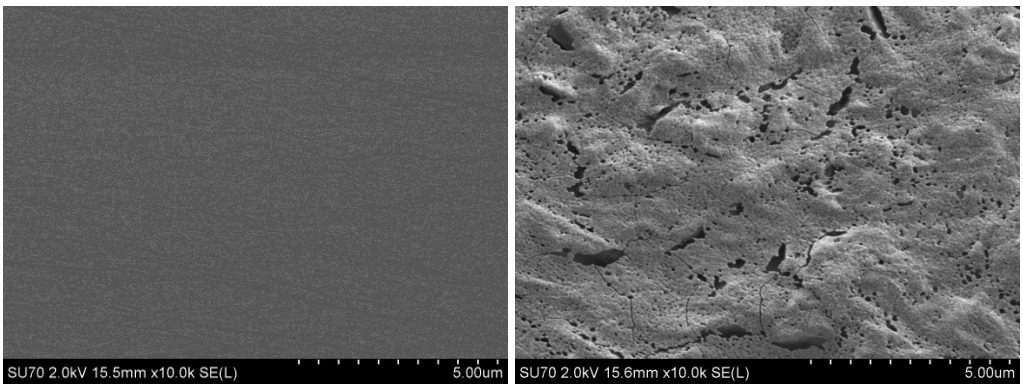

Fig. 52. SEM micrographs of quartz substrate (at left) and sample containing 1 layer (at right) of Ca-P-O sol-gel deposited by dip-coating technique and calcined at 1000 °C.

As seen, the surface of substrate is very smooth and differs significantly from coated one which contains material with clearly expressed cracks. The SEM micrographs of films containing 5, 15 and 30 layers of Ca-P-O sol-gel precursor are presented in Fig. 53. Apparently, the surfaces appeared to be highly dense, monolithic, with fewer amounts of cracks and relatively rough due to increased crystallinity of different phases. Besides, the continuous formation of plate-like crystals with increasing amount of layers could be observed.

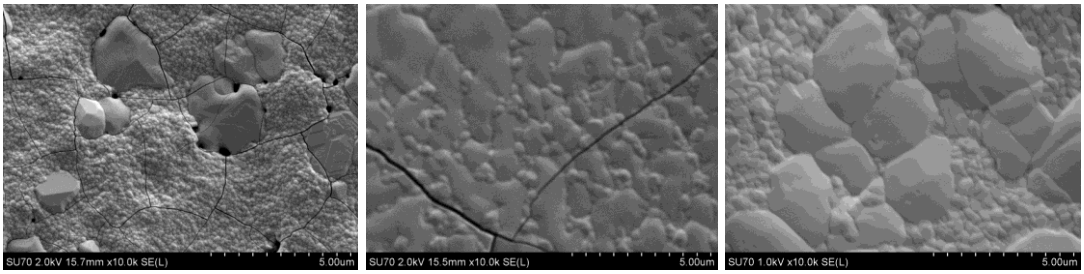

Fig. 53. SEM micrographs of samples containing 5 layers (at left), 15 layers (at middle) and 30 layers (at right) of Ca-P-O sol-gel deposited by dip-coating technique and calcined at 1000 °C.

Atomic force microscopy (AFM) 3D images of quartz substrate and sample containing one layer of CHAp obtained using dip-coating technique are presented in Fig. 54.

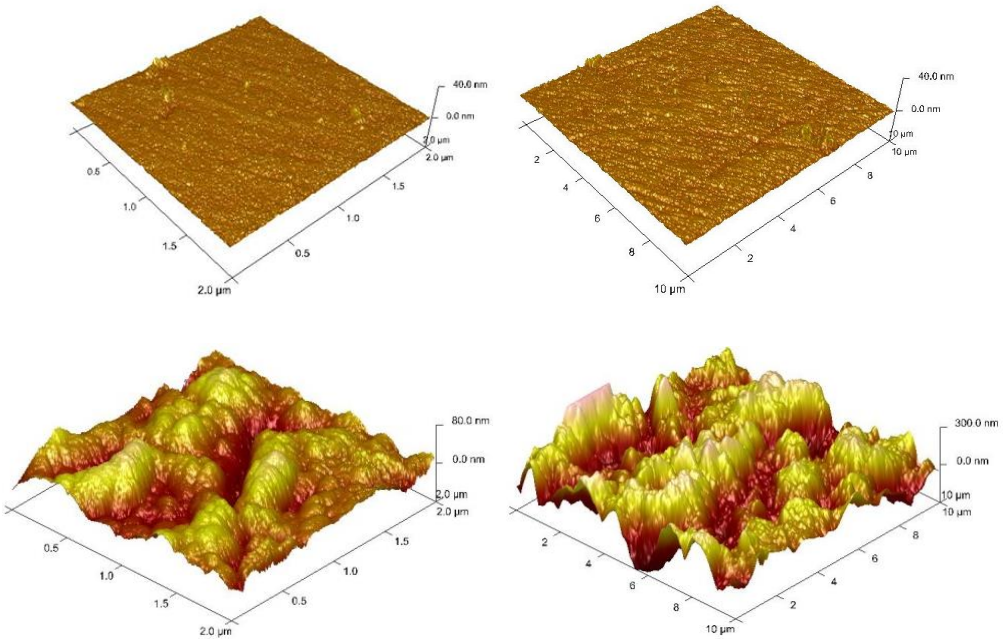

Fig. 54. AFM images of different areas of quartz substrate (at top) and sample containing 1 layer (at bottom) of Ca-P-O sol-gel deposited by dip-coating technique and calcined at 1000 °C.

Apparently, the AFM images show important differences between morphology of coated and uncoated surfaces. The surface of quartz substrate is rather smooth, however, the surface of coated sample is rough with bumps of about 300 nm in size located in the film. The AFM images of films containing 5, 15 and 30 layers of Ca-P-O sol-gel precursor are presented in Fig. 55 showing similar morphology of all specimens. The surfaces are not smooth having symmetrically and homogeneously distributed similar in size bumps.

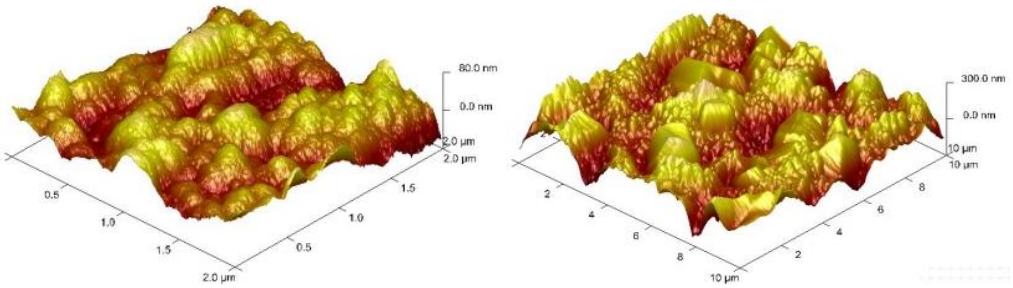

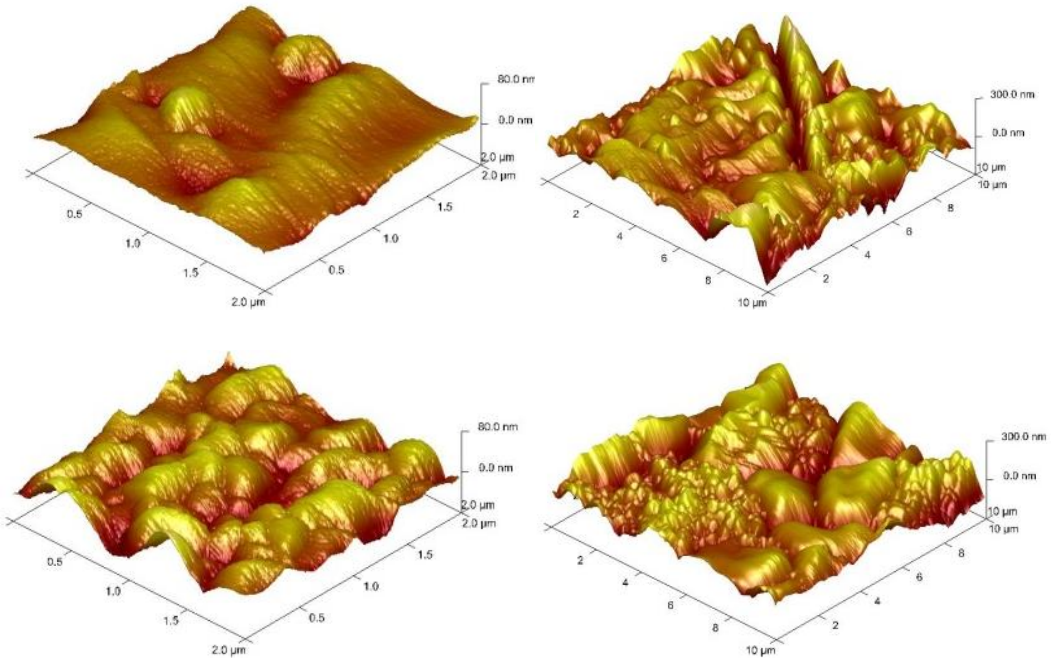

Fig. 55. AFM images of different areas of samples containing 5 layers (at top), 15 layers (at middle) and 30 layers (at bottom) of Ca-P-O sol-gel deposited by dip-coating technique and calcined at 1000 °C.

The results of roughness measurement by AFM for CHAp films from different surface areas are presented in Table 20. As one can see, for the dip-coated samples irregular dependence of the values of roughness on the number of layers could be observed.

Table 20. Surface roughness measured by AFM on CHAp films deposited using dip-coating technique.

Number of layers	RMS (Rq, nm)[a]	
	Surface area 2/2μm	Surface area 10/10μm
1	18.2	81.7
5	16.9	65.0
15	9.4	38.3
30	15.5	39.6

[a] The RMS roughness values for quartz substrate are 0.7 and 0.8, respectively.

The variable angle spectroscopic ellipsometric data of determination of thickness of CHAp layers deposited using dip-coating technique are presented in Table 21. Apparently, the thickness of CHAp layers deposited using dip-

coating technique increases monotonically with increasing number of dipping times.

To estimate hydrophobic and hydrophilic properties of CHAp films obtained using dip-coating technique the contact angle measurements (CAM) were recorded. The results of these investigations are summarized in Fig. 56 and Table 22. The hydrophobic properties depend on a number of layers of samples using dip-coating technique. As seen, the contact angle of dip-coated samples increases monotonically from 65.9° till 95.9° with increasing the amount of layers. The main increase was observed enhancing the amount of layers from 5 to 15. This very interesting tendency could be related with phase composition of CHAp films. As seen from Fig. 51 the crystallinity of CHAp also increases significantly after obtaining 15 and 30 layers on the substrate. Moreover, the only peaks of calcium hydroxyapatite and calcium phosphate phases could be detected in these specimens.

Table 21. The results for the determination of thickness of CHAp layers deposited using dip-coating technique.

Number of layers	Thickness (nm)
1	64.29 ± 0.13
5	244.71 ± 0.41
15	1255.69 ± 0.44
30	3170.07 ± 0.56

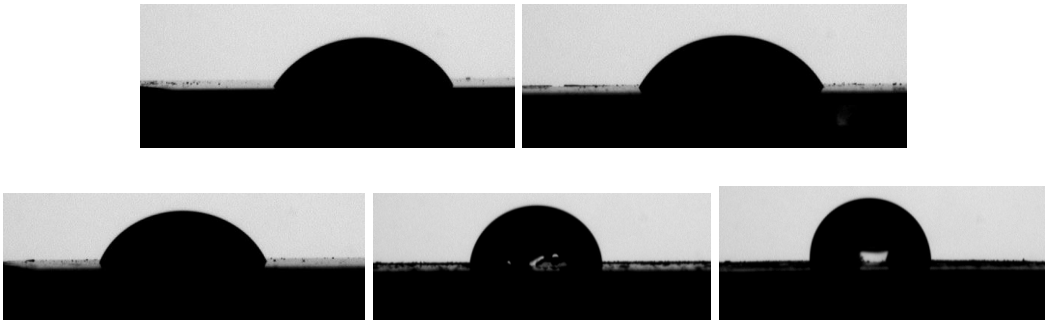

Fig. 56. Images of water droplets on the surfaces of quartz substrate (at top, at left) and CHA coatings (continuously from 1 to 30 layers) obtained by dip-coating technique.

Table 22. CAM results for CHAp films obtained using dip-coating technique.

Number of layers	Mean contact angle (degrees)[a]
1	65.9 ± 0.4
5	69.7 ± 0.4
15	86.4 ± 0.6
30	95.9 ± 0.6

[a] The contact angle value for quartz substrate is 47.2.

4.3.2. Spin-coating approach

In Fig. 57 the XRD patterns of CHAp films obtained by using spin-coating technique are shown. As seen, after the first spin-coating and annealing procedures the small diffraction lines of calcium hydroxyapatite could be observed. The intensity of these peaks evidently increases with increasing the amount of spinning procedures showing the better crystallization of $Ca_{10}(PO_4)_6(OH)_2$. Interestingly, the spin-coating derived CHAp thin films contains calcium phosphate as side phase, however, the formation of minor amount of $CaH_2P_2O_7$ phase has been detected. These XRD results let us to conclude that the crystallization of calcium hydroxyapatite on quartz substrate was influenced by number of spin-coating procedures. Apparently, more pure and crystalline CHAp has formed using spin-coating technique.

Fig. 58 represents the SEM micrographs of CHAp coatings obtained by spin-coating technique. As seen, the surface of substrate after deposition one layer of Ca–P–O sol-gel is very smooth and differs only slightly from the surface of the substrate. The formation of homogeneously distributed small particles on the surface of substrate after five spin-coating and annealing processes could be observed. The morphology of CHAp coatings changes dramatically with further increasing amount of layers. The formation of small crystals on the rough surface could be easily determined.

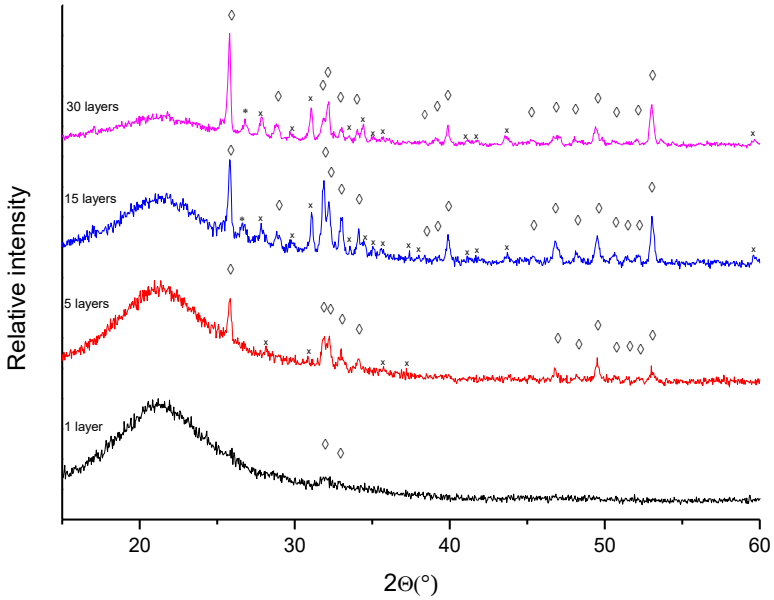

Fig. 57. XRD patterns of the Ca-P-O sol-gel annealed at 1000 °C after each spinning procedure for 5 h in air. Diffraction lines are marked: ◊ - $Ca_{10}(PO_4)_6(OH)_2$ [PDF: 74-0566], × - $Ca_3(PO_4)_2$ [PDF: 70-2065] and ∗ - $CaH_2P_2O_7$ [PDF: 51-0200].

In Fig. 59 AFM 3D images of samples containing 1, 5, 15 and 30 layers of CHAp synthesized by spin-coating technique are presented. The images show quite noticeable differences between morphological features of different samples. The surface of CHAp specimens with 15 and 30 layers is not smooth and contains more bumps in comparison with samples with fewer amounts of layers.

The results of roughness measurement by AFM for CHAp films from different surface areas are presented in Table 23. The values of roughness R_{RMS} of samples increases monotonically from 7.7 till 39.5 (at surface area of 10/10 μm) with increasing number of layers using spin-coating technique.

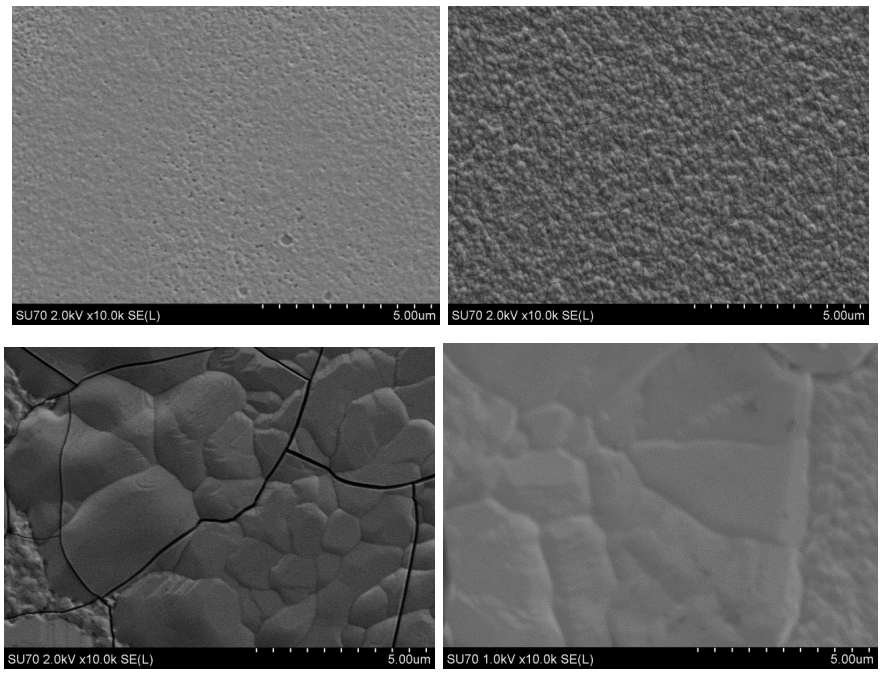

Fig. 58. SEM micrographs of samples containing 1 layer (at top, at left), 5 layers (at top, at right), 15 layers (at bottom, at left) and 30 layers (at bottom, at right) of Ca-P-O sol-gel deposited by spin-coating technique and calcined at 1000 °C.

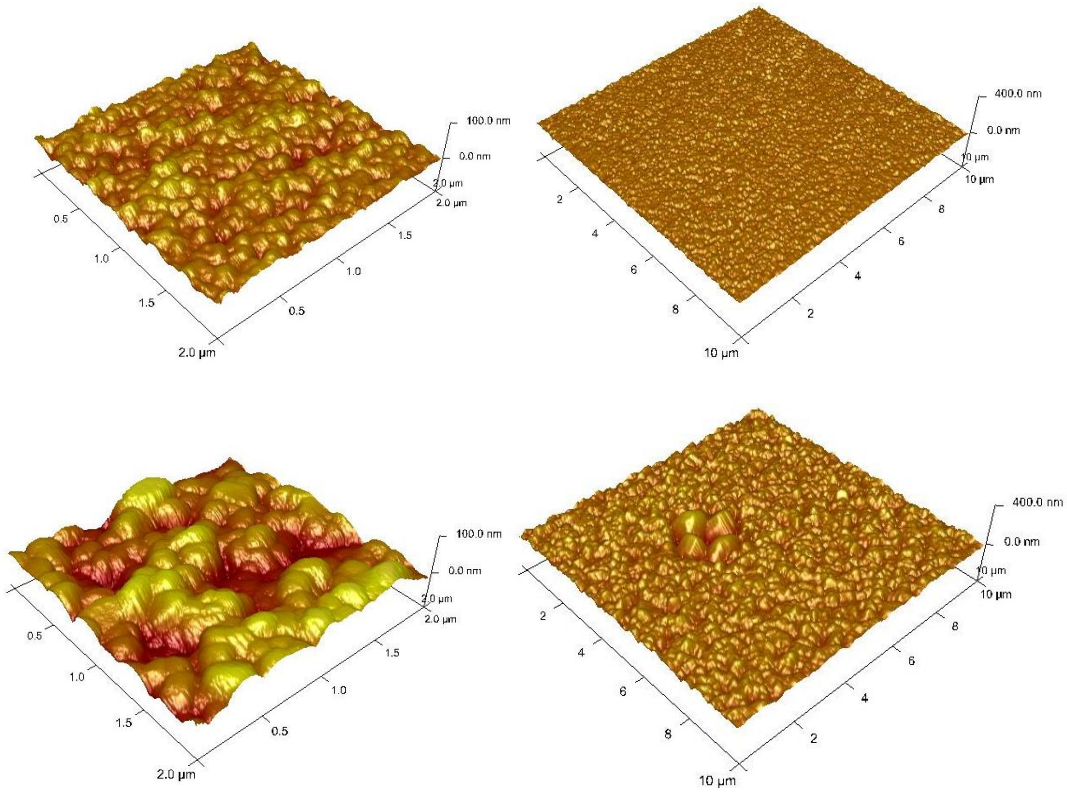

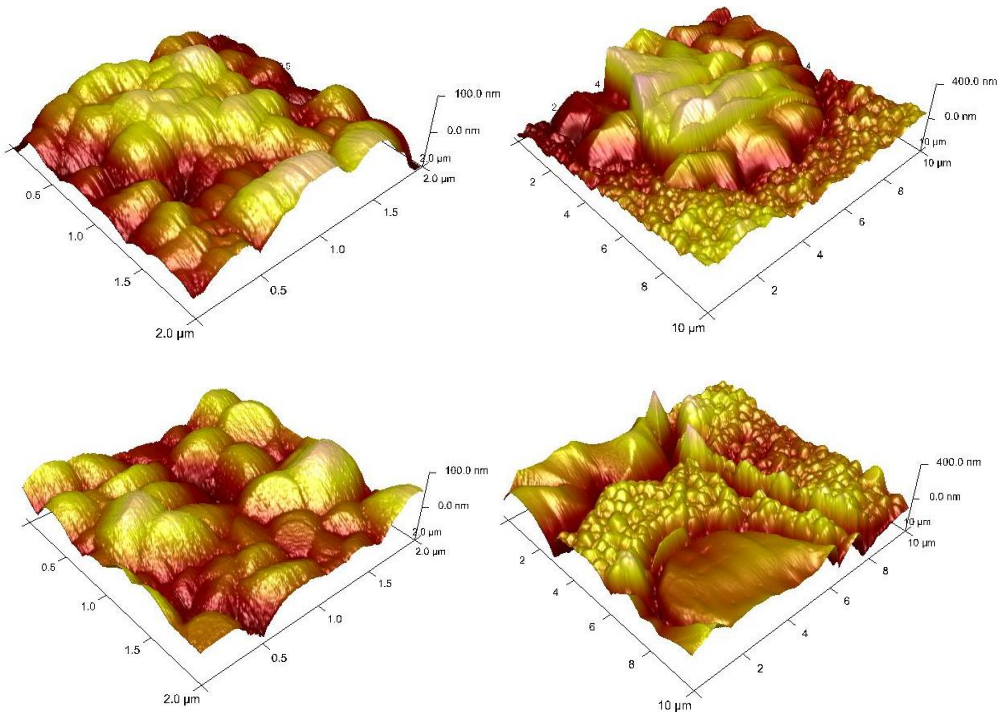

Fig. 59. AFM images of different areas of samples containing different layers of Ca-P-O sol-gel deposited by spin-coating technique and calcined at 1000 °C (from top to bottom: 1 layer, 5 layers, 15 layers and 30 layers.

Table 23. Surface roughness measured by AFM on CHAp films deposited using spin-coating technique.

Number of layers	RMS (Rq, nm)[a]	
	Surface area 2/2µm	Surface area 10/10µm
1	7.6	7.7
5	14.4	18.6
15	14.9	31.1
30	27.0	39.5

[a] The RMS roughness values for quartz substrate are 0.7 and 0.8, respectively.

The variable angle spectroscopic ellipsometric data of determination of thickness of CHAp layers using spin-coating technique are presented in Table 24. Apparently, the thickness of CHAp layers increases monotonically with increasing number spinning procedures.

FTIR spectra of CHAp samples containing 1, 5 and 15 layers showed intensive absorption lines located at ~1000 and 750 cm^{-1}, which unambiguously could be attributed to Si–O vibrations of quartz (Fig. 60).

Table 24. The results for the determination of thickness of CHAp layers deposited using spin-coating technique.

Number of layers	Thickness (nm)
1	20.13 ± 0.10
5	168.11 ± 0.32
15	994.55 ± 0.38
30	2704.17 ± 0.35

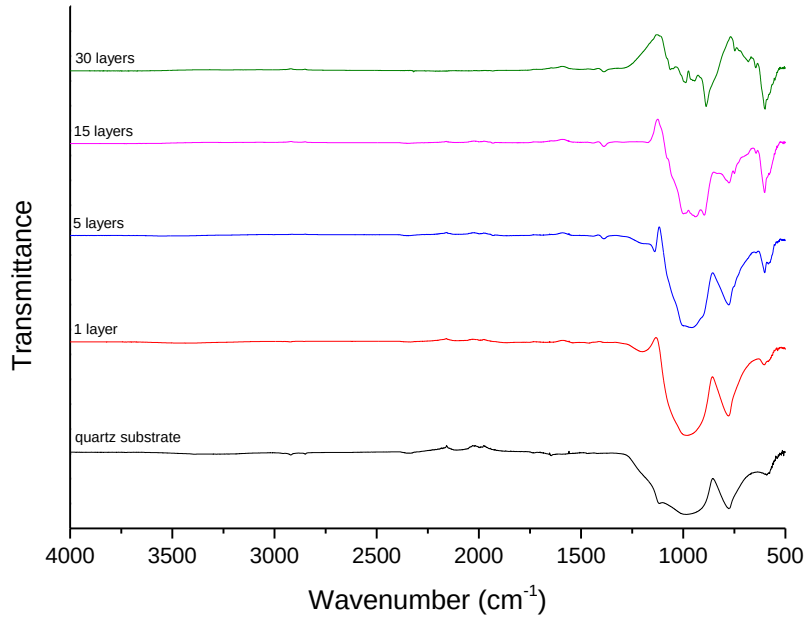

Fig. 60. FTIR spectra of quartz substrate and CHAp coatings obtained by spin-coating technique.

However, these bands almost disappeared in the FTIR spectra of CHAp samples containing 30 layers. In the spectra of these samples a complex band of the asymmetric stretching vibration of the phosphate group at 900–1100 cm^{-1} dominates. For the most of the samples, especially obtained by spin-coating technique with higher amount of spinnings, the region of symmetric stretching vibration of phosphate group at 940–970 cm^{-1} characteristic for β-$Ca_3(PO_4)_2$ and CHAp are observed in the FTIR spectra [138].

To estimate hydrophobic and hydrophilic properties of CHAp films obtained using spin-coating technique the contact angle measurements (CAM)

were recorded. The results of these investigations are summarized in Fig. 61 and Table 25.

The hydrophobic properties depend on a number of layers of samples using spin-coating technique. The same tendency like in the samples prepared by dip-coating technique was observed and for the samples obtained by spin-coating technique. Results clearly show the correlations between number of layers and contact angle values. With increasing number of layers, the hydrophobicity of surfaces increases as well. Again, the most considerable increase of contact angle from 56.3° till 72.3° was observed by changing spin-coating procedures from 5 to 15. This very interesting tendency could be related with phase composition of CHAp films like in the samples prepared by dip-coating procedure.

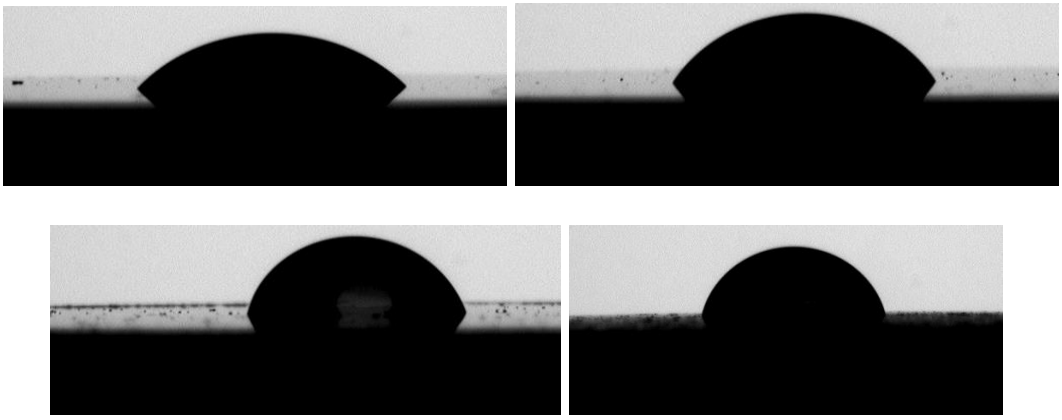

Fig. 61. Images of water droplets on the surfaces of CHA coatings (continuously from 1 to 30 layers) obtained by spin-coating technique.

Table 25. CAM results for CHAp films obtained using spin-coating technique.

Number of layers	Mean contact angle (degrees)[a]
1	47.2 ± 0.3
5	56.3 ± 0.3
15	72.3 ± 0.5
30	74.6 ± 0.5

[a] The contact angle value for quartz substrate is 47.2

4.3.3. Conclusions

Aqueous sol–gel method was used for the synthesis of calcium hydroxyapatite thin films on quartz substrate. Two different dip-coating and spin-coating techniques were applied for preparation of CHAp and compared in this study. The XRD results let us to conclude that the crystallization of calcium hydroxyapatite on the substrate was influenced by both number of dip- or spin-coating procedures and type of applied technique. The phase purity and crystallinity also depend on the amount of layers of end product. It was demonstrated, that more pure and crystalline CHAp has formed using spin-coating technique. SEM micrographs and AFM images were recorded to determine surface morphological features of thin films. The spin-coated films are slightly thicker in comparison with ones obtained using dip-coating technique. However, with increasing amount of layers the difference between thicknesses of differently obtained CHAp films increases with different rate. The obtained results of contact angle measurements clearly showed correlations between number of layers and contact angle values of CHAp surfaces. With increasing number of layers, the hydrophobicity of surfaces increased. Besides, the contact angle values of CHAp samples synthesized by two different coating techniques are also slightly different. The coatings obtained using spin-coating technique were more hydrophilic in comparison with dip-coated samples. The obtained materials could be effectively used as multifunctional delivery systems for biotechnological applications [254–257].

5. General conclusions

1. New sol-gel method for the preparation of calcium ($Ca_{10}(PO_4)_6(OH)_2$, CHAp) thin films on titanium substrate using dip-coating and spin-coating techniques has been developed. For the first time to the best our knowledge, it was demonstrated that an aqueous sol-gel technique is suitable for the formation of calcium hydroxyapatite/phosphate composite coatings $Ca_{10}(PO_4)_6(OH)_2$ and $Ca_3(PO_4)_2$ on titanium substrate. The XRD and FTIR measurements confirmed that the samples also contain TiO_2 (rutile).

2. Interestingly, the repetition of immersing, withdrawal and annealing procedures for 5, 15 and 30 times did not change phase composition of coating dramatically. The SEM micrographs of Ca-P-O sol-gel calcined at 1000 °C showed highly uniform and crystalline particles with smooth surfaces. The hydrophobic properties of thin films measured by CAM were associated with phase composition of CHAp-TCP coatings. It was demonstrated, that calcium titanate sub-layer did not promote the formation of CHAp. Finally, the proposed sol-gel method appeared to be very attractive way to make a high density, homogeneous CHAp-TCP coatings on Ti substrate using both, dip-coating and spin-coating deposition techniques.

3. An aqueous sol-gel method was suggested for the synthesis of calcium hydroxyapatite thin films on silicon substrate. The substrates were coated 1, 5, 15 and 30 times using both, dip- and spin-coating techniques and annealed at 1000 °C after each dipping or spinning procedure. It was demonstrated, that crystallization of calcium hydroxyapatite depends on number of layers. Using dip-coating technique, the formation of calcium hydroxyapatite was evident only with increasing of number of layers up to 30. The $Ca_3(PO_4)_2$ and $Ca_2P_2O_7$ phases also remained in the sample obtained after 30 immersing and annealing procedures. Using spin-coating technique, the XRD results showed that calcium hydroxyapatite phase was formed in the samples containing 5, 15 and 30 layers of Ca-P-O precursor sol-gel.

4. The progressive changes in the surface morphology of CHAp films with increasing the dipping or spinning time were detected. The SEM micrographs

of sol-gel calcined at 1000 °C showed highly uniform and crystalline particles with smooth surfaces. Additionally, homogeneous CHAp coatings of regular polygons with narrow particle size distribution (300-400 nm) have formed in the samples prepared with 15 and 30 spinning and annealing procedures.

5. The AFM results were in a good agreement with SEM observations. The highest roughness (44.2 at surface area of 2/2μm) was observed in the sample containing of 30 layers. The thickness of CHAp films increased monotonically with increasing number of spin-coating and annealing procedures. The results of Raman spectrometry showed the peak at 961 cm^{-1}, which corresponds to symmetric stretching vibration of phosphate groups in calcium hydroxyapatite proving the formation of high quality $Ca_{10}(PO_4)_6(OH)_2$ thin films on Si substrate using an aqueous sol-gel chemistry approach.

6. Fourier transform infrared (FTIR) spectroscopy revealed that intensity of ν_4 infrared absorption bands at 549 cm^{-1}, 570 cm^{-1}, 602 cm^{-1} and ν_1 infrared absorption bands at 945 cm^{-1}, 972 cm^{-1} increases with increasing the number of deposited layers. The specific OH^- vibration mode near 635–630 cm^{-1} and band near 3571 cm^{-1} was not visible in FTIR spectra. The well-defined ν_1 band at 945 cm^{-1} corresponds to peak position of totally symmetric vibrational mode from oxyhydroxyapatite $Ca_{10}(PO_4)_6(OH)_{2-2x}O_x$. Position of infrared bands observed in this work both in the ν_1 and ν_4 spectral regions coincides well with the β-$Ca_3(PO_4)_2$ structure. The results obtained demonstrated that calcium oxyhydroxyapatite, probably, have formed on Si substrate.

7. Aqueous sol-gel method was developed for the synthesis of calcium hydroxyapatite thin films on quartz substrate. Two different dip-coating and spin-coating techniques were applied for preparation of CHAp and compared. The XRD results let us to conclude that the crystallization of calcium hydroxyapatite on the substrate was influenced by both number of dip- or spin-coating procedures and type of applied technique. The phase purity and crystallinity also depend on the amount of layers of end product. It was

demonstrated, that more pure and crystalline CHAp has formed using spin-coating technique.

8. SEM micrographs and AFM images were recorded to determine surface morphological features of thin films. The main morphological features of films obtained by dip- and spin-coating techniques were very similar. However, the surface of dip-coated sample containing 30 layers was rougher and with more expressed crystallization of smaller particles. The thickness of CHAp layers have changed from ~64 nm to ~3170 nm (dip-coating technique) and from ~20 nm to ~2704 nm (spin-coating technique) by increasing number of annealing procedures from 1 to 30, respectively. The obtained results of contact angle measurements clearly showed correlations between number of layers and contact angle values of CHA surfaces. With increasing number of layers, the hydrophobicity of surfaces increased. Finally, the results presented in this study demonstrated that suggested sol-gel process is perfectly suitable for the synthesis of calcium hydroxyapatite on the quartz substrate allowing to control phase purity and morphological properties of CHAp.

6. List of author‘s publications

Articles in journals

1. A. Beganskienė, Ž. Stankevičiūtė, M. Malakauskaitė, I. Bogdanovičienė, V. Mikli, K. Tönsuaadu, A. Kareiva. Sol-gel approach to the calcium phosphate nanocomposites. Proceedings of The 37th Int. Conf. & Expo. on Advanced Ceramics & Composites (ICACC2013). In Nanostructured Materials and Nanotechnology VII (eds S. Mathur, F. Hernandez-Ramirez, S. Kirihara and S. Widjaja), John Wiley & Sons, Inc., Hoboken, NJ, USA, 34 (2013) p. 1-11. doi: 10.1002/9781118807828.ch1.
2. Ž. Stankevičiūtė, M. Malakauskaitė, A. Beganskienė, A. Kareiva. Sol-gel synthesis of calcium phosphate coatings on Ti substrate using dip-coating technique. Chemija, 24 (2014) 288–295.
3. M. Malakauskaitė-Petrulevičienė, Ž. Stankevičiūtė, A. Beganskienė, A. Kareiva. Sol–gel synthesis of calcium hydroxyapatite thin films on quartz substrate using dip-coating and spin-coating techniques. Journal of Sol-Gel Science and Technology, 71 (2014) 437–446.
4. M. Malakauskaitė-Petrulevičienė, Ž. Stankevičiūtė, G. Niaura, A. Prichodko, A. Kareiva. Synthesis and characterization of sol-gel derived calcium hydroxyapatite thin films spin-coated on silicon substrate. Ceramics International, 41 (2015) 7421-7428.
5. M. Malakauskaite-Petruleviciene, Z. Stankeviciute, G. Niaura, E. Garskaite, A. Beganskiene, A. Kareiva. Characterization of sol-gel processing of calcium phosphate thin films on silicon substrate by FTIR spectroscopy. Vibrational Spectroscopy, 85 (2016) 16–21.

Published contributions to academic conferences

1. Ž. Stankevičiūtė, M. Malakauskaitė. Dip-coating of calcium hydroxyapatite on Ti substrates. International conference of young chemists “Nanochemistry and nanomaterials”. Palanga, Lithuania, 7-9 December (2012) 44.
2. M. Malakauskaitė, Ž. Stankevičiūtė, A. Beganskienė, A. Kareiva.

Calcium phosphate bioceramic thin films prepared by sol-gel method on different substrates. Scientific conference “Chemistry and chemical technology”. Lithuania, Kaunas, 24-25 April, (2013) 83-88.

3. Ž. Stankevičiūtė, M. Malakauskaitė, A. Beganskienė, A. Kareiva. Spin-coated hydroxyapatite thin films on silica substrate: preparation and characterization. European Congress and Exhibition on Advanced Materials and Processes “FEMS EUROMAT 2013”. Spain, Sevilla, 8-13 September (2013) 145.

4. D. Jasaitis, M. Malakauskaitė, Ž. Stankevičiūtė, A. Beganskienė, A. Kareiva. Sol-gel synthesis of calcium hydroxyapatite films on titanium substrate using dip-coating technique. The 17h International Sol-Gel Conference. Spain, Madrid, 25-30 August (2013) 321.

5. M. Malakauskaitė-Petrulevičienė, V. Jonauskė, Ž. Stankevičiūtė, R. Raudonis, A. Beganskienė, A. Kareiva. Spin-coated and dip-coated hydroxyapatite thin films on silica substrate: preparation and characterization. Bio-inspired materials. Germany, Potsdam, 18-21 March (2014) 111.

6. Ž. Stankevičiūtė, R. Raudonis, M. Malakauskaitė-Petrulevičienė, A. Kareiva. Formation of calcium hydroxyapatite (CHAp) thin films on Ti substrate using spin-coating. 16-th international conference “Advanced materials and technologies”. Palanga, Lithuania, 27-31 August (2014) 105.

7. M. Malakauskaitė-Petrulevičienė, Ž. Stankevičiūtė, A. Prichodko, A. Kareiva. Spin-coated and dip-coated calcium hydroxyapatite thin films on titanium, silicon and quartz substrates: preparation and characterization. European Symposium and Exhibition on Biomaterials and Related Areas “Euro BioMAT 2015”. Weimar, Germany, 21 - 22 April (2015) [C-5].

8. V. Jonauskė, A. Prichodko, A. Kareiva, M. Malakauskaitė-Petrulevičienė. Spin-coated calcium hydroxyapatite thin films prepared using an aqueous sol-gel chemistry approach. Fourth international conference on multifunctional, hybrid and nanomaterials. Spain, Sitges, 9-13 March (2015) [P1.285].

9. M. Malakauskaitė-Petrulevičienė, A. Prichodko, Ž. Stankevičiūtė, R.

Raudonis, A. Beganskienė, A. Kareiva. Peculiarities of formation of hydroxyapatite on Si substrate. Fourth international conference on multifunctional, hybrid and nanomaterials. Spain, Sitges, 9-13 March (2015) [P1.302].

10. A. Momot, E. Garškaitė, V. Jonauskė, M. Drienovsky, M. Palcut, A. Kareiva, M. Malakauskaitė-Petrulevičienė. Engineering scaffolds for bone regeneration: Hydroxyapatite-polymer composite synthesized via sol-gel method. Fourth international conference on multifunctional, hybrid and nanomaterials. Spain, Sitges, 9-13 March (2015) [P1.237].

11. M. Malakauskaitė-Petrulevičienė, Ž. Stankevičiūtė, G. Niaura, A. Prichodko, A. Kareiva. FTIR analysis of spin-coated calcium hydroxyapatite thin films on silicon substrate. 2nd international conference of chemists "Nanochemistry and nanomaterials 2015". Lithuania, Vilnius, 22-23 October (2015) 26.

7. Acknowledgements

I would like to rejoice over a possibility to study PhD in the Faculty of Chemistry in Vilnius University. Studies were very interesting with many challenges along the way. I would not be able to achieve the set goals without the help of people I am surrounded by.

First of all, I would like to thank my scientific supervisor Prof. Dr. Habil. Aivaras Kareiva for his major help in scientific research, his understanding in difficult situations and motivation throughout my journey in the Faculty of Chemistry. I am very happy to have had such a good, sincere and professional supervisor.

Also I would like to thank all members of sol-gel research group for their support and help during all my studies. Especially I want to thank my colleague Dr. Živilė Stankevičiūtė, who assisted me in all situations during my research.

And my special thanks go to my family, who were patient, supportive and very helpful.

8. Curriculum Vitae

Milda Malakauskaitė-Petrulevičienė

2012-2016	Department of Inorganic Chemistry, Faculty of Chemistry, Vilnius University	PhD studies
2007-2009	Department of Analytical and Environmental Chemistry, Faculty of Chemistry, Vilnius University	Master's Degree in Chemistry
2003-2007	Department of Analytical and Environmental Chemistry, Faculty of Chemistry, Vilnius University	Bachelor's Degree in Chemistry
1991-2003	Vilnius Mykolas Biržiška Gymnasium	Secondary Education Diploma majoring in Chemists

9. Literature references

[1] P. Bartolo, J.P. Kruth, J. Silva, G. Levy, A. Malshe, K. Rajurkar, et al., Biomedical production of implants by additive electro-chemical and physical processes, CIRP Ann. - Manuf. Technol. 61 (2012) 635–655. doi:10.1016/j.cirp.2012.05.005.

[2] M. Bohner, L. Galea, N. Doebelin, Calcium phosphate bone graft substitutes: Failures and hopes, J. Eur. Ceram. Soc. 32 (2012) 2663–2671. doi:10.1016/j.jeurceramsoc.2012.02.028.

[3] A. Mizuno, N. Amizuka, K. Irie, A. Murakami, N. Fujise, T. Kanno, et al., Severe Osteoporosis in Mice Lacking Osteoclastogenesis Inhibitory Factor/ Osteoprotegerin, 247 (1998) 610–615.

[4] H. Zhou, J. Lee, Nanoscale hydroxyapatite particles for bone tissue engineering, Acta Biomater. 7 (2011) 2769–2781. doi:10.1016/j.actbio.2011.03.019.

[5] S. Wu, X. Liu, K.W.K. Yeung, C. Liu, X. Yang, Biomimetic porous scaffolds for bone tissue engineering, Mater. Sci. Eng. R Reports. 80 (2014) 1–36. doi:10.1016/j.mser.2014.04.001.

[6] J. Wierzchos, T. Falcioni, A. Kiciak, J. Wolinski, R. Koczorowski, P. Chomicki, et al., Advances in the ultrastructural study of the implant-bone interface by backscattered electron imaging, Micron. 39 (2008) 1363–1370. doi:10.1016/j.micron.2008.01.022.

[7] L. Le Guéhennec, A. Soueidan, P. Layrolle, Y. Amouriq, Surface treatments of titanium dental implants for rapid osseointegration., Dent. Mater. 23 (2007) 844–854. doi:10.1016/j.dental.2006.06.025.

[8] S. Lavenus, J. Roze, A. Hoornaert, G. Louarn, P. Layrolle, Impact of Nanotechnology on Dental Implants, in: Emerg. Nanotechnologies Dent., 2012: pp. 71–84. doi:10.1016/B978-1-4557-7862-1.00005-5.

[9] A. Abdal-hay, A.S. Hamdy, K.A. Khalil, J.H. Lim, A novel simple one-step air jet spinning approach for deposition of poly(vinyl acetate)/hydroxyapatite composite nanofibers on Ti implants, Mater. Sci. Eng. C. 49 (2015) 681–690. doi:10.1016/j.msec.2015.01.008.

[10] V. Goriainov, R. Cook, J. M Latham, D. G Dunlop, R.O.C. Oreffo, Bone and metal: An orthopaedic perspective on osseointegration of metals., Acta Biomater. 10 (2014) 4043–4057. doi:10.1016/j.actbio.2014.06.004.

[11] H.Q. Nguyen, D.A. Deporter, R.M. Pilliar, N. Valiquette, R. Yakubovich, The effect of sol-gel-formed calcium phosphate coatings on bone ingrowth and osteoconductivity of porous-surfaced Ti alloy implants, Biomaterials. 25 (2004) 865–876. doi:10.1016/S0142-9612(03)00607-0.

[12] N. Cao, J. Dong, Q. Wang, Q. Ma, C. Xue, M. Li, An experimental bone defect healing with hydroxyapatite coating plasma sprayed on carbon/carbon composite implants, Surf. Coatings Technol. 205 (2010) 1150–1156. doi:10.1016/j.surfcoat.2010.05.008.

[13] L. Xu, A. Yamamoto, Characteristics and cytocompatibility of biodegradable polymer film on magnesium by spin coating, Colloids

Surfaces B Biointerfaces. 93 (2012) 67–74. doi:10.1016/j.colsurfb.2011.12.009.
[14] S.L. Iconaru, P. Chapon, P. Le Coustumer, D. Predoi, Antimicrobial activity of thin solid films of silver doped hydroxyapatite prepared by sol-gel method, Sci. World J. 2014 (2014) 165351. doi:10.1155/2014/165351.
[15] S.B. Lang, S.A.M. Tofail, A.A. Gandhi, M. Gregor, C. Wolf-Brandstetter, J. Kost, et al., Pyroelectric, piezoelectric and photoeffects in hydroxyapatite thin films on silicon, Proc. - Int. Symp. Electrets. 123703 (2011) 87–88. doi:10.1109/ISE.2011.6084995.
[16] D.B. Haddow, P. James, R. Van Noort, Sol-gel derived calcium phosphate coatings for biomedical applications, J. Sol-Gel Sci. Technol. 13 (1998) 261–265. doi:10.1023/A:1008699421635.
[17] E.D. Spoerke, N.G. Murray, H. Li, L.C. Brinson, D.C. Dunand, S.I. Stupp, A bioactive titanium foam scaffold for bone repair, Acta Biomater. 1 (2005) 523–533. doi:10.1016/j.actbio.2005.04.005.
[18] E. Schiegnitz, V. Palarie, V. Nacu, B. Al-Nawas, P.W. Kämmerer, Vertical osteoconductive characteristics of titanium implants with calcium-phosphate-coated surfaces - a pilot study in rabbits, Clin. Implant Dent. Relat. Res. 16 (2014) 194–201. doi:10.1111/j.1708-8208.2012.00469.x.
[19] A. Kolk, J. Handschel, W. Drescher, D. Rothamel, F. Kloss, M. Blessmann, et al., Current trends and future perspectives of bone substitute materials - From space holders to innovative biomaterials, J. Cranio-Maxillofacial Surg. 40 (2012) 706–718. doi:10.1016/j.jcms.2012.01.002.
[20] H. Wang, N. Eliaz, Z. Xiang, H.P. Hsu, M. Spector, L.W. Hobbs, Early bone apposition in vivo on plasma-sprayed and electrochemically deposited hydroxyapatite coatings on titanium alloy, Biomaterials. 27 (2006) 4192–4203. doi:10.1016/j.biomaterials.2006.03.034.
[21] S. Saska, L.S. Mendes, A.M.M. Gaspar, T.S. de Oliveira Capote, Bone Substitute Materials in Implant Dentistry, in: Curr. Concepts Dent. Implantol., 2015: pp. 25–57. doi:10.5772/59487.
[22] H. Zhang, Q.-W. Fu, T.-W. Sun, F. Chen, C. Qi, J. Wu, et al., Amorphous Calcium Phosphate, Hydroxyapatite and Poly(D,L-Lactic Acid) Composite Nanofibers: Electrospinning Preparation, Mineralization and In Vivo Bone Defect Repair, Colloids Surfaces B Biointerfaces. 136 (2015) 27-36. doi:10.1016/j.colsurfb.2015.08.015.
[23] F. Peters, K. Schwarz, M. Epple, The structure of bone studied with synchrotron X-ray diffraction , X-ray absorption spectroscopy and thermal analysis, Thermochim. Acta. 361 (2000) 131–138.
[24] C. Rey, C. Combes, C. Drouet, M.J. Glimcher, Bone mineral : update on chemical composition and structure, Osteoporos Int. 20 (2009) 1013–1021. doi:10.1007/s00198-009-0860-y.
[25] M. Vallet-Regi, Calcium phosphates as substitution of bone tissues, Prog. Solid State Chem. 32 (2004) 1–31.

doi:10.1016/j.progsolidstchem.2004.07.001.
[26] M.J. Olszta, X. Cheng, S. Soo, R. Kumar, Y. Kim, M.J. Kaufman, et al., Bone structure and formation : A new perspective, Mterials Sci. Eng. 58 (2007) 77–116. doi:10.1016/j.mser.2007.05.001.
[27] S. Boonrungsiman, E. Gentleman, R. Carzaniga, N.D. Evans, D.W. Mccomb, The role of intracellular calcium phosphate in osteoblast-mediated bone apatite formation, PNAS. 109 (2012) 14170–14175. doi:10.1073/pnas.1208916109/-/DCSupplemental.www.pnas.org/cgi/doi/10.1073/pnas.1208916109.
[28] D. Bayraktar, A.C. Tas, Chemical preparation of carbonated calcium hydroxyapatite powders at 37°C in urea-containing synthetic body fluids, J. Eur. Ceram. Soc. 19 (1999) 2573–2579. doi:10.1016/S0955-2219(99)00132-6.
[29] C. Xu, P. Su, X. Chen, Y. Meng, W. Yu, A. Peng, et al., Biocompatibility and osteogenesis of biomimetic Bioglass-Collagen-Phosphatidylserine composite scaffolds for bone tissue engineering, Biomaterials. 32 (2011) 1051–1058. doi:10.1016/j.biomaterials.2010.09.068.
[30] R.Z. Legeros, Calcium Phosphate-Based Osteoinductive Materials, Chem. Rev. 108 (2008) 4742–4753.
[31] M. Okada, T. Furuzono, Hydroxylapatite nanoparticles: fabrication methods and medical applications, Sci. Technol. Adv. Mater. 13 (2012) 064103. doi:10.1088/1468-6996/13/6/064103.
[32] C. Rey, B. Collins, T. Goehl, I.R. Dickson, M.J. Glimcher, The Carbonate Environment in Bone Mineral : A Resolution-Enhanced Fourier Transform Infrared Spectroscopy Study, Calcif Tissue Int. 45 (1989) 157–164.
[33] A. Antonakos, E. Liarokapis, T. Leventouri, Micro-Raman and FTIR studies of synthetic and natural apatites, Biomaterials. 28 (2007) 3043–3054. doi:10.1016/j.biomaterials.2007.02.028.
[34] E. Landi, G. Celotti, G. Logroscino, A. Tampieri, Carbonated hydroxyapatite as bone substitute, J. Eur. Ceram. Soc. 23 (2003) 2931–2937. doi:10.1016/S0955-2219(03)00304-2.
[35] E.G. Nordstrom, K.H. Karlsson, Carbonate-doped hydroxyapatite, Journals Mater. Sci. Mater. Med. I. 1 (1990) 182–184.
[36] L. Yang, S. Perez-Amodio, F.Y.F. Barrere-de Groot, V. Everts, C.A. van Blitterswijk, P. Habibovic, The effects of inorganic additives to calcium phosphate on in vitro behavior of osteoblasts and osteoclasts, Biomaterials. 31 (2010) 2976–2989. doi:10.1016/j.biomaterials.2010.01.002.
[37] S. Osamu, N. Masanori, M. Yoshinori, K. Manabu, S. Minoru, Bone Formation on Synthetic Precursors of Hydroxyapatite, Tohoku J. Exp. Med. 164 (1991) 37–50.
[38] S. V Dorozhkin, M. Epple, Biological and Medical Significance of Calcium Phosphates, WILEY-VCH Verlag. 41 (2002) 3130–3146.
[39] S. Bose, S. Tarafder, Calcium phosphate ceramic systems in growth

factor and drug delivery for bone tissue engineering : A review, Acta Biomater. 8 (2012) 1401–1421. doi:10.1016/j.actbio.2011.11.017.
[40] B. Nc, A.S. Posner, Hydroxyapatite - Mechanism of Formation and Properties, Calcif. Tissue Res. 13 (1973) 235–243. doi:10.1007/bf02015413.
[41] C. Rey, V. Renugopalakrishnan, B. Collins, M.J. Glimcher, Fourier Transform Infrared Spectroscopic Study of the Carbonate Ions in Bone Mineral During Aging, Calcif. Tissue Int. 49 (1991) 251–258.
[42] D.J. Hadjidakis, I.I. Androulakis, Bone Remodeling, New York Acad. Sci. 1092 (2006) 385–396. doi:10.1196/annals.1365.035.
[43] J. Venkatesan, I. Bhatnagar, P. Manivasagan, K. Kang, S. Kim, Alginate composites for bone tissue engineering : A review, Int. J. Biol. Macromol. 72 (2015) 269–281. doi:10.1016/j.ijbiomac.2014.07.008.
[44] M. Sadat-Shojai, M.-T. Khorasani, E. Dinpanah-Khoshdargi, A. Jamshidi, Synthesis methods for nanosized hydroxyapatite with diverse structures, Acta Biomater. 9 (2013) 7591–7621. doi:10.1016/j.actbio.2013.04.012.
[45] R. Murugan, S. Ramakrishna, Development of nanocomposites for bone grafting, Compos. Sci. Technol. 65 (2005) 2385–2406. doi:10.1016/j.compscitech.2005.07.022.
[46] J.Y. Rho, L. Kuhn-Spearing, P. Zioupos, Mechanical properties and the hierarchical structure of bone, Med. Eng. Phys. 20 (1998) 92–102. doi:10.1016/S1350-4533(98)00007-1.
[47] R. Bhowmik, K.S. Katti, D.R. Katti, Mechanics of molecular collagen is influenced by hydroxyapatite in natural bone, J. Mater. Sci. 42 (2007) 8795–8803. doi:10.1007/s10853-007-1914-1.
[48] A.F. Khan, M. Awais, A.S. Khan, A.A. Chaudhry, I.U. Rehman, Raman Spectroscopy of Natural Bone and Synthetic Apatites, Appl. Spectrosc. Rev. 48 (2013) 329–355. doi:10.1080/05704928.2012.721107.
[49] R. Khanna, K.S. Katti, D.R. Katti, Bone nodules on chitosan – polygalacturonic acid – hydroxyapatite nanocomposite films mimic hierarchy of natural bone, Acta Biomater. 7 (2011) 1173–1183. doi:10.1016/j.actbio.2010.10.028.
[50] A. Marina, P. Gentile, V. Chiono, G. Ciardelli, Collagen for bone tissue regeneration, Acta Biomater. 8 (2012) 3191–3200. doi:10.1016/j.actbio.2012.06.014.
[51] N. Rodriguez-Florez, M.L. Oyen, S.J. Shefelbine, Insight into differences in nanoindentation properties of bone, J. Mech. Behav. Biomed. Mater. 18 (2013) 90–99. doi:10.1016/j.jmbbm.2012.11.005.
[52] N. Ozgür Engin, A.C. Tas, Manufacture of macroporous calcium hydroxyapatite bioceramics, J. Eur. Ceram. Soc. 19 (1999) 2569–2572. doi:10.1016/S0955-2219(99)00131-4.
[53] K. Kandori, M. Oketani, M. Wakamura, Effects of Ti(IV) substitution on protein adsorption behaviors of calcium hydroxyapatite particles, Colloids Surfaces B Biointerfaces. 101 (2013) 68–73. doi:10.1016/j.colsurfb.2012.06.017.

[54] H. Imaizumi, M. Sakurai, O. Kashimoto, T. Kikawa, O. Suzuki, Comparative study on osteoconductivity by synthetic octacalcium phosphate and sintered hydroxyapatite in rabbit bone marrow, Calcif. Tissue Int. 78 (2006) 45–54. doi:10.1007/s00223-005-0170-0.
[55] R. Murugan, S. Ramakrishna, Crystallographic Study of Hydroxyapatite Bioceramics Derived from Various Sources, Cryst. Growth Des. 5 (2005) 111–112.
[56] X. Wang, J. Ye, Variation of crystal structure of hydroxyapatite in calcium phosphate cement by the substitution of strontium ions, J. Mater. Sci. Mater. Med. 19 (2007) 1183–1186. doi:10.1007/s10856-007-3209-0.
[57] V. Jokanović, D. Izvonar, M.D. Dramićanin, B. Jokanović, V. Živojinović, D. Marković, et al., Hydrothermal synthesis and nanostructure of carbonated calcium hydroxyapatite, J. Mater. Sci. Mater. Med. 17 (2006) 539–546. doi:10.1007/s10856-006-8937-z.
[58] M.P. Ferraz, F.J. Monteiro, C.M. Manuel, Hydroxyapatite nanoparticles : A review of preparation methodologies, J. Appl. Biomater. 2 (2004) 74–80. http://www.ncbi.nlm.nih.gov/pubmed/20803440.
[59] M.H. Fathi, A. Hanifi, V. Mortazavi, Preparation and bioactivity evaluation of bone-like hydroxyapatite nanopowder, J. Mater. Process. Technol. 202 (2008) 536–542. doi:10.1016/j.jmatprotec.2007.10.004.
[60] H. Tanaka, M. Futaoka, R. Hino, K. Kandori, T. Ishikawa, Structure of synthetic calcium hydroxyapatite particles modified with pyrophosphoric acid, J. Colloid Interface Sci. 283 (2005) 609–612. doi:10.1016/j.jcis.2004.09.013.
[61] K.K. Kandori, A. Fudo, T. Ishikawa, Study on the particle texture dependence of protein adsorption by using synthetic micrometer-sized calcium hydroxyapatite particles, Colloids Surfaces B Biointerfaces. 24 (2002) 145–153. doi:10.1016/S0927-7765(01)00227-2.
[62] H.B. Lu, C.T. Campbell, D.J. Graham, B.D. Ratner, Surface characterization of hydroxyapatite and related calcium phosphates by XPS and TOF-SIMS, Anal. Chem. 72 (2000) 2886–2894. doi:10.1021/ac990812h.
[63] K. Kandori, M. Mitsui, Synthesis and characterization of Ti(IV)-substituted calcium hydroxyapatite particles by forced hydrolysis of Ca(OH)2-Na5P3O10-TiCl4 mixed solution, Colloid Polym. Sci. 292 (2014) 2849–2856. doi:10.1007/s00396-014-3320-y.
[64] W. Masat, K. Hashimoto, T. Watanabe, Photocatalysis by Calcium Hydroxyapatite Modifiedwith Ti (IV): Albumin Decomposition and Bactericidal Effect, 19 (2003) 3428–3431.
[65] J.H. Kim, S.H. Kim, H.K. Kim, T. Akaike, S.C. Kim, Synthesis and characterization of hydroxyapatite crystals: A review study on the analytical methods, J. Biomed. Mater. Res. 62 (2002) 600–612. doi:10.1002/jbm.10280.
[66] M. Wakamura, K. Kandori, T. Ishikawa, Surface composition of calcium hydroxyapatite modified with metal ions, Colloids Surfaces A

Physicochem. Eng. Asp. 142 (1998) 107–116. doi:10.1016/S0927-7757(98)00486-5.
[67] S. Samavedi, A.R. Whittington, A.S. Goldstein, Calcium phosphate ceramics in bone tissue engineering: A review of properties and their influence on cell behavior, Acta Biomater. 9 (2013) 8037–8045. doi:10.1016/j.actbio.2013.06.014.
[68] L.M. Rodriguez-Lorenzo, M. Vallet-Regi, Controlled Crystallization of Calcium Phosphate Apatites, Chem. Mater. 12 (2000) 2460–2465.
[69] B. Susmita, S.K. Saha, Synthesis and Characterization of Hydroxyapatite Nanopowders by Emulsion Technique, Chem. Mater. 15 (2003) 4464–4469.
[70] S.-C.C. Liou, S.-Y.Y. Chen, H.-Y.Y. Lee, J.-S.S. Bow, Structural characterization of nano-sized calcium deficient apatite powders, Biomaterials. 25 (2004) 189–196. doi:10.1016/S0142-9612(03)00479-4.
[71] A.M. Pietak, J.W. Reid, M.J. Stott, M. Sayer, Silicon substitution in the calcium phosphate bioceramics, Biomaterials. 28 (2007) 4023–4032. doi:10.1016/j.biomaterials.2007.05.003.
[72] J. Kolmas, E. Groszyk, D. Kwiatkowska-Różycka, Substituted hydroxyapatites with antibacterial properties, Biomed Res. Int. 2014 (2014) 178123 (15pp). doi:10.1155/2014/178123.
[73] S. Ghanaati, M. Barbeck, R. Detsch, U. Deisinger, U. Hilbig, V. Rausch, et al., The chemical composition of synthetic bone substitutes influences tissue reactions in vivo: histological and histomorphometrical analysis of the cellular inflammatory response to hydroxyapatite, beta-tricalcium phosphate and biphasic calcium phosphate cer, Biomed. Mater. 7 (2012) 015005 (14pp). doi:10.1088/1748-6041/7/1/015005.
[74] M. Markovic, B.O. Fowler, M.S. Tung, Preparation and comprehensive characterization of a calcium hydroxyapatite reference material, J. Res. Natl. Inst. Stand. Technol. 109 (2004) 553. doi:10.6028/jres.109.042.
[75] T. Leventouri, Synthetic and biological hydroxyapatites: Crystal structure questions, Biomaterials. 27 (2006) 3339–3342. doi:10.1016/j.biomaterials.2006.02.021.
[76] G. Ma, X.Y. Liu, Hydroxyapatite: Hexagonal or monoclinic?, Cryst. Growth Des. 9 (2009) 2991–2994. doi:10.1021/cg900156w.
[77] K. Kandori, K. Miyagawa, T. Ishikawa, Adsorption of immunogamma globulin onto various synthetic calcium hydroxyapatite particles, J. Colloid Interface Sci. 273 (2004) 406–413. doi:10.1016/j.jcis.2004.01.069.
[78] K. Kandori, A. Masunari, T. Ishikawa, Study on Adsorption Mechanism of Proteins Onto Synthetic Calcium Hydroxyapatites Through Ionic Concentration Measurements, Calcif. Tissue Int. 76 (2005) 194–206. doi:10.1007/s00223-004-0102-4.
[79] K. Kandori, T. Kuroda, S. Togashi, E. Katayama, Preparation of calcium hydroxyapatite nanoparticles using microreactor and their characteristics of protein adsorption, J. Phys. Chem. B. 115 (2011) 653–659. doi:10.1021/jp110441e.

[80] T.I. Ivanova, O.V. Frank-Kamenetskaya, A.B. Koltsov, V.L. Ugolkov, Crystal Structure of Calcium-Deficient Carbonated Hydroxyapatite. Thermal Decomposition, J. Solid State Chem. 160 (2001) 340–349. doi:10.1006/jssc.2000.9238.
[81] D. Laurencin, N. Almora-Barrios, N.H. de Leeuw, C. Gervais, C. Bonhomme, F. Mauri, et al., Magnesium incorporation into hydroxyapatite, Biomaterials. 32 (2011) 1826–1837. doi:10.1016/j.biomaterials.2010.11.017.
[82] A. Aminian, M. Solati-Hashjin, A. Samadikuchaksaraei, F. Bakhshi, F. Gorjipour, A. Farzadi, et al., Synthesis of silicon-substituted hydroxyapatite by a hydrothermal method with two different phosphorous sources, Ceram. Int. 37 (2011) 1219–1229. doi:10.1016/j.ceramint.2010.11.044.
[83] R.Z. Legeros, S. Lin, R. Rohanizadeh, D. Mijares, J.P. Legeros, Biphasic calcium phosphate bioceramics: Preparation, properties and applications, J. Mater. Sci. Mater. Med. 14 (2003) 201–209. doi:10.1023/A:1022872421333.
[84] I. Mobasherpour, M.S. Heshajin, A. Kazemzadeh, M. Zakeri, Synthesis of nanocrystalline hydroxyapatite by using precipitation method, J. Alloys Compd. 430 (2007) 330–333. doi:10.1016/j.jallcom.2006.05.018.
[85] N. Monmaturapoj, Nano-size Hydroxyapatite Powders Preparation by Wet-Chemical Precipitation Route, J. Mater. Mater. Miner. 18 (2008) 15–20.
[86] A. Cüneyt Taş, F. Korkusuz, M. Timuçin, N. Akkaş, An investigation of the chemical synthesis and high-temperature sintering behaviour of calcium hydroxyapatite (HA) and tricalcium phosphate (TCP) bioceramics., J. Mater. Sci. Mater. Med. 8 (1997) 91–96. doi:10.1023/A:1018506800033.
[87] C. Kothapalli, M. Wei, a. Vasiliev, M.T. Shaw, Influence of temperature and concentration on the sintering behavior and mechanical properties of hydroxyapatite, Acta Mater. 52 (2004) 5655–5663. doi:10.1016/j.actamat.2004.08.027.
[88] A. Cuneyt Tas, Molten salt synthesis of calcium hydroxyapatite whiskers, J. Am. Ceram. Soc. 84 (2001) 295–300.
[89] J. Pena, M. Vallet-Regí, Hydroxyapatite, tricalcium phosphate and biphasic materials prepared by a liquid mix technique, J. Eur. Ceram. Soc. 23 (2003) 1687–1696. doi:10.1016/S0955-2219(02)00369-2.
[90] J. Chen, Z. Wen, S. Zhong, Z. Wang, J. Wu, Q. Zhang, Synthesis of hydroxyapatite nanorods from abalone shells via hydrothermal solid-state conversion, Mater. Des. 87 (2015) 445–449. doi:10.1016/j.matdes.2015.08.056.
[91] S. Pramanik, A.K. Agarwal, K.N. Rai, A. Garg, Development of high strength hydroxyapatite by solid-state-sintering process, Ceram. Int. 33 (2007) 419–426. doi:10.1016/j.ceramint.2005.10.025.
[92] S. Cox, Synthesis method of hydroxyapatite, Lucideon, Insight Creat. Advant. 1 (2014) 1–7.

[93] S.-H. Rhee, Synthesis of hydroxyapatite via mechanochemical treatment, Biomaterials. 23 (2002) 1147–1152. doi:10.1016/S0142-9612(01)00229-0.
[94] W.F. Ho, H.C. Hsu, S.K. Hsu, C.W. Hung, S.C. Wu, Calcium phosphate bioceramics synthesized from eggshell powders through a solid state reaction, Ceram. Int. 39 (2013) 6467–6473. doi:10.1016/j.ceramint.2013.01.076.
[95] D.M. Liu, T. Troczynski, W.J. Tseng, Water-based sol-gel synthesis of hydroxyapatite: Process development, Biomaterials. 22 (2001) 1721–1730. doi:10.1016/S0142-9612(00)00332-X.
[96] K. Agrawal, G. Singh, D. Puri, S. Prakash, Synthesis and Characterization of Hydroxyapatite Powder by Sol-Gel Method for Biomedical Application, J Miner. Mater. Char Eng. 10 (2011) 727–734.
[97] H. Zhang, K. Zhou, Z. Li, S. Huang, Plate-like hydroxyapatite nanoparticles synthesized by the hydrothermal method, J. Phys. Chem. Solids. 70 (2009) 243–248. doi:10.1016/j.jpcs.2008.10.011.
[98] K. Byrappa, T. Adschiri, Hydrothermal technology for nanotechnology, Prog. Cryst. Growth Charact. Mater. 53 (2007) 117–166. doi:10.1016/j.pcrysgrow.2007.04.001.
[99] J. Liu, X. Ye, H. Wang, M. Zhu, B. Wang, H. Yan, The influence of pH and temperature on the morphology of hydroxyapatite synthesized by hydrothermal method, Ceram. Int. 29 (2003) 629–633. doi:10.1016/S0272-8842(02)00210-9.
[100] J. Zhao, Y.J. Zhu, G.F. Cheng, Y.J. Ruan, T.W. Sun, F. Chen, et al., Microwave-assisted hydrothermal rapid synthesis of amorphous calcium phosphate nanoparticles and hydroxyapatite microspheres using cytidine 5′-triphosphate disodium salt as a phosphate source, Mater. Lett. 124 (2014) 208–211. doi:10.1016/j.matlet.2014.03.054.
[101] J.K. Han, H.Y. Song, F. Saito, B.T. Lee, Synthesis of high purity nano-sized hydroxyapatite powder by microwave-hydrothermal method, Mater. Chem. Phys. 99 (2006) 235–239. doi:10.1016/j.matchemphys.2005.10.017.
[102] N. Bala, C. Khosla, B. Banda, S. Bahadur, F. Sahib, Preparation and Deposition of Hydroxyapatite on Biomaterials by Sol-Gel Technique-A Review, Chitkara Chem. Rev. 1 (2013) 59–69.
[103] E.I. Ko, Sol-Gel process, in: G. Ertl, H. Knozinger, J. Weitkamp (Eds.), Prep. Solid Catal., WILEY-VCH Verlag GmbH, 1999: pp. 85–97.
[104] J. Chen, Y. Wang, X. Chen, L. Ren, C. Lai, W. He, et al., A simple sol-gel technique for synthesis of nanostructured hydroxyapatite, tricalcium phosphate and biphasic powders, Mater. Lett. 65 (2011) 1923–1926. doi:10.1016/j.matlet.2011.03.076.
[105] O. Kaygili, S. V. Dorozhkin, S. Keser, Synthesis and characterization of Ce-substituted hydroxyapatite by sol-gel method, Mater. Sci. Eng. C. 42 (2014) 78–82. doi:10.1016/j.msec.2014.05.024.
[106] F. Bakan, O. Laçin, H. Sarac, A novel low temperature sol-gel synthesis process for thermally stable nano crystalline hydroxyapatite, Powder

Technol. 233 (2013) 295–302. doi:10.1016/j.powtec.2012.08.030.
[107] O. Kaygili, C. Tatar, The investigation of some physical properties and microstructure of Zn-doped hydroxyapatite bioceramics prepared by sol-gel method, J. Sol-Gel Sci. Technol. 61 (2012) 296–309. doi:10.1007/s10971-011-2627-0.
[108] B. Jokić, M. Mitrić, V. Radmilović, S. Drmanić, R. Petrović, D. Janaćković, Synthesis and characterization of monetite and hydroxyapatite whiskers obtained by a hydrothermal method, Ceram. Int. 37 (2011) 167–173. doi:10.1016/j.ceramint.2010.08.032.
[109] L.X. Yang, J.J. Yin, L.L. Wang, G.X. Xing, P. Yin, Q.W. Liu, Hydrothermal synthesis of hierarchical hydroxyapatite: Preparation, growth mechanism and drug release property, Ceram. Int. 38 (2012) 495–502. doi:10.1016/j.ceramint.2011.07.033.
[110] C.J. Tredwin, A.M. Young, G. Georgiou, S.H. Shin, H.W. Kim, J.C. Knowles, Hydroxyapatite, fluor-hydroxyapatite and fluorapatite produced via the sol-gel method. Optimisation, characterisation and rheology, Dent. Mater. 29 (2013) 166–173. doi:10.1016/j.dental.2012.11.008.
[111] H.-S. Ryu, K.S. Hong, J.-K. Lee, D.J. Kim, J.H. Lee, B.-S. Chang, et al., Magnesia-doped HA/β-TCP ceramics and evaluation of their biocompatibility, Biomaterials. 25 (2004) 393–401. doi:10.1016/S0142-9612(03)00538-6.
[112] S. Raynaud, E. Champion, Calcium phosphate apatites with variable Ca / P atomic ratio II . Calcination and sintering, Biomaterials. 23 (2002) 1073–1080.
[113] R.A. Surmenev, A review of plasma-assisted methods for calcium phosphate-based coatings fabrication, Surf. Coatings Technol. 206 (2012) 2035–2056. doi:10.1016/j.surfcoat.2011.11.002.
[114] S.R. Paital, N.B. Dahotre, Calcium phosphate coatings for bio-implant applications: Materials, performance factors, and methodologies, Mater. Sci. Eng. R Reports. 66 (2009) 1–70. doi:10.1016/j.mser.2009.05.001.
[115] Y. Li, I.S. Lee, F.Z. Cui, S.H. Choi, The biocompatibility of nanostructured calcium phosphate coated on micro-arc oxidized titanium, Biomaterials. 29 (2008) 2025–2032. doi:10.1016/j.biomaterials.2008.01.009.
[116] L.L. Hench, Bioceramics: From Concept to Clinic, J. Am. Ceram. Soc. 74 (1991) 1487–1510. doi:10.1111/j.1151-2916.1991.tb07132.x.
[117] E. Mohseni, E. Zalnezhad, A.R. Bushroa, Comparative investigation on the adhesion of hydroxyapatite coating on Ti–6Al–4V implant: A review paper, Int. J. Adhes. Adhes. 48 (2014) 238–257. doi:10.1016/j.ijadhadh.2013.09.030.
[118] N.A. Trujillo, R.A. Oldinski, H. Ma, J.D. Bryers, J.D. Williams, K.C. Popat, Antibacterial effects of silver-doped hydroxyapatite thin films sputter deposited on titanium, Mater. Sci. Eng. C. 32 (2012) 2135–2144. doi:10.1016/j.msec.2012.05.012.
[119] S.M. Best, A.E. Porter, E.S. Thian, J. Huang, Bioceramics: Past, present

and for the future, J. Eur. Ceram. Soc. 28 (2008) 1319–1327. doi:10.1016/j.jeurceramsoc.2007.12.001.
[120] Y. Yang, K. Kim, J. Ong, A review on calcium phosphate coatings produced using a sputtering process an alternative to plasma spraying, Biomaterials. 26 (2005) 327–337. doi:10.1016/j.biomaterials.2004.02.029.
[121] Q. Bao, C. Chen, D. Wang, Q. Ji, T. Lei, Pulsed laser deposition and its current research status in preparing hydroxyapatite thin films, Appl. Surf. Sci. 252 (2005) 1538–1544. doi:10.1016/j.apsusc.2005.02.127.
[122] C.F. Koch, S. Johnson, D. Kumar, M. Jelinek, D.B. Chrisey, A. Doraiswamy, et al., Pulsed laser deposition of hydroxyapatite thin films, Mater. Sci. Eng. C. 27 (2007) 484–494. doi:10.1016/j.msec.2006.05.025.
[123] C.M. Lopatin, V. Pizziconi, T.L. Alford, T. Laursen, Hydroxyapatite powders and thin films prepared by a sol-gel technique, Thin Solid Films. 326 (1998) 227–232. doi:10.1016/S0040-6090(98)00531-8.
[124] M.A. Surmeneva, T.M. Mukhametkaliyev, A.I. Tyurin, A.D. Teresov, N.N. Koval, T.S. Pirozhkova, et al., Effect of silicate doping on the structure and mechanical properties of thin nanostructured RF magnetron sputter-deposited hydroxyapatite films, Surf. Coatings Technol. 275 (2015) 176–184. doi:10.1016/j.surfcoat.2015.05.021.
[125] G. Xu, I.A. Aksay, J.T. Groves, Continuous crystalline carbonate apatite thin films. A biomimetic approach, J. Am. Chem. Soc. 123 (2001) 2196–2203. doi:10.1021/ja002537i.
[126] E. Gyorgy, S. Grigorescu, G. Socol, I.N. Mihailescu, D. Janackovic, A. Dindune, et al., Bioactive glass and hydroxyapatite thin films obtained by pulsed laser deposition, Appl. Surf. Sci. 253 (2007) 7981–7986. doi:10.1016/j.apsusc.2007.02.146.
[127] L. Duta, F.N. Oktar, G.E. Stan, G. Popescu-Pelin, N. Serban, C. Luculescu, et al., Novel doped hydroxyapatite thin films obtained by pulsed laser deposition, Appl. Surf. Sci. 265 (2013) 41–49. doi:10.1016/j.apsusc.2012.10.077.
[128] S. Durdu, Ö.F. Deniz, I. Kutbay, M. Usta, Characterization and formation of hydroxyapatite on Ti6Al4V coated by plasma electrolytic oxidation, J. Alloys Compd. 551 (2013) 422–429. doi:10.1016/j.jallcom.2012.11.024.
[129] Y.W. Gu, K.A. Khor, P. Cheang, In vitro studies of plasma-sprayed hydroxyapatite/Ti-6Al-4V composite coatings in simulated body fluid (SBF), Biomaterials. 24 (2003) 1603–1611. doi:10.1016/S0142-9612(02)00573-2.
[130] J. Cizek, K.A. Khor, Role of in-flight temperature and velocity of powder particles on plasma sprayed hydroxyapatite coating characteristics, Surf. Coatings Technol. 206 (2012) 2181–2191. doi:10.1016/j.surfcoat.2011.09.058.
[131] M.C. Kuo, S.K. Yen, The process of electrochemical deposited hydroxyapatite coatings on biomedical titanium at room temperature, Mater. Sci. Eng. C. 20 (2002) 153–160. doi:10.1016/S0928-

4931(02)00026-7.
[132] K. Kuroda, M. Okido, Hydroxyapatite coating of titanium implants using hydroprocessing and evaluation of their osteoconductivity, Bioinorg. Chem. Appl. 2012 (2012) 730693. doi:10.1155/2012/730693.
[133] D.-M. Liu, Q. Yang, T. Troczynski, Sol-gel hydroxyapatite coatings on stainless steel substrates, Biomaterials. 23 (2002) 691–698. doi:10.1016/S0142-9612(01)00157-0.
[134] W. Jie, L. Yubao, Tissue engineering scaffold material of nano-apatite crystals and polyamide composite, Eur. Polym. J. 40 (2004) 509–515. doi:10.1016/j.eurpolymj.2003.10.028.
[135] H.R. Ramay, M. Zhang, Preparation of porous hydroxyapatite scaffolds by combination of the gel-casting and polymer sponge methods, Biomaterials. 24 (2003) 3293–3302. doi:10.1016/S0142-9612(03)00171-6.
[136] L. Gan, R. Pilliar, Calcium phosphate sol–gel-derived thin films on porous-surfaced implants for enhanced osteoconductivity. Part I: Synthesis and characterization, Biomaterials. 25 (2004) 5303–5312. doi:10.1016/j.biomaterials.2003.12.038.
[137] E.S. Thian, J. Huang, S.M. Best, Z.H. Barber, R.A. Brooks, N. Rushton, et al., The response of osteoblasts to nanocrystalline silicon-substituted hydroxyapatite thin films, Biomaterials. 27 (2006) 2692–2698. doi:10.1016/j.biomaterials.2005.12.019.
[138] H. Zeng, W.R. Lacefield, XPS, EDX and FTIR analysis of pulsed laser deposited calcium phosphate bioceramic coatings: the effects of various process parameters, Biomaterials. 21 (2000) 23–30. doi:10.1016/S0142-9612(99)00128-3.
[139] I. Demnati, D. Grossin, C. Combes, M. Parco, I. Braceras, C. Rey, A comparative physico-chemical study of chlorapatite and hydroxyapatite: from powders to plasma sprayed thin coatings, Biomed. Mater. 7 (2012) 054101. doi:10.1088/1748-6041/7/5/054101.
[140] Y. Huang, Q. Ding, S. Han, Y. Yan, X. Pang, Characterisation, corrosion resistance and in vitro bioactivity of manganese-doped hydroxyapatite films electrodeposited on titanium, J. Mater. Sci. Mater. Med. 24 (2013) 1853–1864. doi:10.1007/s10856-013-4955-9.
[141] E.S. Thian, J. Huang, S.M. Best, Z.H. Barber, W. Bonfield, Magnetron co-sputtered silicon-containing hydroxyapatite thin films—an in vitro study, Biomaterials. 26 (2005) 2947–2956. doi:10.1016/j.biomaterials.2004.07.058.
[142] E.S. Thian, J. Huang, M.E. Vickers, S.M. Best, Z.H. Barber, W. Bonfield, Silicon-substituted hydroxyapatite (SiHA): A novel calcium phosphate coating for biomedical applications, J. Mater. Sci. 41 (2006) 709–717. doi:10.1007/s10853-006-6489-8.
[143] M. Nakamura, Improvement of Osteoblast Adhesion Through Polarization of Plasma-Sprayed Hydroxyapatite Coatings on Metal, J. Med. Biol. Eng. 34 (2014) 44. doi:10.5405/jmbe.1450.
[144] A. Visan, D. Grossin, N. Stefan, L. Duta, F.M. Miroiu, G.E. Stan, et al.,

Biomimetic nanocrystalline apatite coatings synthesized by Matrix Assisted Pulsed Laser Evaporation for medical applications, Mater. Sci. Eng. B Solid-State Mater. Adv. Technol. 181 (2014) 56–63. doi:10.1016/j.mseb.2013.11.007.
[145] S. Pourhashem, A. Afshar, Double layer bioglass-silica coatings on 316L stainless steel by sol–gel method, Ceram. Int. 40 (2014) 993–1000. doi:10.1016/j.ceramint.2013.06.096.
[146] S. Langstaff, M. Sayer, T.J.N. Smith, S.M. Pugh, Resorbable bioceramics based on stabilized calcium phosphates. Part II: Evaluation of biological response, Biomaterials. 22 (2001) 135–150. doi:10.1016/S0142-9612(00)00139-3.
[147] S. Catros, J.-C. Fricain, B. Guillotin, B. Pippenger, R. Bareille, M. Remy, et al., Laser-assisted bioprinting for creating on-demand patterns of human osteoprogenitor cells and nano-hydroxyapatite, Biofabrication. 3 (2011) 025001 (11pp). doi:10.1088/1758-5082/3/2/025001.
[148] Z. Hong, L. Luan, S.-B. Paik, B. Deng, D.E. Ellis, J.B. Ketterson, et al., Crystalline hydroxyapatite thin films produced at room temperature — An opposing radio frequency magnetron sputtering approach, Thin Solid Films. 515 (2007) 6773–6780. doi:10.1016/j.tsf.2007.02.089.
[149] J. Holopainen, E. Santala, M. Heikkilä, M. Ritala, Electrospinning of calcium carbonate fibers and their conversion to nanocrystalline hydroxyapatite, Mater. Sci. Eng. C. Mater. Biol. Appl. 45 (2014) 469–476. doi:10.1016/j.msec.2014.09.035.
[150] R. Surmenev, M. Ryabtseva, E. V Shesterikov, V.F. Pichugin, T. Peitsch, M. Epple, The release of nickel from nickel-titanium (NiTi) is strongly reduced by a sub-micrometer thin layer of calcium phosphate deposited by rf-magnetron sputtering, J. Mater. Sci. Mater. Med. 21 (2010) 1233–1239. doi:10.1007/s10856-010-3989-5.
[151] E.S. Bogya, Z. Károly, R. Barabás, Atmospheric plasma sprayed silica–hydroxyapatite coatings on magnesium alloy substrates, Ceram. Int. 41 (2015) 6005–6012. doi:10.1016/j.ceramint.2015.01.041.
[152] M. Tomozawa, S. Hiromoto, Growth mechanism of hydroxyapatite-coatings formed on pure magnesium and corrosion behavior of the coated magnesium, Appl. Surf. Sci. 257 (2011) 8253–8257. doi:10.1016/j.apsusc.2011.04.087.
[153] A. Yanovska, V. Kuznetsov, A. Stanislavov, S. Danilchenko, L. Sukhodub, Calcium-phosphate coatings obtained biomimetically on magnesium substrates under low magnetic field, Appl. Surf. Sci. 258 (2012) 8577–8584. doi:10.1016/j.apsusc.2012.05.052.
[154] S. Shadanbaz, G.J. Dias, Calcium phosphate coatings on magnesium alloys for biomedical applications: A review, Acta Biomater. 8 (2012) 20–30. doi:10.1016/j.actbio.2011.10.016.
[155] H. Hornberger, S. Virtanen, A.R. Boccaccini, Biomedical coatings on magnesium alloys – A review, Acta Biomater. 8 (2012) 2442–2455. doi:10.1016/j.actbio.2012.04.012.
[156] S. V. Dorozhkin, Calcium orthophosphate coatings on magnesium and

its biodegradable alloys, Acta Biomater. 10 (2014) 2919–2934. doi:10.1016/j.actbio.2014.02.026.
[157] R. Sultana, J. Yang, X. Hu, Deposition of micro-porous hydroxyapatite/tri-calcium phosphate coating on zirconia-based substrate, J. Am. Ceram. Soc. 95 (2012) 1212–1215. doi:10.1111/j.1551-2916.2012.05114.x.
[158] K. Iijima, A. Sakai, A. Komori, Y. Sakamoto, H. Matsuno, T. Serizawa, et al., Control of biomimetic hydroxyapatite deposition on polymer substrates using different protein adsorption abilities, Colloids Surfaces B Biointerfaces. 130 (2015) 77–83. doi:10.1016/j.colsurfb.2015.04.010.
[159] L.D. Piveteau, M.I. Girona, L. Schlapbach, P. Barboux, J.P. Biolot, B. Gasser, Thin films of calcium phosphate and titanium dioxide by a sol-gel route: A new method for coating medical implants, J. Mater. Sci. Mater. Med. 10 (1999) 161–167. doi:10.1023/A:1008985423644.
[160] U. Ripamonti, L.C. Roden, L.F. Renton, Osteoinductive hydroxyapatite-coated titanium implants, Biomaterials. 33 (2012) 3813–3823. doi:10.1016/j.biomaterials.2012.01.050.
[161] T. Laonapakul, Y. Otsuka, A.R. Nimkerdphol, Y. Mutoh, Acoustic emission and fatigue damage induced in plasma-sprayed hydroxyapatite coating layers, J. Mech. Behav. Biomed. Mater. 8 (2012) 123–133. doi:10.1016/j.jmbbm.2011.11.011.
[162] W.K. Yeung, G.C. Reilly, A. Matthews, A. Yerokhin, In vitro biological response of plasma electrolytically oxidized and plasma-sprayed hydroxyapatite coatings on Ti-6Al-4V alloy, J. Biomed. Mater. Res. - Part B Appl. Biomater. 101 B (2013) 939–949. doi:10.1002/jbm.b.32899.
[163] L. Mishnaevsky, E. Levashov, R.Z. Valiev, J. Segurado, I. Sabirov, N. Enikeev, et al., Nanostructured titanium-based materials for medical implants: Modeling and development, Mater. Sci. Eng. R Reports. 81 (2014) 1–19. doi:10.1016/j.mser.2014.04.002.
[164] L. Wang, S. He, X. Wu, S. Liang, Z. Mu, J. Wei, et al., Polyetheretherketone/nano-fluorohydroxyapatite composite with antimicrobial activity and osseointegration properties, Biomaterials. 35 (2014) 6758–6775. doi:10.1016/j.biomaterials.2014.04.085.
[165] A. Arsiwala, P. Desai, V. Patravale, Recent advances in micro/nanoscale biomedical implants, J. Control. Release. (2014) 25–45. doi:10.1016/j.jconrel.2014.06.021.
[166] J.D. Long, S. Xu, J.W. Cai, N. Jiang, J.H. Lu, K.N. Ostrikov, et al., Structure, bonding state and in-vitro study of Ca–P–Ti film deposited on Ti6Al4V by RF magnetron sputtering, Mater. Sci. Eng. C. 20 (2002) 175–180. doi:10.1016/S0928-4931(02)00029-2.
[167] L. Sun, C.C. Berndt, K. a Gross, A. Kucuk, Material Fundamentals and Clinical Performance of Plasma- Sprayed Hydroxyapatite Coatings : A Review, J. Biomed. Mater. Res. 58 (2001) 570–592. doi:10.1002/jbm.xxxx.
[168] R.A. Surmenev, M.A. Surmeneva, A.A. Ivanova, Significance of

calcium phosphate coatings for the enhancement of new bone osteogenesis – A review, Acta Biomater. 10 (2014) 557–579. doi:10.1016/j.actbio.2013.10.036.
[169] J. Musil, P. Baroch, J. Vlček, K.H. Nam, J.G. Han, Reactive magnetron sputtering of thin films: present status and trends, Thin Solid Films. 475 (2005) 208–218. doi:10.1016/j.tsf.2004.07.041.
[170] S.J. Ding, Properties and immersion behavior of magnetron-sputtered multi-layered hydroxyapatite/titanium composite coatings, Biomaterials. 24 (2003) 4233–4238. doi:10.1016/S0142-9612(03)00315-6.
[171] A.L. Oliveira, J.F. Mano, R.L. Reis, Nature-inspired calcium phosphate coatings: present status and novel advances in the science of mimicry, Curr. Opin. Solid State Mater. Sci. 7 (2003) 309–318. doi:10.1016/j.cossms.2003.10.009.
[172] D. Perizzolo, W.R. Lacefield, D.M. Brunette, Interaction between topography and coating in the formation of bone nodules in culture for hydroxyapatite- and titanium-coated micromachined surfaces, J. Biomed. Mater. Res. 56 (2001) 494–503. doi:10.1002/1097-4636(20010915)56:4<494::AID-JBM1121>3.0.CO;2-X.
[173] B. Mavis, A. Cuneyt Tas, Dip Coating of Calcium Hydroxyapatite on Ti-6Al-4V Substrates, Society. 91 (2000) 989–991. doi:10.1111/j.1151-2916.2000.tb01314.x.
[174] N. Ohtsu, Y. Nakamura, S. Semboshi, Thin hydroxyapatite coating on titanium fabricated by chemical coating process using calcium phosphate slurry, Surf. Coatings Technol. 206 (2012) 2616–2621. doi:10.1016/j.surfcoat.2011.11.022.
[175] U. Vijayalakshmi, S. Rajeswari, Influence of process parameters on the sol–gel synthesis of nano hydroxyapatite using various phosphorus precursors, J. Sol-Gel Sci. Technol. 63 (2012) 45–55. doi:10.1007/s10971-012-2762-2.
[176] J. Hernandez-Montelongo, D. Gallach, N. Naveas, V. Torres-Costa, a. Climent-Font, J.P. García-Ruiz, et al., Calcium phosphate/porous silicon biocomposites prepared by cyclic deposition methods: Spin coating vs electrochemical activation, Mater. Sci. Eng. C. 34 (2014) 245–251. doi:10.1016/j.msec.2013.09.022.
[177] J.X. Zhang, R.F. Guan, X.P. Zhang, Synthesis and characterization of sol-gel hydroxyapatite coatings deposited on porous NiTi alloys, J. Alloys Compd. 509 (2011) 4643–4648. doi:10.1016/j.jallcom.2011.01.196.
[178] C.S. Chai, B. Ben-Nissan, Bioactive nanocrystalline sol-gel hydroxyapatite coatings, J. Mater. Sci. Mater. Med. 10 (1999) 465–469. doi:10.1023/A:1008992807888.
[179] D.B. Hall, P. Underhill, J.M. Torkelson, Spin Coating of Thin and Ultrathin Polymer Films, Polym. Eng. Sci. 38 (1998) 2039–2045. doi:10.1002/pen.10373.
[180] University of Louisville, Spin Coating Theory, Www.Cpmt.Org. (2011) 2–3.

[181] Cristian-Albrechts-Universitat, Basic Laboratory. Materials Science and Engineering. Spin Coating, (2011) 1–6.
[182] N.M. Site, P. Street, Production of thin film silicon-doped hydroxyapatite via sputter deposition, 9 (2004) 1895–1898. doi:10.1023/B:JMSC.0000016213.77001.71.
[183] L. Keller, W.A. Dollase, X-ray determination of crystalline hydroxyapatite to amorphous calcium- phosphate ratio in plasma sprayed coatings, J. Biomed. Mater. Res. 49 (2000) 244–249. doi:10.1002/(SICI)1097-4636(200002)49:2<244::AID-JBM13>3.0.CO;2-H.
[184] A. Cattini, D. Bellucci, A. Sola, L. Pawłowski, V. Cannillo, Microstructural design of functionally graded coatings composed of suspension plasma sprayed hydroxyapatite and bioactive glass, J. Biomed. Mater. Res. Part B Appl. Biomater. 102 (2014) 551–560. doi:10.1002/jbm.b.33034.
[185] C.J. Liao, F.H. Lin, K.S. Chen, J.S. Sun, Thermal decomposition and reconstruction of hydroxyapatite in air atmosphere, Biomed. Sci. Instrum. 35 (1999) 99–104. doi:10.1016/S0142-9612(99)00076-9.
[186] F. Fazan, P.M. Marquis, Dissolution behavior of plasma-sprayed hydroxyapatite coatings, J. Mater. Sci. Mater. Med. 11 (2000) 787–792. doi:10.1023/A:1008901512273.
[187] K.A. Gross, V. Gross, C.C. Berndt, Thermal Analysis of Amorphous Phases in Hydroxyapatite Coatings, J. Am. Ceram. Soc. 81 (1998) 106–112.
[188] P. Robotti, G. Zappini, S.M. Kurtz, Thermal Plasma Spray Deposition of Titanium and Hydroxyapatite on Polyaryletheretherketone Implants, in: PEEK Biomater. Handb., 2012: pp. 119–143. doi:10.1016/B978-1-4377-4463-7.10009-0.
[189] G.P. Dinda, J. Shin, J. Mazumder, Pulsed laser deposition of hydroxyapatite thin films on Ti-6Al-4V: effect of heat treatment on structure and properties, Acta Biomater. 5 (2009) 1821–1830. doi:10.1016/j.actbio.2009.01.027.
[190] J.T. Gudmundsson, N. Brenning, D. Lundin, U. Helmersson, High power impulse magnetron sputtering discharge, J. Vac. Sci. Technol. A Vacuum, Surfaces, Film. 30 (2012) 030801. doi:10.1116/1.3691832.
[191] P.J. Kelly, R.D. Arnell, Magnetron sputtering : a review of recent developments and applications, Vaccum. 56 (2000) 159–172.
[192] M.A. Surmeneva, E.A. Chudinova, I.Y. Grubova, O.S. Korneva, I.A. Shulepov, A.D. Teresov, et al., Effect of pulsed electron beam treatment on the physico-mechanical properties of hydroxyapatite-coated titanium, Ceram. Int. 42 (2016) 1470–1475. doi:10.1016/j.ceramint.2015.09.092.
[193] V.F. Pichugin, R.A. Surmenev, E. V. Shesterikov, M.A. Ryabtseva, E. V. Eshenko, S.I. Tverdokhlebov, et al., The preparation of calcium phosphate coatings on titanium and nickel-titanium by rf-magnetron-sputtered deposition: Composition, structure and micromechanical properties, Surf. Coatings Technol. 202 (2008) 3913–3920.

doi:10.1016/j.surfcoat.2008.01.038.
[194] J. Harle, H.W. Kim, N. Mordan, J.C. Knowles, V. Salih, Initial responses of human osteoblasts to sol-gel modified titanium with hydroxyapatite and titania composition, Acta Biomater. 2 (2006) 547–556. doi:10.1016/j.actbio.2006.05.005.
[195] M.-F. Hsieh, L.-H. Perng, T.-S. Chin, Hydroxyapatite coating on Ti6Al4V alloy using a sol–gel derived precursor, Mater. Chem. Phys. 74 (2002) 245–250. doi:10.1016/S0254-0584(01)00474-6.
[196] M. Catauro, F. Bollino, F. Papale, Surface modifications of titanium implants by coating with bioactive and biocompatible poly (ε-caprolactone)/SiO2 hybrids synthesized via sol-gel, Arab. J. Chem. (2014) 0–7. doi:10.1016/j.arabjc.2015.02.010.
[197] U. Vijayalakshmi, S. Rajeswari, Preparation and characterization of microcrystalline hydroxyapatite using sol gel method, Trends Biomater. Artif. Organs. 19 (2006) 57–62.
[198] J. Qu, X. Lu, D. Li, Y. Ding, Y. Leng, J. Weng, et al., Silver/hydroxyapatite composite coatings on porous titanium surfaces by sol-gel method, J. Biomed. Mater. Res. B. Appl. Biomater. 97 (2011) 40–48. doi:10.1002/jbm.b.31784.
[199] L. Gan, J. Wang, R.M. Pilliar, Evaluating interface strength of calcium phosphate sol-gel-derived thin films to Ti6Al4 V substrate, Biomaterials. 26 (2005) 189–196. doi:10.1016/j.biomaterials.2004.02.022.
[200] P. Habibovic, F. Barrere, Biomimetic hydroxyapatite coating on metal implants, J. Am. Ceram. Soc. 85 (2002) 517–522. doi:10.1111/j.1151-2916.2002.tb00126.x.
[201] T. Wang, A. Dorner-Reisel, Thermo-analytical investigations of the decomposition of oxyhydroxyapatite, Mater. Lett. 58 (2004) 3025–3028. doi:10.1016/j.matlet.2004.05.033.
[202] P. Hartmann, C. Jäger, S. Barth, J. Vogel, K. Meyer, Solid State NMR, X-Ray Diffraction, and Infrared Characterization of Local Structure in Heat-Treated Oxyhydroxyapatite Microcrystals: An Analog of the Thermal Decomposition of Hydroxyapatite during Plasma-Spray Procedure, J. Solid State Chem. 160 (2001) 460–468. doi:10.1006/jssc.2001.9274.
[203] L.M. Rodríguez-Lorenzo, M. Vallet-Regí, J.M. Ferreira, Fabrication of hydroxyapatite bodies by uniaxial pressing from a precipitated powder, Biomaterials. 22 (2001) 583–8. doi:10.1016/S0142-9612(00)00218-0.
[204] Y. Liu, Z. Shen, Dehydroxylation of hydroxyapatite in dense bulk ceramics sintered by spark plasma sintering, J. Eur. Ceram. Soc. 32 (2012) 2691–2696. doi:10.1016/j.jeurceramsoc.2012.02.025.
[205] T. Narushima, K. Ueda, T. Goto, H. Masumoto, T. Katsube, H. Kawamura, et al., Preparation of Calcium Phosphate Films by Radiofrequency Magnetron Sputtering, Mater. Trans. 46 (2005) 2246–2252. doi:10.2320/matertrans.46.2246.
[206] O. Blind, L.H. Klein, B. Dailey, L. Jordan, Characterization of hydroxyapatite films obtained by pulsed-laser deposition on Ti and Ti-

6AL-4v substrates, Dent. Mater. 21 (2005) 1017–1024. doi:10.1016/j.dental.2004.12.003.
[207] H.-W. Kim, J.C. Knowles, H.-E. Kim, Hydroxyapatite/poly (ε-caprolactone) composite coatings on hydroxyapatite porous bone scaffold for drug delivery, Biomaterials. 25 (2004) 1279–1287. doi:10.1016/j.biomaterials.2003.07.003.
[208] C. Zhou, C. Deng, X. Chen, X. Zhao, Y. Chen, Y. Fan, et al., Mechanical and biological properties of the micro-/nano-grain functionally graded hydroxyapatite bioceramics for bone tissue engineering, J. Mech. Behav. Biomed. Mater. 48 (2015) 1–11. doi:10.1016/j.jmbbm.2015.04.002.
[209] Y.C. Tsui, C. Doyle, T.W. Clyne, Plasma sprayed hydroxyapatite coatings on titanium substrates Part 1: Mechanical properties and residual stress levels, Biomaterials. 19 (1998) 2015–2029. doi:10.1016/S0142-9612(98)00103-3.
[210] S. Vahabzadeh, M. Roy, A. Bandyopadhyay, S. Bose, Phase stability and biological property evaluation of plasma sprayed hydroxyapatite coatings for orthopedic and dental applications, Acta Biomater. 17 (2015) 47–55. doi:10.1016/j.actbio.2015.01.022.
[211] Y. Huang, J. He, L. Gan, X. Liu, Y. Wu, F. Wu, et al., Osteoconductivity and osteoinductivity of porous hydroxyapatite coatings deposited by liquid precursor plasma spraying: in vivo biological response study, Biomed. Mater. 9 (2014) 065007. doi:10.1088/1748-6041/9/6/065007.
[212] W. Chen, Y. Liu, H.S. Courtney, M. Bettenga, C.M. Agrawal, J.D. Bumgardner, et al., In vitro anti-bacterial and biological properties of magnetron co-sputtered silver-containing hydroxyapatite coating, Biomaterials. 27 (2006) 5512–5517. doi:10.1016/j.biomaterials.2006.07.003.
[213] S. Samani, S.M. Hossainalipour, M. Tamizifar, H.R. Rezaie, In vitro antibacterial evaluation of sol-gel-derived Zn-, Ag-, and (Zn + Ag)-doped hydroxyapatite coatings against methicillin-resistant Staphylococcus aureus, J. Biomed. Mater. Res. A. 101 (2013) 222–30. doi:10.1002/jbm.a.34322.
[214] G.A. Fielding, M. Roy, A. Bandyopadhyay, S. Bose, Antibacterial and biological characteristics of silver containing and strontium doped plasma sprayed hydroxyapatite coatings, Acta Biomater. 8 (2012) 3144–3152. doi:10.1016/j.actbio.2012.04.004.
[215] A. Rakngarm Nimkerdphol, Y. Otsuka, Y. Mutoh, Effect of dissolution/precipitation on the residual stress redistribution of plasma-sprayed hydroxyapatite coating on titanium substrate in simulated body fluid (SBF), J. Mech. Behav. Biomed. Mater. 36 (2014) 98–108. doi:10.1016/j.jmbbm.2014.04.007.
[216] S.S. Jensen, M. Aaboe, E.M. Pinholt, E. Hjørting-Hansen, F. Melsen, I.E. Ruyter, Tissue reaction and material characteristics of four bone substitutes., Int. J. Oral Maxillofac. Implants. 11 (1996) 55–66.
[217] W. Xu, W. Hu, M. Li, C. Wen, Sol-gel derived hydroxyapatite/titania

biocoatings on titanium substrate, Mater. Lett. 60 (2006) 1575–1578. doi:10.1016/j.matlet.2005.11.072.
[218] J.Y. Han, Z.T. Yu, L. Zhou, Hydroxyapatite/titania composite bioactivity coating processed by sol-gel method, Appl. Surf. Sci. 255 (2008) 455–458. doi:10.1016/j.apsusc.2008.06.072.
[219] A. Leleckaite, A. Kareiva, H. Bettentrup, T. Jüstel, H.-J. Meyer, Sol-gel preparation and characterization of codoped yttrium aluminium garnet powders, Zeitschrift Fur Anorg. Und Allg. Chemie. 631 (2005) 2987–2993. doi:10.1002/zaac.200500315.
[220] I. Bogdanovičienė, A. Beganskienė, V. Mikli, Influence of heating conditions on the formation of sol – gel derived calcium hydroxyapatite, Chemija. 21 (2010) 98–105.
[221] J. Trinkūnaitė-Felsen, A. Kareiva, Characterization of naturally derived calcium compounds used in food industry, Chemija. 23 (2012) 76–85.
[222] S.H. Jun, E.J. Lee, S.W. Yook, H.E. Kim, H.W. Kim, Y.H. Koh, A bioactive coating of a silica xerogel/chitosan hybrid on titanium by a room temperature sol-gel process, Acta Biomater. 6 (2010) 302–307. doi:10.1016/j.actbio.2009.06.024.
[223] M. Vilotijević, P. Marković, S. Zec, S. Marinković, V. Jokanović, Hydroxyapatite coatings prepared by a high power laminar plasma jet, J. Mater. Process. Technol. 211 (2011) 996–1004. doi:10.1016/j.jmatprotec.2010.12.018.
[224] C.C. Silva, A. S.B. Sombra, Raman spectroscopy measurements of hydroxyapatite obtained by mechanical alloying, J. Phys. Chem. Solids. 65 (2004) 1031–1033. doi:10.1016/j.jpcs.2003.10.071.
[225] D. V Rokhmistrov, O.T. Nikolov, O.A. Gorobchenko, K.I. Loza, Study of structure of calcium phosphate materials by means of electron spin resonance., Appl. Radiat. Isot. 70 (2012) 2621–2626. doi:10.1016/j.apradiso.2012.07.020.
[226] T. Levchenko, Y. Plyuto, N. Kovtyukhova, Functionalisation of the template-free and template-structured silica films synthesised on glass substrates by sol–gel technique, J. Sol-Gel Sci. Technol. 43 (2007) 269–274. doi:10.1007/s10971-007-1584-0.
[227] N. Dubnikova, E. Garskaite, A. Beganskiene, A. Kareiva, Sol-gel synthesis and characterization of sub-microsized lanthanide (Ho, Tm, Yb, Lu) aluminium garnets, Opt. Mater. (Amst). 33 (2011) 1179–1184. doi:10.1016/j.optmat.2011.02.008.
[228] Z. Feng, Y. Li, Y. Huang, H.J. Seo, Luminescence properties of Eu^{2+} and Eu^{3+} doped calcium-deficient hydroxyapatite prepared in air, J. Alloys Compd. 509 (2011) 7087–7092. doi:10.1016/j.jallcom.2011.04.003.
[229] A. Prichodko, V. Jonauske, M. Cepenko, A. Beganskiene, A. Kareiva, Sol–gel derived two-dimensional nanostructures of calcium phosphates, Adv. Sci. Technol . 91 (2014) 13–18.
[230] K. Salma, N. Borodajenko, A. Plata, L. Berzina-Cimdina, A. Stunda, Fourier transform infrared spectra of technologically modified calcium phosphates, in: 14th Nordic-Baltic Conference on Biomedical

Engineering and Medical Physics. IFMBE Proceedings, 20 (2008) 68–71.
[231] E. Garskaite, K.-A. Gross, S.-W. Yang, T.C.-K. Yang, J.-C. Yang, A. Kareiva, Effect of processing conditions on the crystallinity and structure of carbonated calcium hydroxyapatite (CHAp), Cryst. Eng. Commun. 16 (2014) 3950–3959. doi:10.1039/c4ce00119b.
[232] G.B. Ramirez-Rodriguez, J.M. Delgado-Lopez, J. Gomez-Morales, Evolution of calcium phosphate precipitation in hanging drop vapor diffusion by in situ Raman microspectroscopy, Cryst. Eng. Comm. 15 (2013) 2206–2212.
[233] S.A. Pauline, N. Rajendran, Biomimetic novel nanoporous niobium oxide coating for orthopaedic applications, Appl. Surf. Sci. 290 (2014) 448–457. doi:10.1016/j.apsusc.2013.11.112.
[234] K.L. Mittal, Adhesion Measurement of Thin Films, Electrocompon. Sci. Technol. 3 (1976) 21–42. doi:10.1155/APEC.3.21.
[235] P.R. Chalker, S.J. Bull, D.S. Rickerby, A review of the methods for the evaluation of coating-substrate adhesion, Mater. Sci. Eng. A—Struct. Mater. Prop. Microstruct. Process. 140 (1991) 583–592.
[236] C. Mochizuki, H. Hara, I. Takano, T. Hayakawa, M. Sato, Application of carbonated apatite coating on a Ti substrate by aqueous spray method, Mater. Sci. Eng. C. 33 (2013) 951–958. doi:10.1016/j.msec.2012.11.027.
[237] K. Nakamoto, Infrared and Raman spectra of inorganic and coordination compounds, 4th ed., in: John Wiley New York, 1986: p. Chapters 2 and 3.
[238] G. Niaura, A.K. Gaigalas, V.L. Vilker, Surface-Enhanced Raman Spectroscopy of Phosphate Anions: Adsorption on Silver, Gold, and Copper Electrodes, J. Phys. Chem. B. 101 (1997) 9250–9262. doi:10.1021/jp970097k.
[239] U. Posset, E. Löcklin, R. Thull, W. Kiefer, Vibrational spectroscopic study of tetracalcium phosphate in pure polycrystalline form and as a constituent of a self-setting bone cement., J. Biomed. Mater. Res. 40 (1998) 640–645. doi:10.1002/(SICI)1097-4636(19980615)40:4<640::AID-JBM16>3.0.CO;2-J.
[240] I. Rehman, W. Bonfield, Characterization of hydroxyapatite and carbonated apatite by photo acoustic FTIR spectroscopy, J. Mater. Sci. Mater. Med. 8 (1997) 1–4. doi:10.1023/A:1018570213546.
[241] F. Garcia, J.L. Arias, B. Mayor, J. Pou, I. Rehman, J. Knowles, et al., Effect of heat treatment on pulsed laser deposited amorphous calcium phosphate coatings, J. Biomed. Mater. Res. 43 (1998) 69–76.
[242] G. Ulian, G. Valdre, M. Corno, P. Ugliengo, The vibrational features of hydroxylapatite and type A carbonated apatite: A first principle contribution, Am. Mineral. 98 (2013) 752–759.
[243] A.M. Sofronia, R. Baies, E.M. Anghel, C.A. Marinescu, S. Tanasescu, Thermal and structural characterization of synthetic and natural nanocrystalline hydroxyapatite., Mater. Sci. Eng. C. Mater. Biol. Appl. 43 (2014) 153–63. doi:10.1016/j.msec.2014.07.023.

[244] C. Durucan, P.W. Brown, α-Tricalcium phosphate hydrolysis to hydroxyapatite at and near physiological temperature, J. Mater. Sci. Mater. Med. 11 (2000) 365–371. doi:10.1023/A:1008934024440.
[245] A. Rapacz-Kmita, C. Paluszkiewicz, A. Ślósarczyk, Z. Paszkiewicz, FTIR and XRD investigations on the thermal stability of hydroxyapatite during hot pressing and pressureless sintering processes, J. Mol. Struct. 744-747 (2005) 653–656. doi:10.1016/j.molstruc.2004.11.070.
[246] A.Z. Alshemary, Y.-F. Goh, I. Shakir, R. Hussain, Synthesis, characterization and optical properties of chromium doped β-Tricalcium phosphate, Ceram. Int. 41 (2015) 1663–1669. doi:10.1016/j.ceramint.2014.09.107.
[247] I. Uysal, F. Severcan, Z. Evis, Characterization by Fourier transform infrared spectroscopy of hydroxyapatite co-doped with zinc and fluoride, Ceram. Int. 39 (2013) 7727–7733. doi:10.1016/j.ceramint.2013.03.029.
[248] I.A. Karampas, C.G. Kontoyannis, Characterization of calcium phosphates mixtures, Vib. Spectrosc. 64 (2013) 126–133. doi:10.1016/j.vibspec.2012.11.003.
[249] C.J. Liao, F.H. Lin, K.S. Chen, J.S. Sun, Thermal decomposition and reconstitution of hydroxyapatite in air atmosphere, Biomaterials. 20 (1999) 1807–1813. doi:10.1016/S0142-9612(99)00076-9.
[250] K.A. Gross, C.C. Berndt, P. Stephens, R. Dinnebier, Oxyapatite in hydroxyapatite coatings, J. Mater. Sci. 33 (1998) 3985–3991. doi:10.1023/a:1004605014652.
[251] G. Muralithran, S. Ramesh, The effects of sintering temperature on the properties of hydroxyapatite, Ceram. Int. 26 (2000) 221–230. doi:10.1016/S0272-8842(99)00046-2.
[252] R.W.N. Nilen, P.W. Richter, The thermal stability of hydroxyapatite in biphasic calcium phosphate ceramics, J. Mater. Sci. Mater. Med. 19 (2008) 1693–1702. doi:10.1007/s10856-007-3252-x.
[253] A. Jillavenkatesa, R.A. Condrate, The Infrared and Raman Spectra of β- and α-Tricalcium Phosphate ($Ca_3(PO_4)_2$), Spectrosc. Lett. 31 (1998) 1619–1634. doi:10.1080/00387019808007439.
[254] R. Bosco, M. Iafisco, J. van den Beucken, S. Leeuwenburgh, J. Jansen, Adsorption of alendronate onto biomimetic apatite nanocrystals to develop drug carrier coating for bone implants, Key Eng. Mater. 529-530 (2013) 475–479.
[255] K. Lin, D. Zhai, N. Zhang, N. Kawazoe, G. Chen, J. Chang, Fabrication and characterization of bioactive calcium silicate microspheres for drug delivery, Ceram. Int. 40 (2014) 3287–3293. doi:10.1016/j.ceramint.2013.09.106.
[256] G. Miao, X. Chen, C. Mao, X. Li, Y. Li, C. Lin, Synthesis and characterization of europium-containing luminescent bioactive glasses and evaluation of in vitro bioactivity and cytotoxicity, J. Sol-Gel Sci. Technol. 69 (2013) 250–259. doi:10.1007/s10971-013-3209-0.
[257] L. Shang, G.U. Nienhaus, Small fluorescent nanoparticles at the nano–bio interface, Mater. Today. 16 (2013) 58–66.

doi:10.1016/j.mattod.2013.03.005.